ADSORPTION PROPERTIES OF BORON NITRIDE NANOTUBES

A THESIS SUBMITTED TO
THE GRADUATE SCHOOL OF NATURAL AND APPLIED SCIENCES
OF
MIDDLE EAST TECHNICAL UNIVERSITY

BY

SAEED AHMAD KHAN

IN PARTIAL FULFILLMENT OF THE REQUIREMENTS
FOR
THE DEGREE OF MASTER OF SCIENCE
IN
CHEMICAL ENGINEERING

FEBRUARY 2016

Approval of the thesis:

ADSORPTION PROPERTIES OF BORON NITRIDE NANOTUBES

submitted by **SAEED AHMAD KHAN** in partial fulfillment of the requirements for the degree of **Master of Science in Chemical Engineering Department, Middle East Technical University** by,

Prof. Dr. Gülbin Dural Ünver _____
Dean, Graduate School of **Natural and Applied Sciences**

Prof. Dr. Halil Kalıpçılar _____
Head of Department, **Chemical Engineering**

Prof. Dr. Naime Aslı Sezgi _____
Supervisor, **Chemical Engineering Dept., METU**

Prof. Dr. Fatma Suna Balcı
Co-Supervisor, **Chemical Engineering Dept., Gazi University** _____

Examining Committee Members:

Prof. Dr. Gürkan Karakaş _____
Chemical Engineering Dept., METU

Prof. Dr. Naime Aslı Sezgi _____
Chemical Engineering Dept., METU

Prof. Dr. Fatma Suna Balcı _____
Chemical Engineering Dept., Gazi Univeristy

Prof. Dr. Halil Kalıpçılar _____
Chemical Engineering Dept., METU

Assoc. Prof. Dr. Serkan Kıncal _____
Chemical Engineering Dept., METU

Date: 05.02.2016

I hereby declare that all information in this document has been obtained and presented in accordance with academic rules and ethical conduct. I also declare that, as required by these rules and conduct, I have fully cited and referenced all material and results that are not original to this work.

Name, Last name : Saeed Ahmad KHAN

Signature :

ABSTRACT

ADSORPTION PROPERTIES OF BORON NITRIDE NANOTUBES

Khan, Saeed Ahmad

M.S., Department of Chemical Engineering

Supervisor: Prof. Dr. Naime Aslı Sezgi

Co-Supervisor: Prof. Dr. Fatma Suna Balcı

February 2016, 119 pages

The developments in nanotechnology in last decades have provided use of nanoparticles for many applications in various areas such as electronics, fuel cells, composites, cosmetics, and biomedical. They have excellent mechanical, thermal, and electrical properties. Nanotechnology is one of the fastest growing areas in materials and engineering science and biotechnology. Nanotubes have been one of the most regarded and studied type of nanoparticles up to now. Boron nitride nanotubes (BNNTs) are an important member of nanotube family. BNNTs are structural analogues of carbon nanotubes (CNTs). They are formed by rolling and folding of boron nitride atom sheets into cylindrical forms.

In this study, the nanotubes were synthesized in a tubular reactor at 1300^{o}C, with an ammonia flow rate of 125 sccm and boron to iron oxide or iron ratio of 15/1. Two types of precursor materials (iron oxide and iron) were used in this study for BNNTs synthesis. The material was purified by acid treatment using HNO_3 and HCl and characterized. Adsorption properties of BNNTs were investigated in order to analyze its potential applications as an adsorbent, catalyst support etc. XRD results revealed the presence of mostly hexagonal and little rhombohedral boron nitride solid phases. Some

impurities like cubic iron and compound of boron and iron (FeB_{49}) were also observed in the synthesized material.

Hollow cylindrical, bamboo-like and agglomerated nanotubes were obtained with the diameters range of 10-300 nm and length of several micrometers. Most of the nanotubes were in the diameter range of 15-100 nm. Nitrogen adsorption isotherms were obtained for BNNTs and the type-II isotherms were observed with hysteresis loops resembling to both type A and type B which indicate the presence of cylindrical and slit like pores in the material. The highest BET surface area for material synthesized using iron oxide and iron were found to be 145.2 m^2/g and 141.4 m^2/g, respectively. The average surface area for all the samples synthesized in this study was 133.66 m^2/g. The total pore volume for iron oxide and iron samples were 0.46 cm^3/g and 0.45 cm^3/g while the average BJH pore diameters were 41.7 Å and 37.5 Å, respectively. The micropore volume obtained for both synthesized materials from t-plot was 0.05 cm^3/g. The micropore volumes (D-R method) obtained from carbon dioxide adsorption for materials synthesized using iron oxide and iron were 0.053 cm^3/g and 0.040 cm^3/g, respectively. Chemisorption results showed the presence of acid sites on the material. The total acidity was found to be 0.136 and 0.155 mmol/g for BNNTs synthesized using iron oxide and iron, respectively. The properties of samples, synthesized from both precursors, were compared and it was observed that properties of the synthesized material were almost the same.

Keywords: Boron nitride, Nanotubes, Nanotechnology, Adsorption, Desorption, Isotherm

ÖZ

BOR NİTRÜR NANOTÜPLERİN ADSORPSİYON ÖZELLİKLERİ

Khan, Saeed Ahmad

Yüksek Lisans, Kimya Mühendisliği Bölümü
Tez Yöneticisi: Prof. Dr. Naime Aslı Sezgi
Ortak Tez Yöneticisi: Prof. Dr. Fatma Suna Balcı
Şubat 2016, 119 sayfa

Son yıllarda nanoteknolojideki ilerlemeler nanopartiküllerin elektronik, yakıt pilleri, kompozitler, kozmetik ve biyomedikal gibi birçok alanda kullanımını sağlamıştır. Nanopartiküllerin mükemmel mekanik, termal ve elektriksel özellikleri bulunmaktadır. Biyoteknoloji ve malzeme ve mühendislik biliminde en hızlı gelişen alanlarından biri nanoteknolojidir. Nanotüpler şu zamana kadar en çok üzerinde çalışılan ve değerlendirme yapılan nanopartiküllerden bir tanesi olmuşlardır. Bor nitrür nanotüpleri, nanotüp ailesinin en önemli üyesidir. Bor nitrür nanotüpleri (BNNT) karbon nanotüplerin (CNT) yapısal analoglarıdır. Bunlar bor nitrür atomik levhalarının yuvarlama ve katlanmasıyla silindirik yapıya çevrilmesiyle oluşturulurlar.

Bu çalışmada, nanotüpler tübüler bir reaktör içerisinde 1300^{o}C'de 125 sccm amonyak akışı ve 15/1 bor/demir oksit veya demir oranıyla sentezlenmiştir. Bu çalışmada, BNNT sentezi için iki çeşit öncül malzeme (demir oksit ve demir) kullanılmıştır. Malzeme HNO_3 ve HCl kullanılarak asit ile saflaştırılmış ve karakterize edilmiştir. Katalizör destek malzemesi, adsorbant olarak potansiyel uygulamalarını analiz etmek için BNNTl'in adsorbsiyon özellikleri araştırılmıştır. XRD sonuçları hekzagonal ve rombohedral bor nitrür katı fazlarının varlığını ortaya çıkarmıştır. Kübik demir ve bor-demir bileşikleri (FeB_{49}) gibi bazı safsızlıklar sentezlenen malzemede gözlenmiştir

Oyuk silindir, bambuya benzer ve aglomere nanotüpler 10-300 nm çap aralığında ve birkaç mikrometre uzunluğunda elde edilmiştir. Nanotüplerin çoğunluğu 15-100 nm çap aralığındadır. BNNT için azot adsorbsiyon izotermleri elde edilmiş ve ikinci tür (Type-II) izoterm çeşitlerinin yanında A ve B türü gecikme döngüleri (hysteresis loops) malzeme içinde silindirik ve kesik benzeri gözeneklerin varlığına işaret etmiştir. Malzemeler için en yüksek BET yüzey alanı ölçüm sonuçları demir oksit ve demir örnekleri için sırasıyla 145,2 m^2/g ve 141,4 m^2/g olarak çıkmıştır. Demir oksit ve demir örnekleri için sırasıyla toplam gözenek hacmi 0,46 cm^3/g ve 0,45 cm^3/g, ortalama gözenek çapları ise 41,7 Å ve 37,5 Å'dür. Mikrogözenek hacmi sentezlenen iki malzeme için de 0,05 cm^3/g'dır. Sentezlenen demir oksit ve demir için karbondioksit adsorbsiyonundan elde edilen mikro gözenek hacmi sırasıyla 0,053 cm^3/g ve 0,040 cm^3/g'dır. Kimyasal adsorpsiyon sonuçları malzemede asit aktiv sitelerin olduğunu göstermiştir. Toplam asidite sırasıyla demir oksit ve demir kullanılarak sentezlenen BNNTler için 0,136 ve 0,155 mmol/g olarak bulunmuştur. İki ayrı öncül malzemeden sentezlenen örneklerin özellikleri karşılaştırılmış ve sentezlenen malzemelerin özelliklerinin neredeyse aynı olduğu gözlenmiştir.

Anahtar kelimeler: Bor nitrür, Nanotüpler, Nanoteknoloji, Adsorbsiyon, Desorpsiyon, Izotherm

To my beloved family……

ACKNOWLEDGMENTS

The most important thing in life is the people and their values. People around you are part of your success and I am very grateful to have met such people in my life. I would like to express my deepest appreciation to Prof. Dr. Naime Aslı Sezgi, my supervisor and Prof. Dr. Suna BALCI, my co-supervisor, for their patient guidance, enthusiastic encouragement and useful critiques of this research work. Their guidance helped me in all phases of my research and writing of this thesis. Without their guidance and persistent help this thesis would not have been possible.

I am particularly grateful to Dr Funda TURGUT, Candan Karaeyvaz of Chemical Engineering Dept., Gazi University and Erdem Balık of Chemical Engineering Dept., METU, for their generous support and help during my experimental work. I owe my deepest gratitude to all professors of Chemical Engineering Department for encouragement and enormous help. I am obliged to many of my colleagues in the department who continuously supported me and made my life easy away from home.

Furthermore, I want to acknowledge the assistance that I received from all the technical staff in the labs of Chemical Engineering department METU and Gazi University for giving me generous help during my laboratory work. I would like to thank METU Central Laboratory for carrying out XRD, EDX, SEM and TEM of my samples. I am sincerely thankful to Prof. Dr. Selahattin YILMAZ for chemical adsorption analysis and Can Ağca for helping me with Turkish translation. I am grateful to Higher Education Commission (HEC) of Pakistan for the financial support (HRDI-UESTP) during my studies.

I am thankful to all my friends from Pakistan studying in METU (it is difficult to mention all their names here) for their lovely company and the joyful moments we spent here in Turkey.

I don’t have the words to express what my parents and my brothers have done for me. My family encouraged me to continue working hard. I thank them for their untiring support and guidance. Without them this dissertation and my education would not have been possible.

TABLE OF CONTENTS

LIST OF TABLES

TABLES

LIST OF FIGURES

FIGURES

NOMENCLATURE

A	Cross sectional adsorbate area, m^2
BNNT	Boron Nitride Nanotube
BET	Brunauer-Emmett-Teller
C	BET constant
CNT	Carbon Nanotube
CVD	Chemical Vapor Deposition
E_0	Characteristic energy of adsorption
EDX	Energy Dispersive X-Ray Spectroscopy
FTIR	Fourier Transform Infrared Spectroscopy
GPa	Giga Pascal
h-BN	Hexagonal Boron Nitride
IUPAC	International union of pure and applied chemistry
MWBNNT	Multi-wall Boron Nitride Nanotube
N_A	Avogadro's number (6.023×10^{23} molecules/mol)
P	Equilibrium pressure
Po	Saturation vapor pressure of the adsorbate
r-BN	Rhombohedral Boron Nitride
R	Gas constant, $atm.cm^3.mol^{-1}.K^{-1}$
SEM	Scanning Electron Microscopy
S	Total surface area
SWBNNT	Single-wall Boron Nitride Nanotube
T	Temperature, K
TPa	Tera Pascal
V_0	Microspore volume
V	Liquid molar volume of a given adsorbate

V_m	Monolayer volume
W	Amount of gas adsorbed
W_m	Amount of adsorbed for monolayer coverage
XRD	X-ray Diffraction
2Ɵ	Bragg angle, degree
ʎ	Wavelength, nm
β	Affinity coefficient

CHAPTER 1

INTRODUCTION

Over the past few decades research community has greatly focused their research on the new intriguing materials of nanoscale because of their tremendous applications in variety of fields like hydrogen storage, drug delivery, polymer nanocomposites etc. These materials got the name of nanomaterial and the field was entitled as nanotechnology. The story of nanomaterials started in 1959 when famous physicist Richard Feynman said his famous sentence “there is plenty of room at the bottom” in the meeting of American Physical Society [1]. The term nanotechnology was introduced by Eric Drexler in 1980s because these materials had dimensions in nanometer region [2].

Research in nanotechnology enabled us to design new materials which have very unique mechanical, thermal, optical, and electrical properties. These properties opened doors to a wide array of applications in the fields of electronics, medicine, composites, agriculture, energy, and aerospace [3]. Most famous nanomaterials are nanotubes and carbon nanotubes (CNTs) are the foremost and well studied since its discovery in 1991 [4]. Discovery of CNTs helped focusing the research on other nanotubes like boron nitride nanotube which is a new emerging member of the nanotube family [5].

The behavior of nanomaterials significantly differs from their respective bulk material. The unique chemistry, structural characteristics and energetic of nanomaterials have formed basis for the field of nanotechnology. Because of new synthesis methods for nanomaterials and latest characterization tools, the field of nanoscience saw a rapid expansion in the past two decades. Latest characterization techniques have made it possible to study thoroughly the properties and behavior of nanomaterials like electrical, optical and magnetic properties. The aim of nanoscience is to synthesize high

performance nanomaterials to explore new concepts in the fields of nanoelectronics, medicine etc. [6].

This study is about boron nitride nanotubes so different aspects of BNNTs will be discussed. BNNTs are one of the famous members of nanomaterials formed by wrapping of hexagonal boron nitride atomic sheets into cylindrical form. Wrapping of single atomic sheet into cylindrical structure forms single-walled nanotube (SWNT) while several concentrically organized nanotubes form multi-walled nanotube (MWNTs). There are different ways to produce BNNTs but in this study it is synthesized by reaction of ammonia with powder mixture of amorphous boron and iron oxide or iron. Adsorption properties of BNNTs were investigated using nitrogen adsorption, carbon dioxide adsorption and chemisorptions. Textural properties like surface area, pore size distribution, pore volumes and structures of BNNTs were studied [6].

Studying adsorption properties of nanomaterials is important to know the nature of their surfaces which can help us to discover about different potential application of these materials. One of the potential applications which is under intense research [7, 8, 9] is hydrogen storage in nanomaterials. Hydrogen can be used as a fuel in the fuel cells driven vehicles. Hydrogen storage capacity for CNTs is also carried out but with changing diameter and helicity the properties of CNTs change which poses significant challenge for its use as a gas adsorbent. On other hand BNNTs have stable thermal and chemical properties which do not depend on diameter and helicity of the nanotube. So BNNTs can be a promising candidate for hydrogen storage. For this purpose study of its adsorption and surface properties are very necessary. BNNTs can withstand high temperatures it can be used as support material in the catalyst or as an adsorbent for effluent gas capture like carbon dioxide. By doping of metal nanoparticles it can potentially be used as a catalyst for different purposes e.g. fuel cell catalyst. Surface funtionalization of BNNTs can help to achieve better dispersion in polymer matrix thus producing high quality nanocomposites for different applications [10, 11].

1.1 Nanotubes

One of the most prominent nanomaterials is nanotubes. Due to their unique properties most of the research in the field of nanomaterials is focused on nanotubes. Nanotubes are nanometer scaled tube structures resulting from folding atomic sheets in cylindrical form. The diameter of nanotube is in nanometer region but the length could be up to several microns. Nanotube formed from a single atomic sheet is called single-walled nanotube and when multiple atomic sheets are wrapped in concentric cylindrical form it is called multi-walled nanotube as shown in Figure 1.1.

Nanotube with two concentric cylindrical structures is called double-walled nanotube. Nanotubes can also be classified according to the rolling directions of atomic sheets as shown in Figure 1.2. These rolling directions can have tremendous effect on the properties of nanotubes. Carbon nanotubes (CNTs) can be either metallic or semiconductor depending upon the chirality (chiral angle between hexagon and tube axis). In Figure 1.2 three charalities of single-walled carbon nanotube; armchair, zigzag and chiral, based on the tube axis orientation with respect to hexagonal lattice are shown.

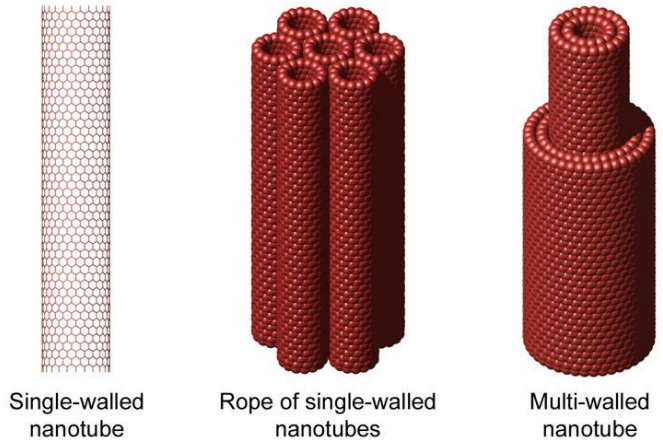

Figure 1.1 Single-walled and multi-walled nanotubes [6]

These different chiral structures of CNTs can have different electronic properties (metallic or semiconductor) [12]. Studies showed that size of nanotube diameter also

affects the electronic properties. Nanotubes with same chirality but different diameter can have different band gap values [13].

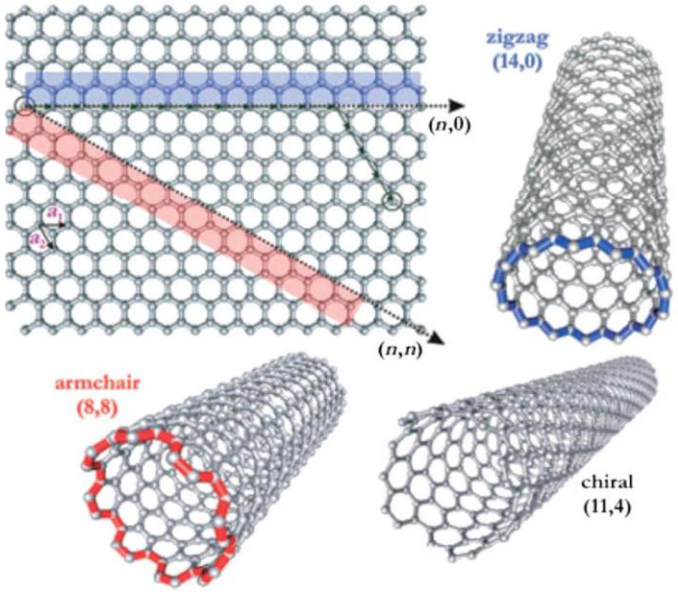

Figure 1.2 Types of carbon nanotubes (CNTs) on basis of rolling-up of graphene sheets [12]

1.2 Boron Nitride Nanotubes

The story of nanotubes started with the discovery of carbon nanotubes by Iijima et al. in 1991 [4]. Since then CNTs have attracted a lot of research attention around the world regarding their synthesis, purification, properties and potential application areas. CNTs are formed from rolling of graphene sheets into hallow cylindrical form. CNTs can be single or multi-walled and also their properties greatly depend on the chirality and diameter of the nanotube [12, 14]. Figure 1.2 shows different types of CNTs in which the graphene sheets are rolled up in armchair, chiral, and zigzag forms. The reason why CNTs attracted considerable research attention is their outstanding mechanical [15], electrical [16], and thermal [17] properties.

The discovery of carbon nanotubes paved the way for discovery of other nanotubes. For this reason theoretical and experimental researches were carried out in the field of nanomaterials. Different nanomaterials were discovered like BNNTs. BNNTs are the structural analogues of CNTs which are formed by wrapping of boron nitride (BN) atomic sheets in to hollow cylindrical tubes as shown in Figure 1.3. BNNTs were theoretically predicted by Cohen, M.L. et al. in 1994 [18] and experimentally prepared by Chopra, N.G et al. in 1995 [5]. Like carbon nanotubes, BNNTs also have different chiralities as shown in Figure 1.4 but their properties do not depend on it [19].

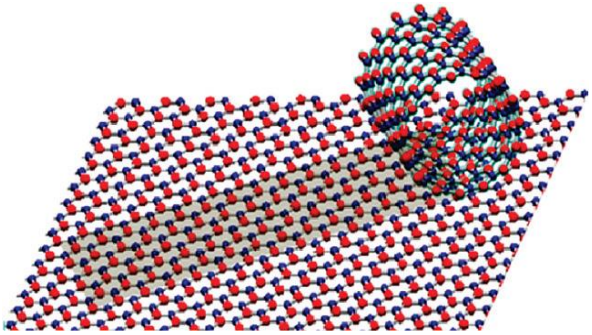

Figure 1.3 Computational model of boron nitride atomic sheet rolled-up into BNNTs (Blue and red colors represent boron and nitrogen, respectively) [20]

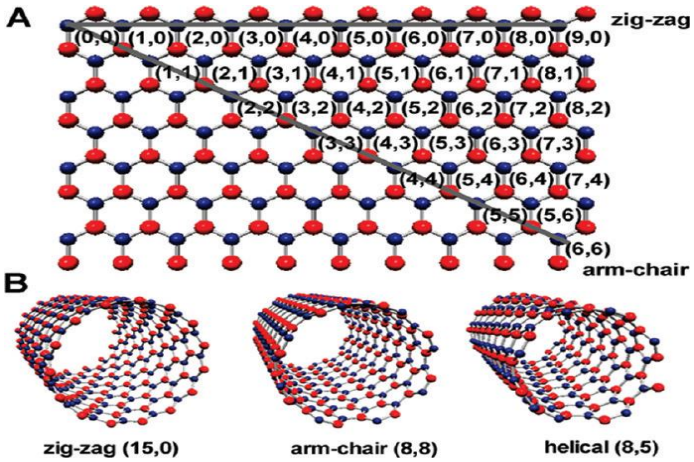

Figure 1.4 Possible wrapping directions of BN atomic sheets. (Red and blue colors represent boron and nitrogen atoms, respectively) [20]

1.2.1 Properties of Boron Nitride Nanotubes

Mechanical properties of BNNTs are good and some researchers have found young's modulus of BNNTs to be 1.18 TPa [21] which is very high as compared to other nanomaterials. CNTs have young's modulus of 0.27-4.15TPa [15]. Tensile strength of BNNTs is 30 GPa which is almost 15 times of steel [22]. BNNT can also recover after bending when the load is released [23]. Thermal conductivity of BNNTs (600 W/m K) [24] is very low as compared to CNTs (3000W/m K) [17]. BNNTs are chemically more stable than CNTs. The oxidation of BNNTs starts at 800^{o}C [25] while CNTs are stable in air up to 400^{o}C [23]. As previously mentioned that electronic properties of CNTs depend on the chirality and diameter of the nanotube so they can be metallic or semiconductor [12, 14] but for boron nitride nanotube it's not the case, it has always uniform band gap of around 5.5eV with semiconductor properties [6]. Interesting feature of BNNTs is that the band gap can be tuned using doping of different atoms like carbon and this property makes it a promising candidate in the field of nanoelectronics. Some researchers have discovered piezoelectric effect when stress is applied on BNNTs [23].

1.3 Application of Boron Nitride Nanotubes

Due to unique and intriguing properties, BNNTs have a wide array of potential application areas in the near future. Some of those applications are discussed here

1.3.1 Drug delivery

BNNTs are chemically stable and non-toxic so they can be used as a carrier for drug molecule in human body without being decomposed or metabolized [22]. Some researchers have envisioned transporting DNA with boron nitride nanotube [23] as shown in Figure 1.5. Funtionalization of BNNTs can have remarkable applications in the field of drug delivery. Tiago et al. have seen the possibility of cancer therapy in

functionalized BNNTs by delivering the respective drug to the damage cells. Functionalized nanotube can pass through the cell wall of a damage cell easily and thus can help in delivery of respective drug for curing [11].

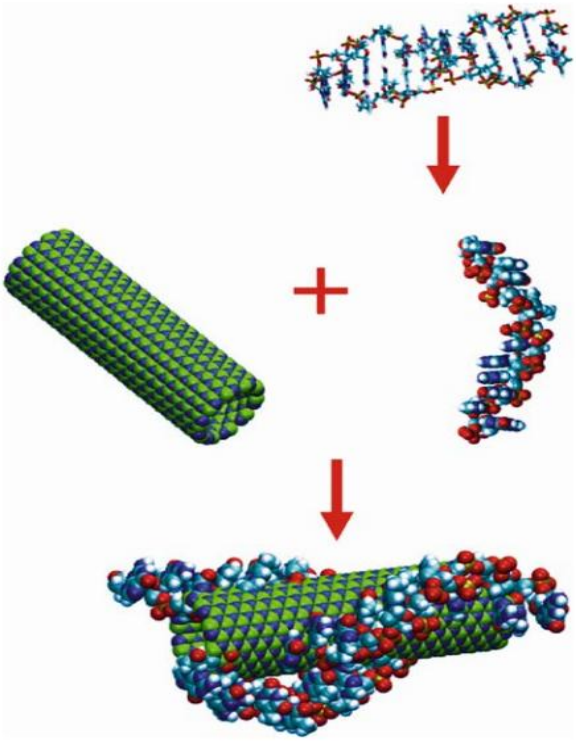

Figure 1.5 Computer model for DNA wrapping around boron nitride nanotube [23].

1.3.2 Electronics

Small electronic devices produce more heat per unit surface area which is getting very problematic. BNNTs are considered a good dissipater of heat [26] and because of this dissipating ability it can be a material of choice for future nanoelectronic devices [22, 23]. The uniform band gap and semiconducting nature of BNNTs [27] has anticipated very promising applications in the field of advance electronics [22]. The band gap can also be tuned by doping another atom or molecule or by bending the BN

nanotube [23]. Functionalization can also change the electronic and transport properties of BN nanotubes [28].

1.3.3 Hydrogen storage

Nanomaterials can be used as a vital material for the storage of hydrogen and in this regard some researches have been done for the storage of H_2 in carbon nanotubes [7] but results are not convincing yet. BNNTs could favor more hydrogen storage than CNTs because of their ionic nature of B-N bonds [23]. Various studies showed that BNNTs can store hydrogen up to 4.8 wt % [8, 9]. Hydrogen is an ideal environmentally friendly fuel and can be proved as vital source of energy around the world but storage of hydrogen is a major obstacle and nanomaterials can help us in this regard. Nanomaterials like BNNTs can be used as hydrogen storage system for fuel cell. Fuel cell is a growing technology which uses hydrogen as a fuel to produce electricity and to power vehicles without producing any greenhouse gases. But still there are challenges in achieving these goals because the surface and adsorption properties of BNNTs are not well understood yet. Storage of gas in BNNTs will require full understanding its adsorption characteristics and surface nature and this study is a step towards this goal.

1.3.4 Catalyst support

Boron nitride (BN) is previously reported to be used as a catalyst support for different reaction [29, 30]. Due to its stability at high temperatures and porous structure BNNT can also be potentially used for catalyst support. Due to the inert nature of BNNT it will have less interaction with reactants during the reaction and the reactants will interact mostly with active site of catalyst. The surface area of BNNT (140 m^2/g) is greater than BN (24 m^2/g) so much more area could be available for active metal particles. The hydrophobic nature of BN can also have effect on the performance of catalyst. BNNTs can potentially be used as a catalyst by doping metal nanoparticles or

by functionalizing using catalytically active chemical. For this purpose high surface area is desirable and BNNTs has high surface area as compared to BN [30]. To use BNNT as catalyst, support or as an adsorbent for gases, evaluation of its adsorption properties is necessary and which is the aim of this study.

1.3.5 Other Applications

Most of studies have been done for functionalization of carbon nanotubes so that they can be used in composites, electrochemical sensors etc. [10, 12]. It is considered that like CNTs, funtionalization can open new application areas for boron nitride nanotubes. Dispersion of nanotubes in composite materials has tremendous effect on the strength of composites and well dispersion is achieved by funtionalization [23]. Even the band gap tuning can be achieved by bonding molecules on the side walls of nanotubes [31]. Very high tensile strength and young's modulus of BNNTs can lead to their applications in very advance fields like aerospace and materials engineering [3, 22]. Low density and high strength of BNNTs can revolutionize the aircraft industry in future [22]. Some researchers have focused their work on this field like reinforcing polymer composites with BNNTs [32].

1.4 Synthesis Methods for Boron Nitride Nanotube

The biggest challenge that researchers encountered in the production of boron nitride nanotubes is the bulk synthesis. Most of the methods employed for the synthesis of BNNTs produces very little amount of product which is a big hindrance in the path of practical applications of BNNTs. There are several different methods for BNNT production discussed here. The type of method used may have effect the properties and structure of final BN nanotubes [33].

1.4.1 Arc-discharge

The schematic diagram of this method is shown in Figure 1.6. The system contains vacuum chamber, gas flow system and two electrodes connected to a DC power supply. Gas used in a chamber can be either inert (e.g helium or argon) or reactive gas like nitrogen or ammonia. For BNNT synthesis a reactive gas is used and a very low pressure is maintained in the chamber. For CNTs production the electrodes used are made of graphite but for BNNTs anode is made of reactive precursor materials. Voltage is applied between these electrodes which produces an arc that increases the temperature and due to high temperature the anode material is evaporated which reacts with the gas in the chamber and the product is obtained on the water cooled copper cathode and the inner walls of the chamber. During this process the anode is consumed. Some metal borides like HfB_2 and ZrB_2 can also be used as anode for BNNT production [6, 34]. High purity BNNTs are obtained by this method but the drawback of this method is that it is very energy intensive method and produces very little amount of product thus making it very expensive.

Inspired by carbon nanotubes [4], the arc-discharge was also the first method for the production of boron nitride nanotubes in which tungsten electrode filled with h-BN and cooled copper electrode were used [5].

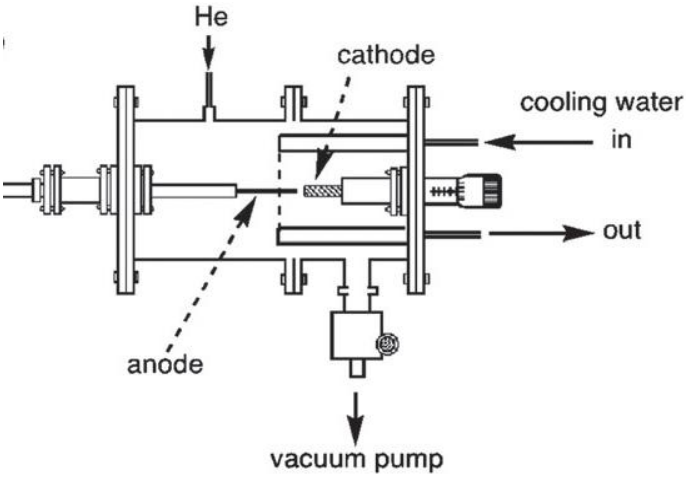

Figure 1.6 Schematic representation of Arc-discharge apparatus [35]

1.4.2 Laser-assisted Method

Instead of electrical energy laser beam is used in this method to evaporate the precursor materials into an ion gas. Schematic representation of this process is shown in Figure 1.7. Laser beam is focused on the target (starting material) which increases the temperature of the material in a very short time. The evaporated target material is carried by inert gas (argon). The product is collected on the water cooled metallic trap. Pure BN is used as a target material in the laser method thus final product is free from catalyst particles. If pure boron is used as target, nitrogen as a reactive gas is used and if the target is pure BN, argon gas is used in the chamber. A tube furnace is also utilized in order to keep high temperature environment inside the tube. The advantage of this method is that it can produce a pure crystalline product (up to 1 g). On other hand, very little amount of product can be synthesized using arc-discharge method. Both laser and arc-discharge methods produce product of almost same dimension and size but require very high energy [6].

The laser ablation method for the synthesis of boron nitride nanotubes was firstly used by Golberg et al. in 1996 [36]. Cubic boron nitride (c-BN) in diamond anvil cell (DAC) under the high pressure environment of nitrogen gas was targeted by CO_2 laser. An estimated temperature of 5000^{o}C was reached at the surface of the BN target.

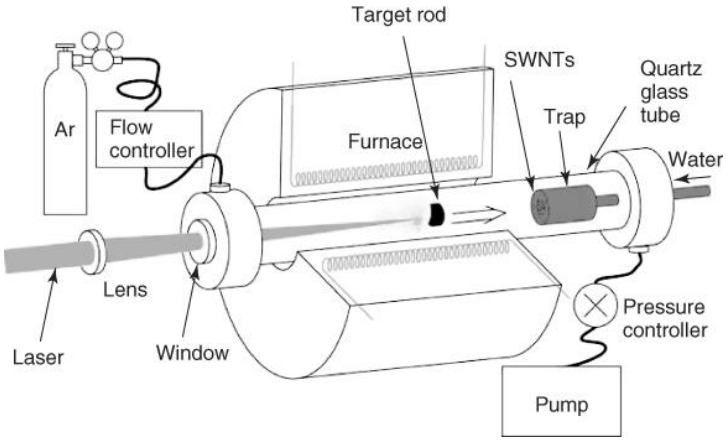

Figure 1.7 Schematic diagram of laser-assisted method for the growth of nanotubes [37].

1.4.3 Ball-milling and annealing

The arc-discharge [5] and laser ablation [36] methods give very little amount of boron nitride nanotubes. This is a two step method by which bulk amount of BNNTs is produced but with low purity. First step involves ball-milling of reactants at room temperature and in the second step the product obtained from ball milling is annealed at high temperature to obtain BNNTs [33, 38].

Boron powder is charged into a small stainless steel ball mill and ammonia gas is provided at a pressure of 300 kPa [23]. Boron powder is then milled for many hours in ammonia atmosphere. The energy from the impact of the balls helps to form a disordered metastable state of BN by reaction of B and ammonia. These impacts in ball milling also create nucleation sites which help in the growth of nanotubes in annealing step. The impact energy of the balls can be controlled by controlling the frequency of the rotating chamber [39]. The product from the ball milling is then annealed at 1000^{o}C-1300^{o}C under nitrogen gas atmosphere for few hours [38]. Ball milling and annealing method takes very long time as ball milling could go on up to 100 hours. Relatively large amount of product is obtained using this method but with a considerable amount of impurities [23].

1.4.4 CNT Substitution Reaction

In this method CNT is used as a template to grow BNNTs. The C-atoms in the tubular hexagonal carbon network is replaced by boron and nitrogen atoms. Nanowires or nanotubes are obtained by this method. Taking advantage of the structural similarities of CNTs and BNNTs Bondo's group in Japan synthesized BNNTs by substitution reaction method [40]. They covered B_2O_3 powder with carbon (MWNTs) and annealed the mixture at 1500^{o}C under nitrogen gas flow which resulted in the following substitution reaction.

B_2O_3 + 3C (CNTs) + N_2 ➔ 2BN (BNNTs) + 3CO

The melting temperature of B_2O_3 (450^oC) is low as compared to boron (2076^oC) and BN (2973^oC). So it can easily be vaporized and the vapor flow up and reacts with CNTs. The final product usually contains trace amount of carbon [6].

1.4.5 Chemical Vapor Deposition

Chemical Vapor Deposition (CVD) is another method of producing nanotubes. In the CVD method reactants in vapor phase are decomposed and reacted on heated substrate to form a layer or film of product. Unlike arc-discharge and laser-assisted methods, The CVD method uses thermal energy. Nowadays, CVD is widely used method for the production of both CNTs and BNNTs. Lourie et al. (2000) were the first researchers to use the CVD method for the BNNTs production [41]. In this method a boron source, sometimes mixed with catalyst, reacts with nitrogen source gas in a horizontal tubular furnace. Different groups of researchers have used different CVD methods and it has been found that the type of CVD method used has effect on the quality and quantity of the final product. The main difference between the CVD techniques is the type of materials used as precursors, temperature and experimental set-up [33]. Typical schematic diagram of CVD is given in Figure 1.8. Different researchers have used CVD method for the synthesis of BNNTs which are briefly explained below.

In the CVD method a boron source and a metal catalyst are used as a precursor sometimes no catalyst is used. The precursor is heated to a high temperature in the presence of catalyst. The nanotubes deposit on the surface of catalyst particle. If pure boron is used as a boron source alongside catalyst a reactive gas (like nitrogen) is necessary for reaction.

The CVD method was employed for the synthesis of BNNTs by Lourie et al. in which nickel boride was used as catalyst and Borazine ($B_3N_3H_6$) as precursor. Silicon wafer substrate and nickel boride catalyst were placed in a tube furnace and were heated up to 1000^oC-1100^oC. Borazine gas was passed through the furnace and the high

temperature leads to the decomposition of borazine into BN and H_2. BN defuses into the catalyst to form BNNTs and hydrogen gas leaves the system. Bulbous shaped nanotubes were produced with this method [41]. Formation of BNNTs on nickel boride catalyst is shown in Figure 1.9.

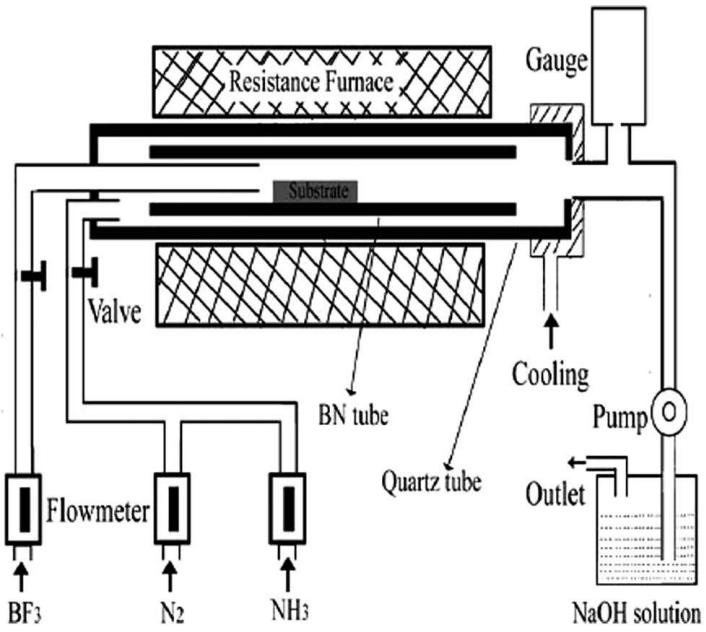

Figure 1.8 Typical CVD setup used for synthesis of boron nitride nanotubes [42]

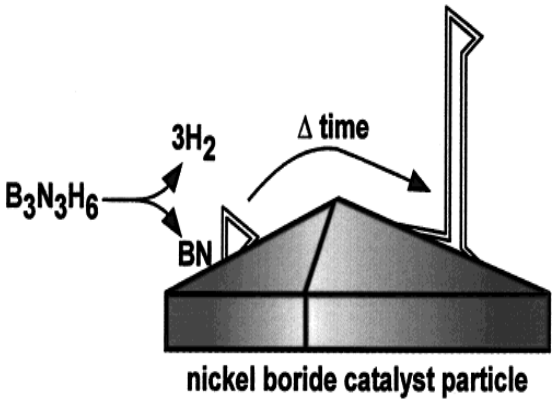

Figure 1.9 Schematic representation of BNNTs formation on nickel boride catalyst particle [41].

These setups for the CVD methods are usually same but sometimes a little change is made in the system according to the experimental requirements. The primary difference between the CVD methods is the type of precursor materials used, quantity and the experimental conditions like temperature, flow rate of gas etc. Some different kinds of CVD methods used by different researchers are discussed in this section.

A new CVD method was introduced by Lee at al. [43] for the production of BNNTs. This is the same method used earlier for the synthesis of CNTs [44]. Its schematic diagram is shown in Figure 1.10. Tube furnace made of quartz is used as reactor in this method. The starting materials are put into an alumina boat which is then placed in a quartz test tube. The quartz test tube is then placed inside the tube furnace. The furnace is heated to a reaction temperature and a reactive gas (NH_3 or N_2) is flown inside the furnace for few hours. The nanotube growth is observed on the substrate and inner wall of the alumina boat.

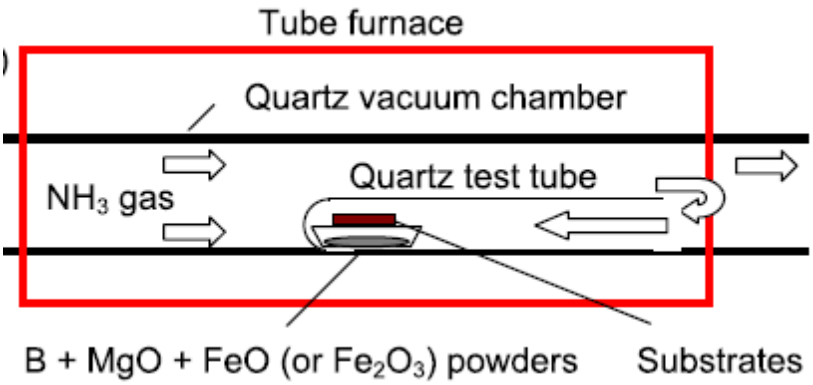

Figure 1.10 Schematic diagram of the tube furnace with quartz test tube inside [43].

Tang et al. (2002) used the CVD method for the synthesis of boron nitride nanotube. Induction furnace was used as a reactor with carbon free precursors. Boron, metal oxide catalyst and a nitrogen source gas were utilized. Boron reacts with metal oxide to form boron oxide which than reacts with nitrogen to form BNNTs [45]. Further

experiments showed that the weight ratios of boron to catalyst and temperature of the reaction has major role in quantity, quality and morphology of resulting BNNTs. BNNTs with up to 70 nm diameter and several micron in length were obtained using CVD [45, 46, 47].

Some other CVD methods are also employed by different research groups for the synthesis of boron nitride nanotubes [48, 49, 50, 51, 52].

All above CVD methods have shown that quality, quantity, morphology and size of BNNTs depend upon the type of materials used, temperature, weight ratios of starting materials and type of catalyst [33].

Non-catalytic CVD is the method in which no catalyst used in the starting material for BNNTs synthesis. The experimental setups for the catalytic and non catalytic CVD are almost same. The difference is only precursors used. A boron and nitrogen source is used as starting material.

Ma et al. (2001) obtained boron nitride nanotubes using the non-catalytic chemical vapor deposition. Melamine ($C_3N_6H_6$) and boric acid (H_3BO_3) were used as precursors in this method without catalyst. A solution mixture was formed of the starting materials which were then heated with nitrogen at high temperature. Multi-walled nanotubes were obtained [53].

1.5 Types of CVD reactors

Different types of CVD reactors are used for synthesis of nanotubes and they have almost the same system for reactant gas delivery, energy source, reactor purging, control equipments for temperature, flow and pressure. The main difference is design of a reactor chamber and substrate heating. Some types of CVD reactor that are presently used for synthesis of nanomaterials are discussed below.

1.5.1 Hot-wall CVD Reactor

Hot-wall CVD reactors are large reactors with several substrates for deposition inside the reactor chamber as shown in Figure 1.11. Several heaters are used to heat the walls and keep the temperature constant in every part of the reactor chamber. The problem in these reactors is that they need regular cleaning as the deposition occurs on both walls of the reactor and substrate. The unwanted layer of the contaminants on the walls of the reactor could result in high thermal loads.

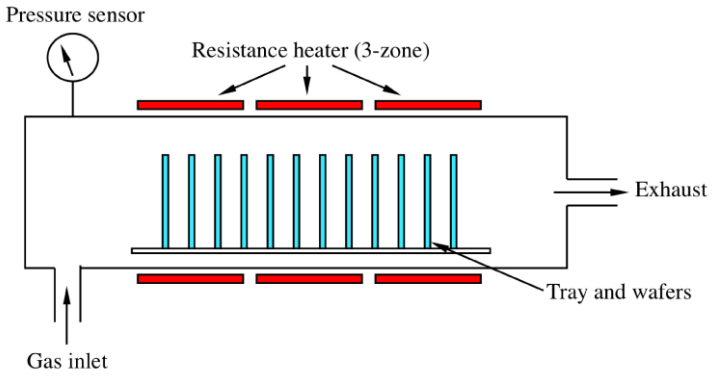

Figure 1.11 Hot-wall CVD reactor general design [54]

1.5.2 Cold-wall CVD reactor

In this type of CVD reactor only substrate is heated to reaction temperature and deposition occurs only on substrate. The walls of the reactor are kept cooled. Figure 1.12 shows general schematic presentation of the cold-wall reactor. The heating is done by induction or radiations. The advantage of cold-wall reactor is that no contaminant deposits on the wall of reactor due to low temperature. Due to cold-wall also there is no depletion of the gas reactants inside the reactor chamber. This type of reactor is mostly used for manufacturing of semiconductors for electronics. Hot-wall and cold-wall CVD reactors are also sometimes called thermal CVD reactors.

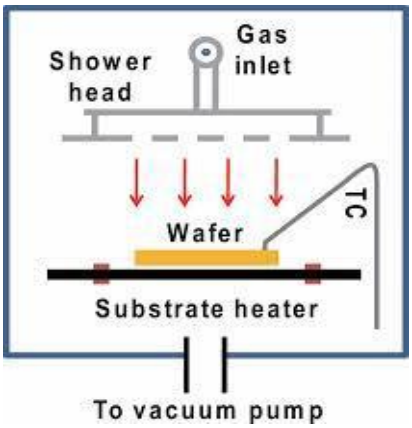

Figure 1.12 Cold-wall CVD reactor [55]

1.5.3 Plasma Enhanced CVD (PECVD) reactor

Plasma CVD reactor is shown in Figure 1.13. Partially ionized gas made up of ions and electrons is called plasma. In this type of reactor reaction occurs in plasma state at low temperatures compared to the temperature of thermal CVD reactors discussed previously. Due to low reaction temperatures (250^{o}C-350^{o}C) polymer can be used as a substrate in PECVD reactors. The wafer substrate acts as an electrode and magnetic drive is used to rotate the substrate. Gas reactants can be introduced from the center or from the sides in order to obtain uniform distribution as shown in Figure 1.13.

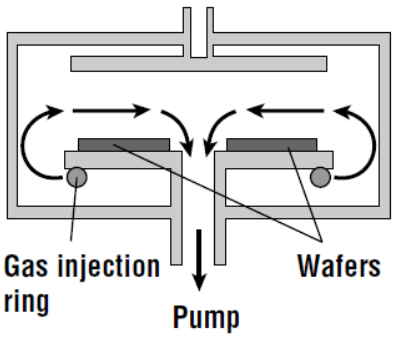

Figure 1.13 Plasma Enhanced CVD reactor [56]

1.5.4 Laser-assisted CVD (LCVD) reactor

These reactors are same in mechanism as thermal CVD reactors but here laser is used as heating source. Energy from the photons of laser is absorbed by reactants to decompose or dissociate and subsequently deposits on the substrate, this is called Photolytic LCVD. Another type of LCVD is Pyrolytic LCVD in which a portion of substrate is heated by laser and deposition occurs on that heated localized spot of the substrate.

1.6 Adsorption

This work is about the study of adsorption properties of BNNTs so in this section some theoretical background about adsorption of gases on solid surfaces is explained. By adsorption of gases on material information about surface of material, structure of material at very small level, porosity and surface active sites for catalytic activity can be obtained. Gas, vapor or liquid molecules may be attached to the surface of solid when it comes close sufficiently to the surface. The phenomenon of adhesion of atoms or molecules of gas or liquid to the surface of solid is called adsorption. There is always possibility of adsorption when gas or vapor interacts with the solid surface. The quantity of gas or vapor adsorbed by surface depends upon the temperature, pressure and interaction potential of gas (adsorbate) and the solid surface (adsorbent). There are two kinds of adsorption depending upon the interaction between vapor or gas and solid surface [57]. Using of BNNTs for different applications needs understanding of their physical and chemical adsorption properties.

a) Physical adsorption
b) Chemical adsorption

1.6.1 Physical adsorption

Physical adsorption also called physisorption, is a weak adsorbate-adsorbent interaction with relatively low heat of adsorption. It is a reversible phenomenon that occurs due to Van der Waal's forces. Physisorption occurs uniformly on the whole surface of adsorbent and is not restricted to specific active sites. That is why this technique is used to find the surface area of the porous powder materials. Unlike chemisorption, physisorption occur in multi-layers on the surface of adsorbent which also results in filling of pores. Physical adsorption occurs at low temperature and it does not occur at high temperatures. Due to no activation energy barrier equilibrium is attained quickly in physical adsorption. Sometimes diffusion in very small pores can limit the adsorption rate [57].

1.6.2 Adsorption Isotherms

Isotherm is a plot of amount (V) of gas or vapor adsorbed versus relative pressure (P/Po) at constant temperature. By visual analysis of isotherms the pore filling mechanism can be understood and information about the porosity of material was obtained. The shape of isotherm also depends upon the interaction between the adsorbate and adsorbent. Based on the research of Brunaur, Deming, Deming and Teller (BDDT) almost all the adsorption isotherms obtained resembles one of the five isotherms shown in Figure 1.14 [57].

1.6.2.1 Type I isotherm

This type of isotherm is obtained when few molecular layers of adsorption have occurred on the surface of the solid. Chemisorption usually gives type I isotherm. For physical adsorption type I isotherm is obtained when adsorption occurs in microporous materials. This type of adsorption occurs in micropores with size of few molecular

diameters (Size<2nm). Thus, the overlapping potential of the pore walls helps the adsorption to occur at very low relative pressure. When micropores filling is completed a plateau is obtained in the plot which shows very little or no adsorption anymore.

1.6.2.2 Type II isotherm

This type of isotherm is associated with adsorption on nonporous or material with pores larger than micropores. The knee called inflection point at the start of the curve indicates the completion of monolayer and start of multi-layers as the relative pressure increases.

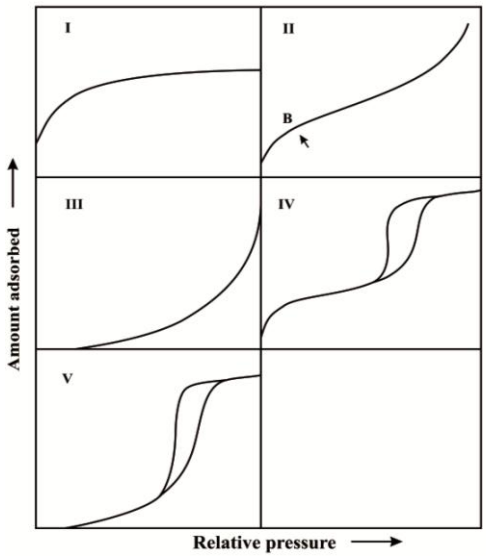

Figure 1.14 Types of adsorption isotherms [57].

1.6.2.3 Type III isotherm

Type III isotherm is obtained when the adsorbate-adsorbate interaction is stronger than the adsorbate-adsorbent interaction. This results in the multilayer adsorption because adsorbate sits on already formed adsorbate layer instead of adsorbent

surface. The gas molecules adsorb on the active sites and a cluster of adsorbate is formed on the favorable sites. So the adsorption is not uniform on the surface because in some areas multilayer adsorption occurs while on others adsorption does not occur at all. Because of this reason there is not clear distinction between the monolayer and multilayers and that is why the inflection point or the knee is absent in this type of isotherm.

1.6.2.4 Type IV isotherm

This type of adsorption is obtained usually when the adsorption occurs on the porous material with pore size range of 2 to 100 nm. As the relative pressure increases the slope of the curve also increases. Inflection point can be observed in type IV isotherm which suggests the completion of monolayer.

1.6.2.5 Type V isotherm

Type V isotherm is same like type III which is obtained when there is weak adsorbate-adsorbent interaction. Like type III isotherm, the inflection point is absent in this type of isotherm. But this isotherm also corresponds to adsorption in the pores of the same size range discussed in type IV isotherm.

1.6.3 Hysteresis

Sometimes adsorption and desorption branches of isotherm do not follow the same path which leads to the formation of hysteresis loop. The reason for formation of hysteresis loop is the fact that the condensation and evaporation mechanisms of gas in pores are different. The phenomena of the hysteresis occur in mesopore region with a pore size range of 2-50 nm. The hysteresis loop creates complexity in analysis but if

correctly interpreted it can give vital information about the pore structures and networks. Hysteresis loop is generally encountered between the relative pressure (P/Po) values of 0.3 to 0.96. In micropore region the adsorption and desorption curves of isotherm follow the same path so no hysteresis loop can be found below P/Po value 0.3 [57].

De Boer explained five kinds of hysteresis loops (Figure 1.15) which correspond to different shape of pores.

Type A hysteresis is obtained when adsorption-desorption occurs in cylindrical pores with both ends open

Type B hysteresis corresponds to slit or plate shaped pores. In the case of nanotubes when adsorption-desorption occurs between the walls of multi-walled nanotubes type B hysteresis is obtained.

Type C hysteresis can be found in open end tapered or wedge-shaped pores

Type D hysteresis is found in irregular pores; they are tapered or wedge shaped but with narrow opening at one or both ends.

Type E hysteresis loop is obtained for bottleneck pores. Evaporation in narrow region of the pore delays desorption in wide region. That is why a small slope is observed in desorption curve at high relative pressure and a large slope at low relative pressure. The large slope region indicates the emptying of wide portion of bottle neck pores.

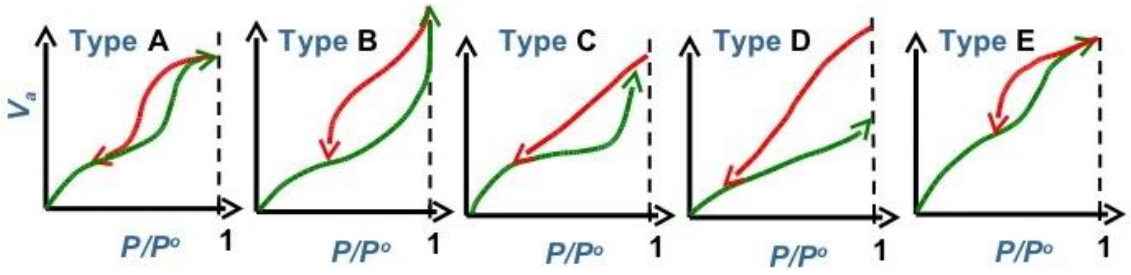

Figure 1.15 Five types of hysteresis loops identified by De Boer [57].

1.6.4 Characterization of porous materials by physical adsorption

1.6.4.1 BET surface area:

Brunauer, Emmett and Teller (BET) theory is base for measuring surface area of porous materials. Small pores (< 2nm) are filled by gas at very low relative pressure (P/Po) values. When these small pores are filled then single layer adsorption occurs on the surface of material and as the P/Po values increase multilayer adsorption starts. BET surface area is usually calculated between P/Po range of 0.05-0.3. Between these relative pressure values it is assumed that single layer adsorption occurs on the surface. Minimum three points are needed in this range to calculate BET surface area. In BET theory, it is also assumed that the surface is homogeneous, there is no lateral interaction between the adsorbed molecules and in multilayer adsorption the upper layer is in equilibrium with the vapor phase of the gas [57].

1.6.4.2 Pore size distribution

Pore distributions can be estimated using Barrett, Joyner and Halanda (BJH) method. BJH method uses Kelvin model for pore filling mechanism. Kelvin model (Kelvin equation) assumes pore condensation phenomena i.e. condensation occurs in pores that already have some layers of adsorbed gas on the walls of the pore. The thickness of that layer can be calculated from statistical thickness (t) equation (de Boer equation). BJH method is only valid for mesopores. Kelvin equation when nitrogen is adsorbing gas is given below [57]

$$r_K(\text{Å}) = \frac{4.15}{\log(P_0 / P)}$$

where r_k is Kelvin radius of pore. de Boer equation for calculating statistical thickness (t) using nitrogen as an adsorbate is given below

$$t(\text{Å}) = \left[\frac{13.99}{\log(P_0 / P) + 0.034} \right]^{1/2}$$

from Kelvin and de Boer equations pore radius (r_p) can be calculated as

$$r_p = r_k + t$$

Based on these equations BJH pore size distribution curves were obtained for BNNTs explained in chapter 4. IUPAC classification of pores according to their sizes is as follow [57]

- Micropore < 2nm in diameter
- 2< Mesopores < 50nm in diameter
- Macropore > 50nm in diameter

1.6.4.3 t-plots

t-plot method is used for estimating micropore volume and external surface area (S_{ext}) i.e. surface area except micropore area. t-plot is a plot of volume adsorbed (V_{ad}) versus statistical thickness calculated from de Boer equation explained earlier. The t-plot contains two linear regions i.e. upper and lower linear regions, generally for micro and mesoporous materials. The slope of upper linear (at high P/Po) region corresponds to external surface area and the intercept gives the micropore volume. The slope of lower linear (at low P/Po) region gives total surface area. So micropore surface area can be calculated from the difference of total and external surface area. [57].

1.6.4.4 H-K method for micropore analysis

Pore size distribution methods are mostly based on the assumption of capillary condensation phenomena which cannot be assumed for adsorption in micropore.

Horvath Kawazoe (H-K) method is generally used for pore size distribution of micropores with slit shape geometry. H-K method is extended by Saito and Foley (SF) for cylindrical pore geometry. H-K pore size distributions were obtained for BNNTs. For H-K method P/P_o values less than 0.02 are used [57].

1.6.4.5 D-R method

Dubinin-Radushkevich (D-R) method is used to calculate micropore volume of porous materials. D-R model gives a linear plot between log (V) and $[\log (Po/P)]^2$ for microporous materials. The linear range is found usually at relative pressure values less than 10^{-2} [57]. The characteristic D-R equation is given below

$$\log_{10} V = \log_{10}(V_0) - 2.303\left(\frac{RT}{\beta E_0}\right)^2 \log_{10}(P_0 / P)^2$$

1.6.5 Characterization of porous material by chemical adsorption

Chemical adsorption is a process where a molecule attaches to the surface through a formation of a chemical bond. Chemical adsorption is also called chemisorption and it is an irreversible adsorption. The heat of adsorption in chemical adsorption is relatively high sometimes even close to chemical bonding. It can occur at temperatures above the critical temperature of the adsorbate. Chemisorption is restricted to single molecular or atomic layer on the surface of adsorbent. In case of chemisorptions the adsorbed molecules did not cover the whole surface and they adsorb only on the active sites of surface. This is why chemisorption is a selective and localized phenomenon. Chemisorption is widely used technique to characterize a catalyst by measuring active metal sites on the surface of catalyst [57]. In our study BNNT chemisorption was performed using ammonia as a probe gas. The surface of material was saturated with adsorbed ammonia gas and then the gas was desorbed by gradual

increase of temperature. This method is called Temperature Programmed Desorption (TPD). The analysis showed us the total acidity of the surface of BNNTs. BNNTs can be potentially used as catalyst or catalyst support, so analysis is necessary for finding the catalytic properties of BNNTs.

CHAPTER 2

LITERATURE SURVEY

Since the discovery of carbon nanotubes (CNTs) [4], nanotubes have attracted a lot of research work in last two decades and while searching for the nanotubes of other materials, boron nitride nanotubes (BNNTs) were theoretically predicted in 1994 [18] and then experimentally prepared in 1995 [5]. The research on CNTs increased rapidly soon after their discovery but BNNTs did not get much attention. In recent years there has been an increase in research on BNNTs but it is still very less as compared to CNTs [50]. In Figure 2.1 number of publications related to CNTs and BNNTs from the year 1992 to 2006 is shown.

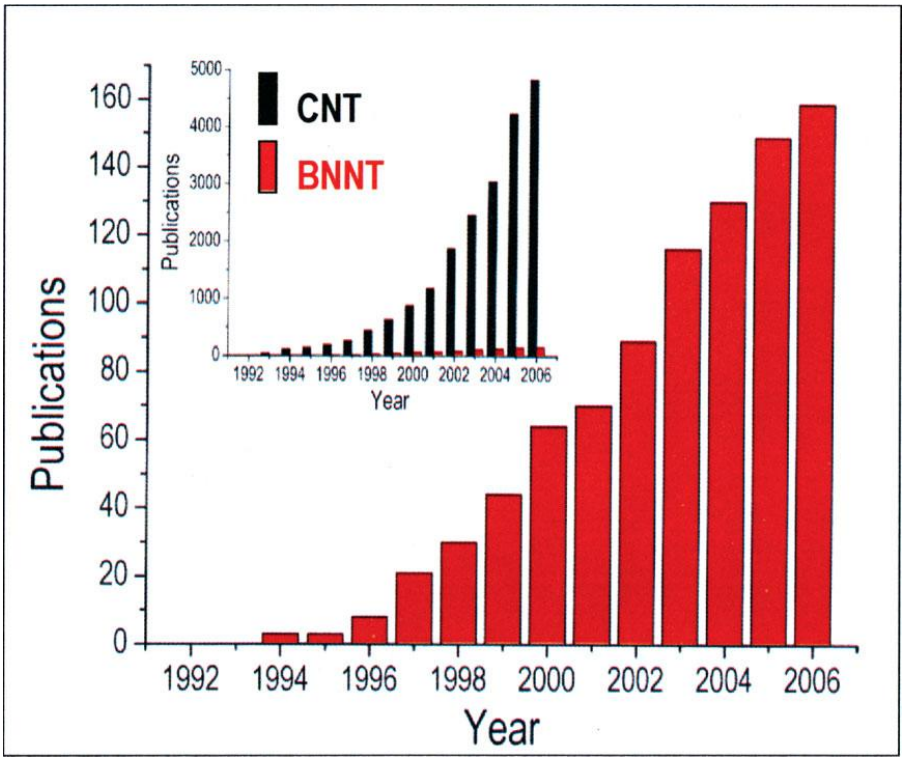

Figure 2.1 Articles published related to CNTs and BNNTs from 1992 to 2006 [50].

Chopra et al. were the first people to synthesize pure boron nitride nanotubes using the arc-discharge method. Tungsten anode packed with boron nitride (h-BN) and cool copper cathode were used. Electric arc was applied to the electrodes which raise the temperature up to 3700 K, subsequently BN was evaporated and pure BNNTs formed were carried by helium gas and collected on copper cathode. Multi-walled BNNTs with diameter in the range of 1-3 nm and length up to 200 nm were obtained. Electron energy loss spectroscopy showed almost B:N ratio of 1 which is same as predicted theoretically [5].

Loiseau et al. used a new route in the arc discharge method for BNNTs synthesis. In the arc-discharge method these electrodes should have at least some conductance and pure BN is not conductive so metal boride (HfB_2) was used in this study instead of h-BN. Stable electric arc of DC current and 20-40V voltage was maintained for 15 min. Nitrogen was used as a gas precursor and grey soot like product was obtained on the chamber walls. Mostly single and double-walled nanotubes were obtained. A unique morphology was observed at the end of some nanotubes which was closed by a flat layer perpendicular to the tube axis. Multi-walled nanotubes with reduced number of layers and inner diameter up to 4 nm were also observed. Some and single-walled nanotubes were also observed [34].

Ichihito et al. synthesized BNNTs using a arc-melting method. Yttrium (Y) had already shown excellent catalytic ability for the production of single-walled CNTs and that's why YB_6 powder was used as electrode in this study. YB_2 powder was placed on copper mold and the furnace chamber was evacuated. Then N_2/Ar mixture was introduced and the arc-melting was applied at voltage of 200V. Multi-walled BNNTs with a diameter in the range of 4-10 nm and length up to 6 microns were observed. This study showed that Y could act as a good catalyst for the formation of BNNTs. The EDX result showed B/N ratio of 1.1:1. It was also observed that conductive boride powder is a good precursor for BN nanotubes synthesized by arc-discharge and no additional material was needed to make it conductive [58].

Golberg et al. worked on the laser ablation method for the production of highly crystalline boron nitride nanotubes. Carbon dioxide laser was used to hit a cubic boron nitride target which raised the temperature up to 5000K. The experiment was carried out at high nitrogen pressure (5-15GPa). Multi-walled nanotubes were formed. BN nanotubes produced from the arc-discharge method usually contain metal particle at one end of nanotube but nanotube synthesized with laser method does not contains metal particles. Impurities in laser assisted methods were found to be amorphous boron and cones of BN. Laser method under nitrogen atmosphere opened new way of producing BN nanotubes and by optimizing different parameters like precursor materials, nitrogen pressure etc. it can replace the traditional arc-discharge method. Both c-BN and h-BN phases were found in final product. High nitrogen pressure has an effect on final product and favors the systematic growth of nanotubes [36].

Zhou et al. synthesized BNNTs using laser ablation method and studied the effect of catalyst on the structure and morphology of the final product. Target materials were pure boron nitride and a mixture of nanosized nickel and cobalt catalysts. Target materials were heated in quartz tube furnace and argon was flowed as a carrier gas. The target was then evaporated using a laser beam at 1200^{o}C and BNNTs were collected on the water cooled collector mounted inside the quartz tube. Boron nitride nanotubes produced with or without catalyst had different atomic structure, tube length and tip morphology. BN nanotubes produced using catalyst was found to be mostly single-walled and smooth outer tube surface. On other hand nanotubes produced without catalyst were multi-walled and their outer surface was rough. In this study it was also confirmed that BNNTs can be synthesized without catalyst using the laser ablation method [59].

Yu, D.P., et al. used a different laser ablation method with plate like target made of powder mixture of boron nitride and Ni/Co nanoparticles. Target was placed inside a tube furnace made of quartz and the furnace was evacuated. The laser was used to heat the target. The ablated target was taken by flowing gas and collected on cool copper collector inside the quartz tube. Argon and nitrogen were used as carrier gas. An

interesting feature was noticed in this method when argon was used as carrier gas mostly single-walled nanotubes were observed and when nitrogen was used multi-walled nanotubes with few layers were formed [60].

Weiqiang Han et al. used template synthesis method to produce BNNTs by CNT substitution reaction. In this method boron oxide (B_2O_3) powder was placed in graphite crucible and covered with carbon nanotube layer. CNTs were prepared through metal catalyzed CVD method. The crucible was placed in induction heating furnace and heated in the flow of nitrogen gas at 1773K for half an hour. When the reaction finished and crucible was taken from the furnace it was observed that the black color layer of CNTs was turned into a grey colored layer. Later characterization confirmed that the grey colored layer was indication of production of BNNTs. It was concluded from this study that the carbon atoms in CNTs were substituted by boron and nitrogen atoms. The average length and diameters of the BN nanotubes were found to be the same as CNTs used for substitution. No carbon impurity was found in the final product. By this method BNNTs of any quantity can be produced depending on the initial amount of CNTs and this is the advantage of this method as CNTs can be produced commercially. But still more understanding is needed for growth mechanism of BNNTs through substitution reaction method and it could help in producing BN nanotubes on mass scale [40].

Jun Dai et al. prepared boron nitride nanotubes at low temperature using mixture of Mg (BO_2).H_2O, NaN_3, NH_2Cl and Mg powder in a small sealed electric heated autoclave. The mixture was heated in autoclave for 60 hours at 600^oC. Typical multi-walled BNNTs with diameter in the range of 30 to 300 nm and length up to 5 microns were obtained. Most of nanotubes have one end close. The advantages of this method are the low cost and straight cylindrical nanotube in final material. Possibility of catalytic process was proposed but it was not clearly evident. This process also produces a lot of impurities in the final product and so as-synthesized materials need a thorough purification procedure [61].

Peiju Cai et al. used the same method used by Jun Dai et al. [56] but with different starting material for the synthesis of BNNTs. Boron powder, Fe_2O_3 and NH_4Cl were mixed and heated in an autoclave for 12 hours at 600^oC. Nitrogen was used as gas environment. Nanotubes were not produced without Fe_2O_3 which suggested that iron oxide had a role in the growth of BN nanotubes. Nanotubes with diameter up to 100 nm were produced [62].

Ying Chen et al. obtained BN nanotubes using a supplementary method of ball milling coupled with annealing after wards. Pure (98%) boron nitride (h-BN) powder was used as a starting material and placed in a lab scale ball mill with steel balls. The system was purge with nitrogen gas and the pressure was maintained at 300 kPa during milling. The milled product was then annealed at 1300^oC in nitrogen environment for 10 hours. BNNTs with inner and outer diameters of 3nm and 11nm were obtained, respectively. No nanotube was observed in the milled product and also there was no nanotube when unmilled BN was heated to the reaction temperature. So it was noted that ball milling played a great role in the formation of nanotubes and it was proposed that milling creates nucleation sites for nanotubes growth. The annealing temperature affects the rate of growth of the nanotube and best product was obtained at 1300 ^oC [38].

Ball milling and annealing method is used for the production of boron nitride nanotubes by Jun Yu et al. with in situ nitriding. Amorphous boron powder is milled under NH_3 environment in a ball mill. During milling nanosized boron nitride phases were formed due to the reaction of boron with ammonia gas under high impact energy of steel ball in mill. These nanosized BN phases acted as nucleation sites for BNNTs growth in annealing process after milling. Amorphous boron was milled for 150 hours and then annealed in tube furnace at 1200^oC for 8 hours. Nanotubes with less than 10 nm diameter and length up to several microns were synthesized in this study without using metal catalyst. The time and temperature of annealing were found to have great effect on the yield and crystallinity of the final product. Another advantage of balling milling and annealing method is that it gives large amount of product [63].

High yield of BNNTs was obtained by Chen et al. using ball milling and annealing process. Boron powder was milled in a lab scale ball mill with stainless steel balls under ammonia atmosphere at 300kPa. High mechanical energy due to impact of steel balls created structural and morphological changes in boron powder which lead to a high yield product after annealing. The annealing of as-milled product was done in nitrogen gas flow at 1200^{o}C for 16 hours. Under the same intensity of milling and heating temperature it was observed that the nanotube yield increased with an increase in milling time. The reason of this increase was the growth of nano-crystalline BN phases which acted as nucleation sites for nanotubes growth. Also milling increased the catalyst (Fe) particles in the mill product. Multi-walled bamboos like nanotubes were the result of the process used in this study. Increasing the milling time can significantly decrease the reaction temperature for the growth of nanotubes and prevents the formation of bulk BN clusters [64].

The first to use Chemical Vapor Deposition (CVD) method for the synthesis of boron nitride nanotubes were Lourie et al. Milled nickel boride (Ni_2B) catalyst was applied to a silicon wafer substrate and then placed in a tube furnace to heat up to 1100^{o}C. In situ prepared borazine ($B_3N_3H_6$) gas was flowed through the furnace for 30 minutes. Borazine was prepared by reacting $(NH_4)_2SO_4$ with $NaBH_4$ according to the following reaction.

$$3(NH_4)_2SO_4 + 6NaBH_4 \rightarrow 2B_3N_3H_6 + 3Na_2SO_4 + 18H_2$$

Bulbous nanotubes with root growth mechanism were obtained. Root growth is a mechanism in which nanotube extends from the ends where catalyst is connected. Almost all nanotubes were grown on the catalyst particles. Hollow and straight cylindrical nanotubes were obtained by this method [41].

Tang et al. produced BN nanotube from boron and magnesium oxide. Boron and magnesium oxide (MgO) mixture with molar ratio of 1:1 was heated in inducting furnace at 1300^{o}C. Boron reacted with MgO and formed vapors of B_2O_2 and Mg vapors. The B_2O_2 vapors were treated with ammonia gas in the reaction chamber at 1100^{o}C to

produce multi-walled boron nitride nanotubes. Vapors of Mg were carried away from the product area and thus a metal free product was obtained. Argon was used as carrier gas for transporting vapors into the reaction chamber. The synthesized nanotubes obtained were up to 70 nm in diameter and length up to 10 micrometers. Open and fractured end nanotubes were observed. The advantage of using MgO is that final product does not contains carbon and by product (Mg) can be easily removed [47].

BNNTs were obtained from the mixture of elemental boron and NiB/Al_2O_3 in the study undertaken by Tang et al. The mixture was ball milled for 8 hours. The mixture was placed in alumina boat and put into tube furnace. Argon gas was used to purge the system while heating the furnace up to reaction temperatures (1000^oC – 1500^oC). Then nitrogen or ammonia was flowed into the tube of furnace for 2 hours. Well crystallized boron nitride nanotubes with 5-30 nm diameter and several microns length were produced. Interlayer spacing of multi-walled nanotubes was found to be 0.33 nm. Bamboo like nanotubes were observed at high temperatures (1400^oC and 1500^oC). Nanotube formation was not observed below 1100^oC. Some agglomeration of catalyst was observed at high temperatures. No noticeable difference in the yield and morphology of nanotubes was observed when nitrogen or ammonia was used as reactant. Unique flat tips were observed for nanotubes less than 10 nm in diameter. Such characteristic was not observed in nanotubes with larger diameters [45].

C. Tang et al. prepared BNNTs using homogenized mixture of amorphous boron and iron oxide (Fe_2O_3) with balance ratio as starting materials. The powder mixture was loaded to alumina boat and boat was placed inside the alumina tube furnace. The furnace was heated and when the desired temperature (1200^oC to 1500^oC) was achieved then ammonia gas was allowed to flow through furnace. Temperature and B/Fe_2O_3 ratio has effect on the nanotube structure. Above 1300^oC flakes like grains of Fe and wool like BN aggregates were observed. Frequent bamboo like nanotubes were found when lower B/Fe_2O_3 ratio was used. Increasing temperature and amount of Fe_2O_3 reduces nanotube formation. It was found that in situ prepared Fe particles are responsible for the growth of nanotubes and Fe particles in nanoscale have greater catalytic activity as compared to

larger particles. BN nanotubes with diameter up to 20 nm were observed on High Resolution Transmission Electron Microscope (HRTEM) [46].

Lee et al. developed a new method for BNNTs production. A mixture of B, MgO, and FeO (or Fe_2O_3) was used as a starting material. The precursor mixture was placed in an one-end closed test tube and loaded into a quartz tube furnace. The quartz tube was evacuated up to 30 mTorr and heated to 1200^oC before the NH_3 flow. Ammonia gas was allowed to flow through the quartz tube while keeping the temperature at 1200^oC. The molar ratio of B:MgO:FeO was kept as 2:1:1. It was believed that BNNTs were formed due to reaction of BxOy vapor and NH_3 at this high temperature. The one-end closed test tube in the furnace was placed opposite to the flow of ammonia gas in order to avoid direct flow of gas through the reaction zone. It was observed that this set-up affected the yield of the nanotubes and low yield was obtained when the open end of test tube was faced directly to the flow of gas. Multi-walled nanotubes with diameter range of 10-100nm were observed [43].

Özmen et al. also studied the synthesis of BNNTs. Elemental boron and Fe_2O_3 were used as precursors and ammonia gas as nitrogen source. For the first time online mass spectroscopy was employed to analyze the reaction effluent gas. Mixture of boron and iron oxide with different weight ratios was loaded to alumina boat which was placed inside horizontal tubular furnace. Different reaction temperatures were used for BNNTs production. When desired reaction temperature was reached ammonia gas was fed to the reactor for 2 hours and 15 minutes. From online mass spectroscopy analysis it was observed that ammonia gas decomposed into nitrogen and oxygen. Nitrogen reacted with boron while the hydrogen gas produced from the decomposition of ammonia was released out of the system. In this study it was found that weight ratios of starting materials, reaction temperatures and flow rate of NH_3 play major role on the structure, crystallinity morphology, quality and quantity of the final product. The nanotubes obtained were mostly bamboo-line. At inlet gas composition of less than 60 mol% nanorods were obtained but above 60 mol% bamboo-like or hollow cylindrical nanotubes were observed. The outer diameters of nanotubes were in the range of 64 to

136 nm while the inner diameters were in the range of 7 to 38 nm. Type-II nitrogen isotherm with type-A and B hysteresis was obtained for the final purified material which showed the presence of both cylindrical and slit like pores. The amount of final material obtained through this method was relatively more as compared to other methods but the as-synthesized material contains considerable amount of impurities [65].

Selin Noyan produced BNNTs from the reaction of boron and iron powder mixture with NH_3 gas in tube furnace. Effluent gases from the furnace were analyzed by online mass spectroscopy. Agglomerated multi-walled nanotubes were obtained in the diameter range of 10-550 nm and interlayer spacing of 0.33 nm. Type II isotherm with type B hysteresis was observed in nitrogen sorption analysis. B/Fe weight ratio and reaction temperature found to have influenced the final product. Maximum BET surface area of BNNTs was 147.6 m^2/g which decreases with the increase in reaction temperature. The deposition rate of boron nitride was maximum at 1300^oC and 15/1 B/Fe weight ratio. In this study the as-synthesized product was treated with acids (HCl and HNO_3) in order to remove the impurities and unreacted materials from the sample [66].

Ma et al. synthesized BNNTs from two different starting materials without using metal catalyst, $B_4N_3O_2H$ and boron nitride powder and measured its hydrogen adsorption capacity at room temperature. The precursors were heated up to 2000K in N_2/NH_3 gas flow. The nanotubes prepared from $B_4N_3O_2H$ precursor were multi-walled cylindrical while from BN powder bamboo like nanotubes were obtained. TEM analysis showed that nanotubes with diameter range of 10 to 30 nm were synthesized. At the room temperature hydrogen capacity at 10 MPa was measured to be 1.8 and 2.6 wt% for multi-walled and bamboo like nanotubes, respectively. Still more researches are needed to improve the adsorption capacity of BNNTs at low pressure and room temperature [8].

Tang et al. obtained unexpectedly structurally collapsed boron nitride nanotubes from novel precursors, B_2O_2 and Mg vapors, using chemical vapor deposition. Relatively pure nanotubes with very high surface area were produced in this study. Due

to high surface area of collapsed nanotubes, hydrogen uptake capacity was found to be high (4 wt %) as compared to multi-walled nanotubes (1.8 wt %) measured by Ma et al. [25]. Nanotubes were prepared on platinum (and other noble metals like tungsten, molybdenum, niobium) plate. This might be considered to be the reason of the collapse structure because when nanotubes were synthesized on graphite plate no noticeable morphological change was observed. This type of BNNTs can prove to be a promising material for gas storage and as a catalyst support due to its very high surface area (789 m^2/g) [9].

Ferriera et al. studied production of BNNTs using novel precursors i.e. boron powder, ammonium nitrate and Fe_2O_3. The powder mixture was charged into alumina boat and heated in tube furnace at 550^oC for 1 hour without gas flow. Then, temperature was increased to 1300^oC and nitrogen was allowed to flow at 50 sccm. Ammonia gas was also introduced following one hour flow of nitrogen. The obtained nanotubes contained particles of metal catalyst. The nanotubes synthesized might be biocompatible for application in biomedical science. By functionalizing the BNNTs, it can be used for cell therapy, cancer treatment and other medical applications [67].

Seo et al. used a method to obtain large amount of BNNTs. In this method starting materials were first ball milled for 24 hours and then annealed at 1200^oC in tube furnace. Boron, MgO, FeO, NH_3, and nitrogen were used as precursors. Alumina boat, charged with precursors, and substrate were placed in one end closed test tube inside the furnace. Mixture of NH_3 (5 vol%) and N_2 (95 vol%) was flown through the furnace. Bamboo like and cylindrical nanotubes were obtained with greater quantity. There was some considerable amount of impurities in the as-synthesized product [68].

Ma et al. achieved synthesis of BN nanotubes using melamine diborate ($C_3N_6H_6.2H_3BO_3$) as precursor without the use of any metal catalyst. The precursor was first calcined for 3 hours in air at 500^oC and annealed in N_2 environment at 800^oC. A B-N-O intermediate was formed which was then heated in a graphite crucible in an induction furnace with flow of nitrogen for two hours at 1700^oC. A white product was

obtained on the wall of the crucible. Bulbous nanotubes were observed. Tip filled with amorphous precursor believed to have played the role of catalyst in the growth process of nanotubes [53].

Lee at al. performed functionalization of pure BNNTs with biocompatible PEGylated phospholipid [methoxy-poly(ethylene glycol)-1,2-distearoylsn- glycero-3-phosphoethanolamine-N conjugates (mPEG-DSPE)]. BNNTs were synthesized with CVD and then functionalized with PEGylated phospholipid in ultrasonic bed for various durations. It was found that the functionalized BNNTs could be kept suspended in water for several months. Noticeable thing was that after several hours of sonication length wise cutting of nanotubes might be achieved. This cutting ability combined with funtionalization of nanotubes could achieve well dispersion in polymer resin and can revolutionize the polymer nanocomposites field [10].

Ahmad et al. used a new method for BNNTs synthesis. Amorphous boron powder, MgO and ϒ-Fe_2O_3 nano-powder mixture was placed in alumina boat and boat was covered with silicon substrate. Alumina boat loaded in one end closed quartz test tube was placed in electrically heated tube furnace. The system was purge by argon gas and heated up to 1100^{o}C. NH_3 was introduced at 1100^{o}C and temperature was raised to 1200^{o}C. Ammonia flow was kept there for one hour after then the system was cooled. Multi-walled nanotubes with up to 57 nm diameter were observed in high resolution TEM. Purging system using argon gas instead of vacuum system has decreased the cost of experiments significantly as no extra accessories are needed. With economic effects, argon also affected the quality of final product and longer BNNTs were obtained [48].

Ma, R. et al [8] and Tang et al. [9] performed experiments to measure the hydrogen adsorption capacity of BNNTs but the results were not convincing. Hydrogen storage capacity was observed to be 2-3 wt% at high pressures but still very low at atmospheric pressure. Tang et al. found a novel morphology of BNNTs when they were synthesized in the presence of metals like tungsten, molybdenum, and niobium. Partially or fully collapsed boron nitride nanotubes were observed. This collapsed BNNTs were

found to have very high surface area (789 m^2/g) which might greatly enhance hydrogen storage capacity of BNNTs [9, 69].

3.1. Objectives of the study

From the literature survey it has been concluded that most of the study for BN nanotubes has been done on its synthesis methods, starting materials, reaction temperature and reaction time effecting the final product. Considerable share of research has been also focused on the effects of flow rates of source and carrier gases. There is also a rare study on the effect of temperature and starting materials on the structure and quantity of the final product. Almost no study has been done on the purification of the final product. The research is mostly focused on finding different ways to increase the amount of final product because very little amount of product can be produced using the present methods. They are investigating different precursors materials, operating temperatures, reaction time, and gas flow rates etc. There is very rare study in literature on the adsorption properties of boron nitride nanotubes and chemisorptions on BNNTs. Based on the literature survey following are the objectives of this study:

- To synthesize two different samples of boron nitride nanotubes using different compounds (Fe and Fe_2O_3) with ammonia and amorphous boron powder and same synthesis parameters
- To purify the as-synthesized product from impurities produced during synthesis
- To characterize the final products using XRD, FTIR, SEM, TEM, and TGA
- To compare the characterization results of two samples prepared from Fe and Fe_2O_3
- To investigate textural properties of BNNTs using nitrogen adsorption technique
- To investigate carbon dioxide adsorption on BNNTs
- To study NH_3 chemisorptions on boron nitride nanotubes

CHAPTER 3

EXPERIMENTAL

The objective of this work is to study the adsorption properties of boron nitride nanotubes. The experimental part of this study can be divided into three sections.

1) Synthesis of BNNTs
2) Purification of BNNTs
3) Studying adsorption properties and structural characterization of BNNTs

BNNTs were synthesized by the reaction of ammonia and boron and iron oxide or iron mixture at 1300^{o}C with an inlet ammonia flow rate of 125 cm^{3}/min and boron to iron oxide or iron ratio of 15/1 [65]. Synthesized product was then purified by acid treatment using nitric and hydrochloric acids. The method [65, 66] used for synthesis of BN nanotubes has advantage over other methods because it produces relatively high amount of final product. The starting materials used are easily available and can be used in different amount keeping the weight ratio constant to get. The final product contains impurities but it can easily be removed by acid treatment [66]. The structural, physical and adsorption properties of purified BNNTs were studied using different characterizing techniques like X-ray Diffraction (XRD), Scanning Electron microscopy (SEM), Energy dispersive X-ray spectroscopy (EDX), Transmission Electron Microscopy (TEM), Fourier Transform Infrared spectroscopy (FTIR), nitrogen and carbon dioxide adsorption and chemical adsorption analyses. Reproductivity of BN was also investigated using some of these characterization methods.

3.1 Synthesis of boron nitride nanotubes

3.1.1 Experimental setup

BNNTs were synthesized by the reaction of ammonia as a nitrogen source with the powder mixture of boron and iron or iron oxide in a horizontal tubular furnace (Protherm PTF 16/50/450). Figure 3.1 shows the experimental set-up. Argon gas (99.99% pure) was used to purge the system before and after the reaction. The reaction gas, ammonia (99.95% pure), and argon gases were connected to the system through ¼ inch stainless steel tubing. The flow rates of gases were adjusted using rotameters which were calibrated for these gases. A three way valve was installed after the ammonia rotameter in order to regulate the flow through a bypass line before entering into the tubular furnace. Soap bubble meters were used to measure the flow rates of gases at the inlet and outlet of the furnace. The powder mixture of boron and iron or iron oxide was loaded into alumina boat and the boat was placed in the centre of tubular furnace that has inner diameter of 5 cm and length of 1 m. Temperature inside the furnace was measured by a thermocouple which is connected to a temperature controller.

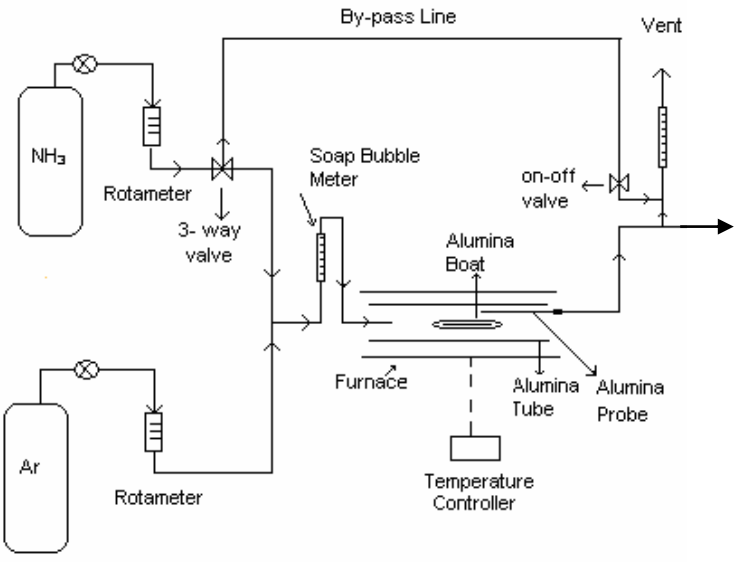

Figure 3.1 Experimental setup of BNNTs production [65]

3.1.2 Experimental procedure

0.8 g of thoroughly mixed and homogenized mixture of boron (Sigma-Aldrich) and iron (Merck) or iron oxide (Sigma-Aldrich) powder with a B/Fe or B/Fe_2O_3 ratio of 15/1 (boron; 0.75 g, Fe_2O_3 or Fe; 0.05 g) was loaded into alumina boat. Alumina boat was placed in the centre of the horizontal tubular furnace and the temperature was adjusted through the controller. The system was heated at a rate of 8^oC/min and argon gas was allowed to flow through the system at 2 bars and 150 cm^3/min. Argon gas was used to purge oxygen from the whole system. When the temperature inside the furnace (Figure 3.2) reached 1200^oC then ammonia was fed to the bypass line using three way valve. This had been done to stabilize and adjust the flow of gas to the desired value before the reaction started as the flow rate of ammonia played important role in the reaction. When the temperature reached to 1300^oC the argon flow was shut off and ammonia was fed in to the furnace at a rate of 125 cm^3/min for 2 hours and 15 minutes. After the completion of reaction time ammonia flow was closed and argon was fed again into the furnace with the same flow rate. The reactor was cooled down at a rate of 5^oC/min and the as-synthesized product was taken from the reactor and weighed. Experimental conditions are given in Table 3.1. These are the optimum experimental conditions deduced from the previous studies of our group [32, 65, 66,] studies which showed that the best and highest amount of product was obtained at these conditions.

Figure 3.2 Horizontal tubular furnace (50 mm diameter, length 1m)

The synthesized materials were named as X-BN-Y-Z where X stands for either purified (P) or unpurified (UP) samples and BN for boron nitride. Y stands for the precursor materials either metal oxide (MO:Fe_2O_3) or metal (M:Fe) from which samples were synthesized. Z represents the number of material synthesized at the same conditions but at different times. The names of samples used in this study are given in Table 3.2. To check the reproducibility of BNNTs production method the material was synthesized at different times and the same conditions.

Table 3.1 Materials and experimental conditions used in the synthesis of BNNTs

Reaction temperature (^oC)	**Reaction time (min)**	**Ammonia flow rate cm^3/min**	**B/Fe_2O_3 weight ratio**	**B/Fe weight ratio**	**Boron and iron oxide source**	**Iron source**
1300	135	125	15/1	15/1	Sigma-Aldrich	Merck

3.2 Purification of as-synthesized Boron Nitride Nanotubes

The as-synthesized BNNTs contain impurities and unreacted materials so the sample was purified using acid treatment (HCl and HNO_3). The purification method used in this study is the same as used in the study of Selin Noyan [66] but with few modifications. Steps that involve in the purification process are as follow.

1.3g of as-synthesized sample was weighed and put into the flask. 25 ml of deionized water was added and the material was sonicated in ultrasonic bath for 2 hours. After sonication 25 ml of HNO_3 was added and the sample in the flask was thoroughly mixed by magnetic stirrer. Again 25 ml of both deionized water and HNO_3 was added and mixed. The solution was then filtered with filter paper. This process is repeated five times in order to remove the unreacted boron completely.

Table 3.2 Names and codes of samples synthesized with the same experimental conditions [65, 66,]

Sample code	Sample Name	Starting materials
SK070714	P-BN-MO-1	Fe_2O_3
SK120814	P-BN-MO-2	Fe_2O_3
SK270814	P-BN-MO-3	Fe_2O_3
SK-3	P-BN-MO-4	Fe_2O_3
SK240714	P-BN-MO-5	Fe_2O_3
Sk230614	P-BN-MO-6	Fe_2O_3
SK300814	P-BN-M-1	Fe
SK020914	P-BN-M-2	Fe
SK-2	P-BN-M-3	Fe
SK271014	UP-BN-M	Fe
CD250310	UP-BN-MO	Fe_2O_3

The material retained on filter paper was poured into 250 ml of deionized water. For removal of iron particles, 20 ml of HCl (37%, Merck) was poured into this solution and its color turned into yellow which is the indication of the presence of elemental iron particles. Then, 10 ml of HNO_3 was added and the solution was heated for 3 hours. During 3 hours of heating Fe reacted with HCl and HNO_3.

After 3 hours of boiling the solution was cooled and filtered. The white solid on the filter paper was purified BNNTs which were then dried at 105^{o}C for 2hours.

3.3 Characterization of BNNTs

Morphological, chemical, surface and adsorption properties of BNNTs were studied using different characterization and adsorption techniques. X-ray Diffraction (XRD) was used to study the crystalline structure and surface morphology was studied using Scanning Electron Microscopy (SEM). Transmission Electron Microscopy (TEM) was used to determine the detail structure of individual nanotube. Chemical composition study was done using Fourier Transform Infrared (FTIR). Energy Dispersive X-ray (EDX) spectroscopy was performed during SEM analysis for finding the elemental composition in the respective image. Nitrogen and carbon dioxide adsorption techniques were used to determine the surface properties like surface area, pore size distribution, total pore volume, micropore volume and other adsorption properties. Chemical adsorption analysis was also performed for BNNTs in order to determine the active sites on the surface.

3.3.1 X-ray Diffraction

X-ray diffraction was used to determine the crystallinity of both the as-synthesized and purified samples. The equipment used for analysis was Rigaku X-ray Diffractometer with CuK_{α} as radiation source and scanning speed of 2^{o}/min. The data was obtained at the Bragg's angle range of 5^{o}-90^{o}. The analysis was performed at voltage 40 kV and current 40 mA.

3.3.2 Fourier Transform Infrared (FTIR) Spectroscopy

Qualitative chemical analysis of the as-synthesized and pure samples was performed using Fourier Transform Infrared Spectroscopy. The sample to be used for analysis was first dried at 110^{o}C and then prepared by mixing with Potassium Bromide (KBr) powder. Approximately 1 mg of sample was well mixed with 100 mg of KBr powder for FTIR analysis. The analysis was done at room temperature. The equipment used in the process was Bruker VERTEX 70 series shown in Figure 3.3.

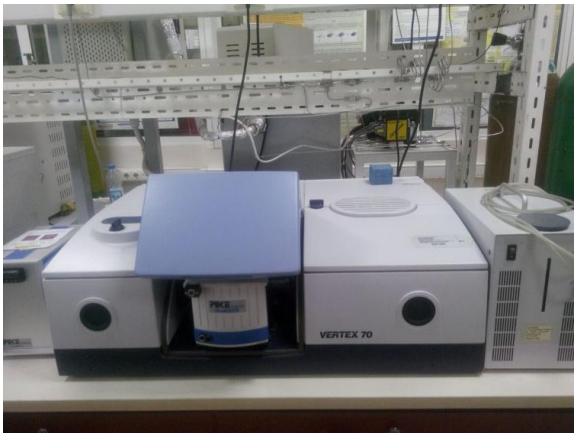

Figure 3.3 FTIR equipment (Brucker Vertex 70)

3.3.3 Scanning Electron Microscopy (SEM) and Energy Dispersive X-ray (EDX) spectroscopy

Surface morphology of the as-synthesized and purified boron nitride nanotubes was studied using SEM. EDX spectroscopy was used to determine the elemental analysis of BNNTs. A small amount of sample was placed on conductive carbon tape and was coated with gold-palladium alloy to make it conductive for analysis. The SEM equipment used for morphological analysis was 30 kV FEI Quanta 400 scanning electron microscope.

3.3.4 Thermogravimetric Analysis (TGA)

Thermogravimetric analysis was performed for the purified product under nitrogen gas flow and air in order to show its oxidation resistance. The experiment was performed from ambient temperature to 900^{o}C with a heating rate of 20^{o}C/min. The air and nitrogen flow rates were 100 ml/min. The model of the TGA equipment used in this study was DTG-60H simultaneous DTA-TGA, SHIMADZU, Japan.

3.3.5 Transmission Electron Microscopy (TEM)

Transmission electron microscopy was used to study the detail structure of different individual nanotubes. Different structural nanotubes were observed in details. For analysis the samples were poured into ethanol and sonicated in ultrasonic bath for 15 minutes. Then, a drop of ethanol solution containing BNNTs was placed on the copper grid (400 square Mesh) coated with carbon. 120 kV FEI Tecnai Transmission Electron Microscope was used in this study.

3.3.6 Nitrogen sorption

To investigate the textural properties of the material nitrogen gas sorption method was employed. Using nitrogen adsorption/desorption isotherms multipoint BET (Brunauer-Emmett-Teller) surface area, pore size distribution, total pore volume etc. were determined for both unpurified and purified samples. BET surface area was calculated (Appendix D) between the relative pressure (P/P_o) range of 0.05-0.30. The total volume adsorbed by the sample was determined at P/P_o value of 0.98. The volume at P/P_o value of 0.02 was the volume adsorbed in only micropores while at 0.96 P/P_o the mesopores volume was obtained. BJH pore size distribution was obtained between P/P_o values of 0.40-0.96. The instrument used in the analysis was Micromeritics TRISTAR II shown in Figure 3.4. The samples were pretreated before the analysis, first dried

overnight at 110^{o}C and then degassed for 3 hours at 300^{o}C in order to remove any moisture or entrapped gasses in the material. The measurements were carried out at liquid nitrogen temperature (77K)

Figure 3.4 Micromeritics surface area and porosity measurement equipment

3.3.7 Carbon dioxide adsorption

Carbon dioxide adsorption was performed for the samples in order to study the micropore volume and micropore surface area. The samples were dried overnight at 110^{o}C and then degassed at 300^{o}C for 3 hours before using for the adsorption analysis. The measurements were carried out at 0^{o}C. The average amount of sample used for analysis was 0.05g. Adsorption isotherm was obtained up to 0.30 relative pressure value.

The instrument used was Autosorb-6 from Quantachrome Corporation (Autosorb 1C) shown in Figure 3.5.

Figure 3.5 Autosorb-6 Quantachrome

3.3.8 Chemical adsorption

Chemical adsorption analysis was performed for purified BNNTs in order to get information about the surface acidity of sample. Temperature Programmed Desorption (TPD) was performed using ammonia as probe molecule.

Firstly, the sample was degassed at 300^{o}C for one hour under helium gas flow at 300 ml/min. Then, the sample was cooled down to 45^{o}C and sample was saturated with NH_3 gas. The flow rate of ammonia was kept at 30 ml/min. Ammonia supply was stooped after one hour and again helium gas was allowed to flow through sample for one hour in order to remove any physisorbed gas from the sample. Finally sample was heated to 800^{o}C with a heating rate of 20^{o}C/min under 30 ml/min flow of helium. A TPD profile was obtained.

The equipment used for analysis was Micromeritics AutiChem II chemisorption analyzer.

3.3.9 Solid density measurement

Skeletal density of powder product was calculated (Appendix F) using gas pycnometer technique. A gas pycnometer detects change in pressure from the displacement of gas by solid material. Helium gas was used as displacement fluid in the equipment. Also, its behavior as an ideal gas was desirable. The amount of sample used was approximately 0.05g. The equipment used in density analysis was Micromeritics Multivolume pycnometer 1305. Figure 3.6 shows the general schematic drawing and picture of the gas pycnometer.

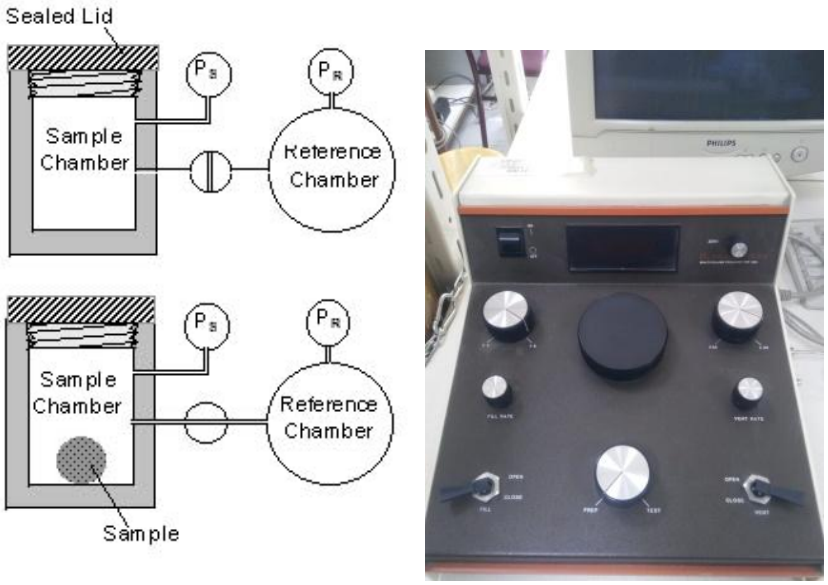

Figure 3.6 General schematic drawing (a) and picture (b) of the gas expansion pycnometer [70]

CHAPTER 4

RESULTS AND DISCUSSION

In this study, boron nitride nanotubes were synthesized and their properties were studied. Powder mixture of amorphous boron and Fe or Fe_2O_3 with ammonia gas was used as reactant for synthesis of boron nitride nanotubes. Ammonia gas was used as a source of nitrogen. Boron to iron oxide or iron weight ratio was kept at 15/1 as previously shown that this ratio gives the best product [65, 66]. The temperature of the reaction was 1300 ^{o}C for 135 minutes with ammonia flow rate of 125 sccm. The amount of reactants (B and iron oxide or iron) used was 0.8 g while the average amount of as-synthesized product obtained was 1.3 g. 1.3 g of as-synthesized product was purified and after purification the average amount of final product left was approximately 0.72g which shows 45 % decrease from the initial amount. The percent yield obtained was 96 % for both purified products synthesized from iron oxide and iron precursors. Yield was calculated from the ratio of purified material weight to boron weight used in reaction. This decrease was due to the removal of impurities and unreacted reactants. The color of the as-synthesized product was mostly grayish with some white color but after purification the color of the material was white. The as-synthesized and pure products were characterized using XRD, FTIR, EDX, SEM, TEM and TGA. Textural properties like BET surface area, pore size distribution, pore volume etc. were analyzed using nitrogen adsorption.

4.1 Characterization of synthesized boron nitride

4.1.1 X-ray Diffraction Patterns

X-ray diffraction patterns of synthesized materials were obtained to get information about crystal structure. XRD patterns of both purified and unpurified product were obtained and compared. The XRD pattern of these samples were given in Appendix A.

XRD patterns of good representive of purified products synthesized from iron oxide and iron are shown in Figure 4.1. The peaks at the Bragg angle 26.4^o, 41.9^o, 43.0^o, 50.1^o, 54.3^o, 76.1^o and 82^o (Figure 4.1a) belong to hexagonal boron nitride while the peaks at 26.7^o, 42.6^o, and 75.9^o are assigned to rhombohedral boron nitride. The small peaks at 44.5^o, 65.2^o, and 77.3^o reveal the presence of cubic iron. d-spacing values of hexagonal boron nitride, rhombohedral boron nitride and cubic iron are given in Appendix A.

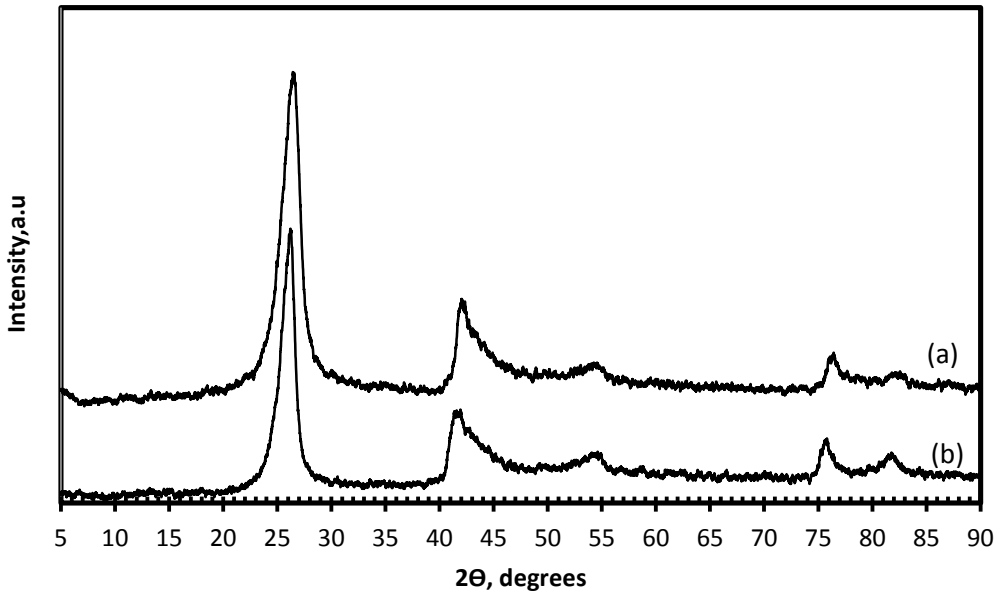

Figure 4.1 X-ray diffraction patterns of purified material synthesized at 1300^{o}C using iron oxide (P-BN-MO-2) (a) and iron (P-BN-M-3) (b)

XRD pattern of purified material synthesized using iron (Figure 4.1b) also shows the presence of hexagonal and rhombohedral boron nitride phases. The XRD pattern of synthesized material were consistent with the XRD patterns of BN in the literature [61, 65, 66]. The effect of using metal oxide or metal in the synthesis of BN was not observed in the XRD patterns.

Figure 4.2 shows comparison between the XRD patterns of the purified product synthesized with same condition using iron oxide (a-d) and iron (e-f). All XRD patterns are same and consistent with the literature and those XRD patterns show reproducibility of the material by the method used in this study. Some additional peaks were observed in the samples shown in Figure 4.2 which were not present in XRD patterns of samples shown in Figure 4.1. They correspond to some impurities in the material. These additional peaks at Bragg angle 44.5^{o}, 65.2^{o}, 78.1^{o} in (Figure 4.2a) corresponds to cubic iron despite the fact that no elemental iron was used in synthesis of this sample but the presence of this peak is because of a reaction proposed by Özmen et al. [65] between iron oxide and boron. Reactions are as follow:

$$2NH_3\,(g) \longleftrightarrow 3H_2(g)+N_2(g) \qquad (4.1)$$

$$(1+x+y)\,B(s) +(1+x)/2\,Fe_2O_3 \longrightarrow Fe(s) +Fe_xB_y\,(s) +(1+x)/2\,B_2O_3\,(s) \qquad (4.2)$$

$$yN_2+2Fe_xB_y(s) \longrightarrow 2y\,BN(s) + 2xFe\,(s) \qquad (4.3)$$

Due to the use of iron as a starting material the iron peak is obvious to be observed in the XRD patterns (Figure 4.2). the following reactions [66] take place in the synthesis of BN from iron.

$$2\,NH_3\,(g) \leftrightarrow\ 3H_2\,(g) + N_2\,(g) \qquad (4.4)$$

$$y\,B\,(s) + x\,Fe\,(s) \rightarrow Fe_xB_y\,(s) \qquad (4.5)$$

$$Fe_xB_y\,(s) + y/2\,N_2\,(g) \rightarrow y\,BN\,(s) + x\,Fe\,(s) \qquad (4.6)$$

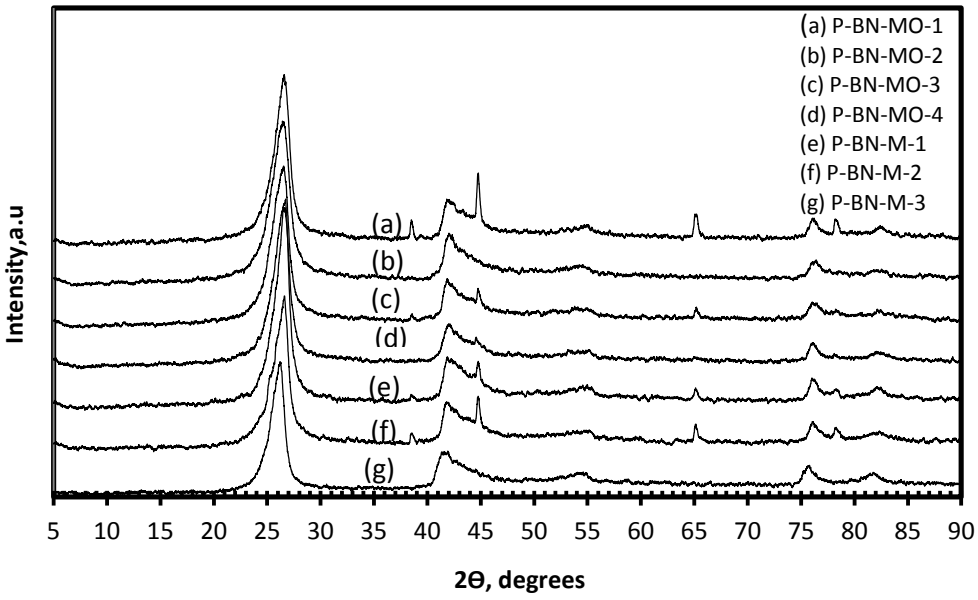

Figure 4.2 X-ray diffraction patterns of purified material synthesized from boron and iron oxide (a,b,c,d) or iron (e,f,g) synthesized under same conditions.

So based on reactions 4.2 and 4.3 Fe is produced and its peak can be observed in some samples synthesized using Fe_2O_3. The peak at 2θ value of 38.5^o belongs to iron boron compound (FeB_{49}) in Figure 4.2 a and this peak can also be found in the XRD pattern of some other samples in Figure 4.2 c, e and f. The iron peak in Figures 4.2 e and f is obvious that iron was used as reactant material for the synthesis of BN. In Figure 4.2 e peaks at 2θ values 44.5^o, 65.2^o, and 78.1^o corresponds to cubic iron.

Presence of iron boron compounds and cubic iron peaks in some of the XRD patterns is the evidence of some impurities remaining in the sample while the synthesized materials in Figures 4.2 b and g are well purified as no extra peaks other than hexagonal and rhombohedral boron nitride can be observed. This might be due to insufficient purification cycle. In other words those samples need more purification cycle. The iron particles may be embedded in the agglomerated areas which were difficult to remove. Probably by increasing the sonication time these entanglements and agglomeration can be reduced which could eventually help to remove the iron impurities from the synthesized materials.

XRD results showed that the final product is mainly composed of hexagonal and with some rhombohedral boron nitride and impurities like cubic iron and iron boron compounds. The starting material has almost no effect on final product.

XRD patterns of purified and unpurified (as-synthesized) samples were compared in Figures 4.3 and 4.4; it was observed that the intensities of the peaks for unpurified samples were very small compared to the peak intensities of purified material. This difference in intensity of peaks was observed in XRD patterns of both samples synthesized from Fe_2O_3 and Fe. This increase in XRD peak intensities suggested the removal of amorphous impurities after the acid purification process. Before purification there were a lot of amorphous boron and impurities in the as-synthesized material and they were removed after purification.

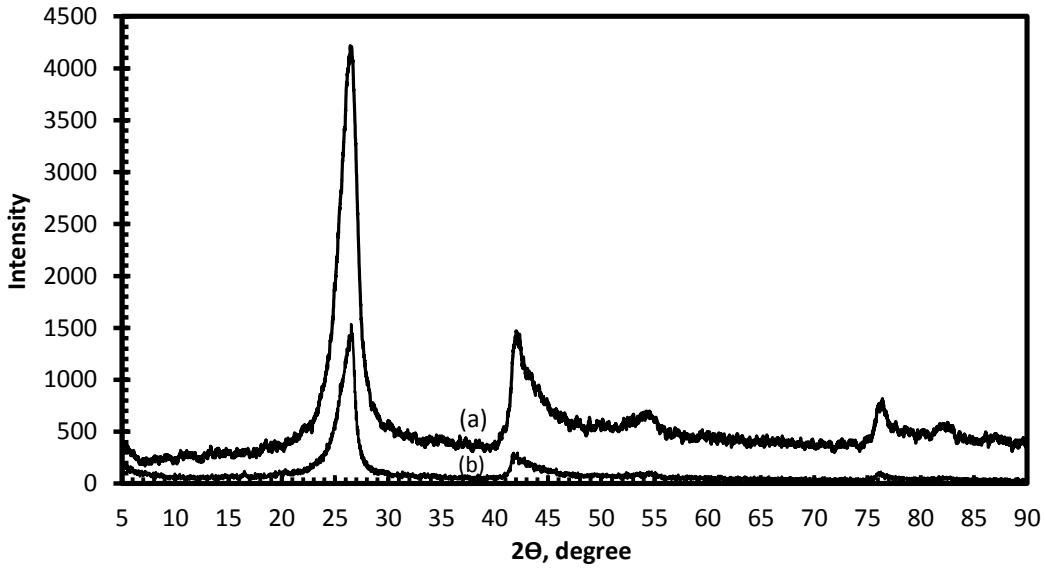

Figure 4.3 XRD patterns of (a) purified and (b) unpurified material synthesized using iron oxide.

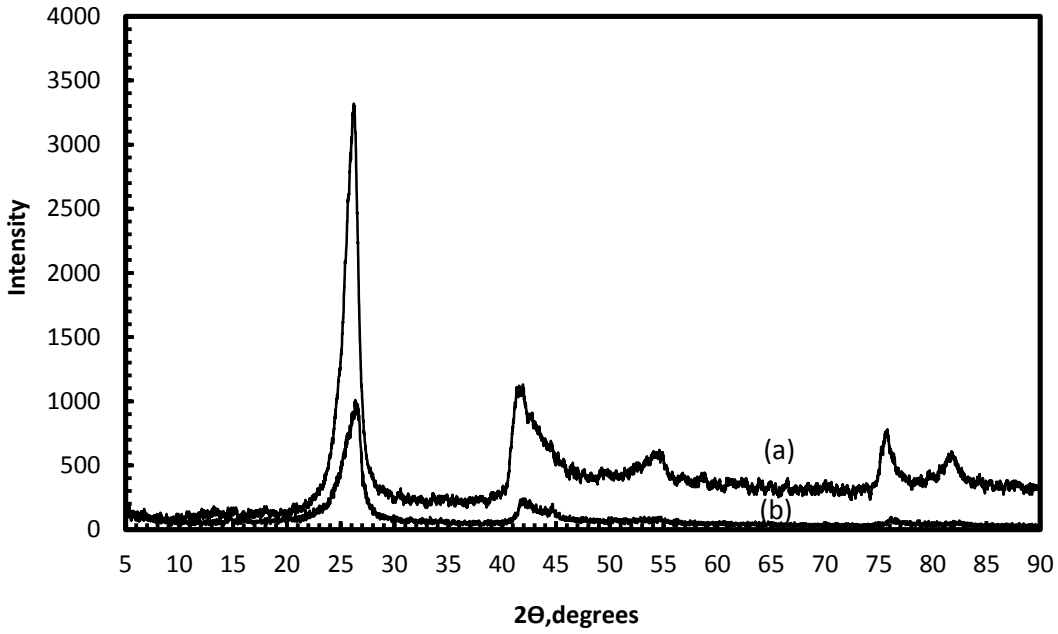

Figure 4.4 XRD patterns of (a) purified and (b) unpurified material synthesized using iron.

4.1.2 Fourier Transform Infrared (FTIR) spectroscopy

For chemical analysis of synthesized material Fourier Transform Infrared Spectroscopy was performed.

Figure 4.5 shows the FTIR spectra representive for purified materials synthesized using iron oxide and iron. The spectra in Figure 4.5 are consistent with the spectra in the literature for boron nitride [11, 61, 62, and 65]. The two strong peaks at 1379 cm^{-1} and 815 cm^{-1} are ascribed to characteristic adsorption peak of BN. The peak at 1379 cm^{-1} can be assigned to in-plane B-N stretching vibrations while the peaks at 815 cm^{-1} can be assigned to out of plane B-N-B bending vibrations. The small broad peak near 2300 cm^{-1} can be ascribed to boron. However, boron peaks were not observed in XRD patterns (Figures 4.1-4.4) because amorphous boron was used in this study. Another

characteristic peak was observed at 3200 cm^{-1} which belong to water absorbed on the sample. The characteristic peak observed between 3400-3500 cm^{-1} belongs to N-H stretching vibration. This might came from raw material used or formed during purification step.

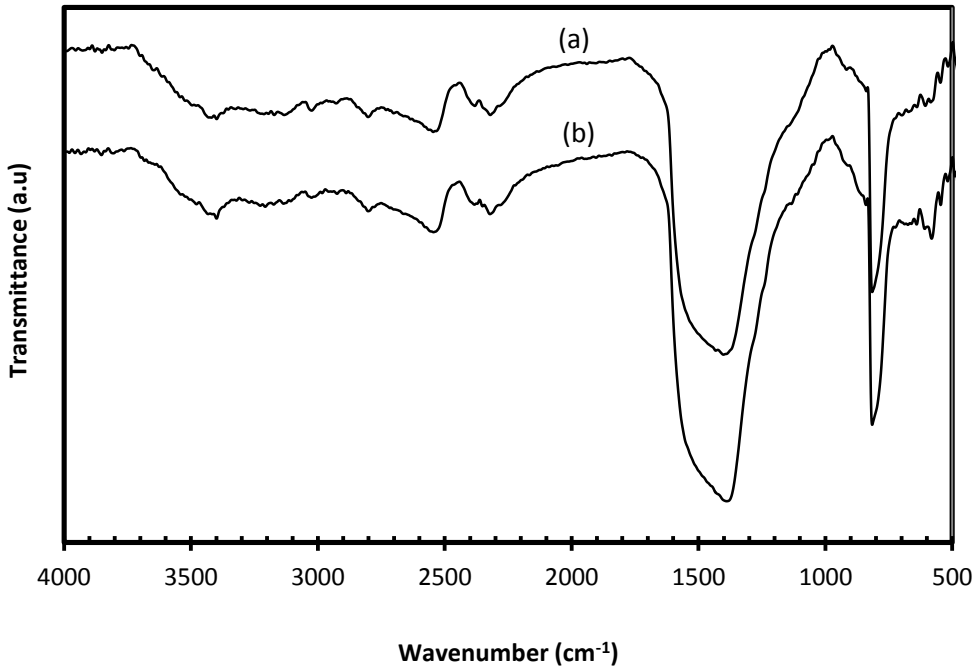

Figure 4.5 FTIR spectra of purified boron nitride synthesized using iron (P- BN-M-2) (a) and iron oxide (P-BN-MO-5) (b)

These peaks were also found in the FTIR spectra of unpurified material (Figure 4.6). So it suggested that these samples are not fully purified. A small peak was observed in Figure 4.5b at wave number 590 cm^{-1} which was assigned to iron oxide.

Figure 4.6 shows the FTIR spectra of unpurified and purified materials synthesized from iron and iron oxide. In all spectra obtained at different times characteristic peaks for BN was observed near 1379 cm^{-1} and 815 cm^{-1}. The spectra in Figure 4.6a and 4.6d showed characteristic peaks in region of 3400-3500 cm^{-1} which

were assigned to N-H stretching vibration. Small peaks were observed in Figure 4.6d and e at wave number 545 cm^{-1} which were assigned to unreacted iron oxide. Spectra in Figure 4.6a and 4.6d correspond to unpurified or as-synthesized material synthesized using iron and iron oxide, respectively while spectra in Figures 4.6 b, c and e belong to purified material. FTIR results are almost consistent with XRD results and same spectra observed for samples produced at different times.

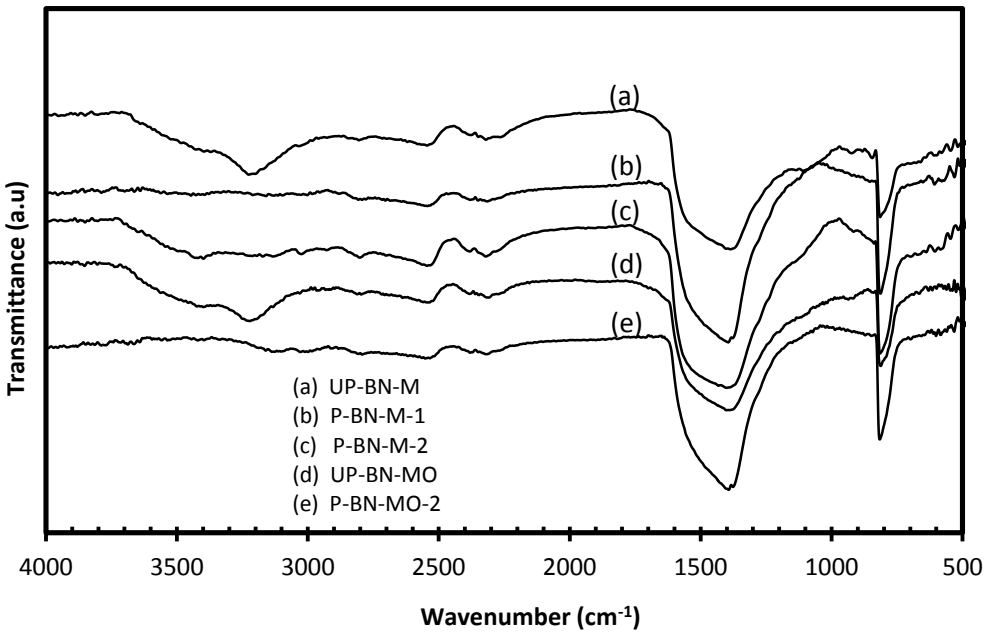

Figure 4.6 FTIR spectra of purified and unpurified BN synthesized using iron and iron oxide.

The FTIR spectra of purified materials were almost the same which was because of the reproducibility of the material by method used in this study. This reproducibility can also be observed previously in the XRD results (Figure 4.1-4.4).

4.1.3 Energy Dispersive X-ray (EDX) spectroscopy

EDX spectroscopy was performed for the synthesized material in order to get information about the elements present in the samples. Figure 4.7 shows EDX spectrum

of sample produced using Fe_2O_3. Clear peaks of boron and nitrogen can be observed in the spectrum confirming that the sample is boron nitride. The gold peaks are due to the conductive coating on the sample applied in pretreatment for analysis. The carbon peak is due to the carbon tape on which the sample was placed for the analysis. Oxygen peak may be assigned to the oxygen adsorption on the surface of the material from atmosphere or the presence of boron oxide in the material.

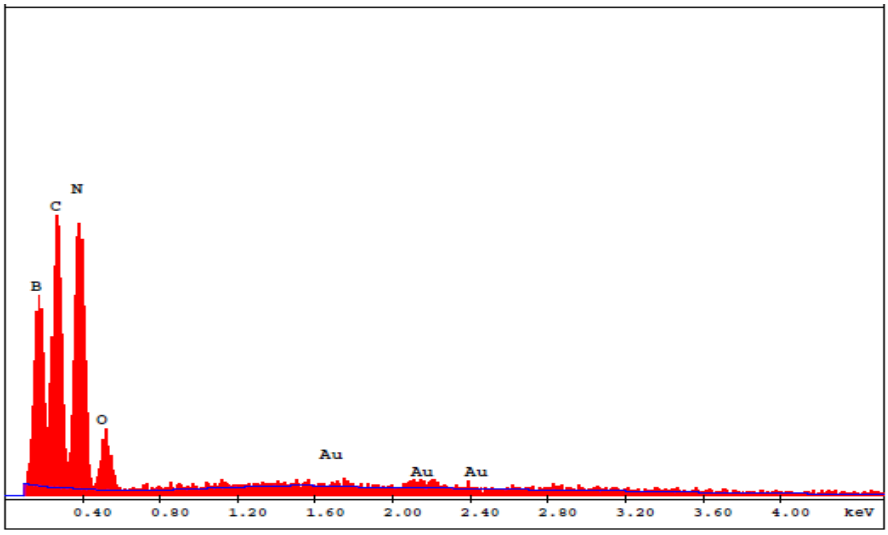

Figure 4.7 EDX spectrum of boron nitride produced from B and Fe_2O_3 (P-BN-MO-5).

Figure 4.8 shows EDX spectrum of sample synthesized using iron. Sharp peaks of boron and nitrogen can be clearly observed suggesting that sample is boron nitride. Some iron peaks can also be seen because Fe was used in a reactant material for synthesis of BN. The EDX results were consistent with the XRD (Figure 4.1-4.4) results showing presence of B and N with iron impurities in some samples. Gold and palladium peaks are due to the Au-Pd alloy coating on the sample before the analysis to make it conductive. Carbon peaks comes from the carbon tape while the oxygen peak may be assigned to the oxygen gas adsorption on the material.

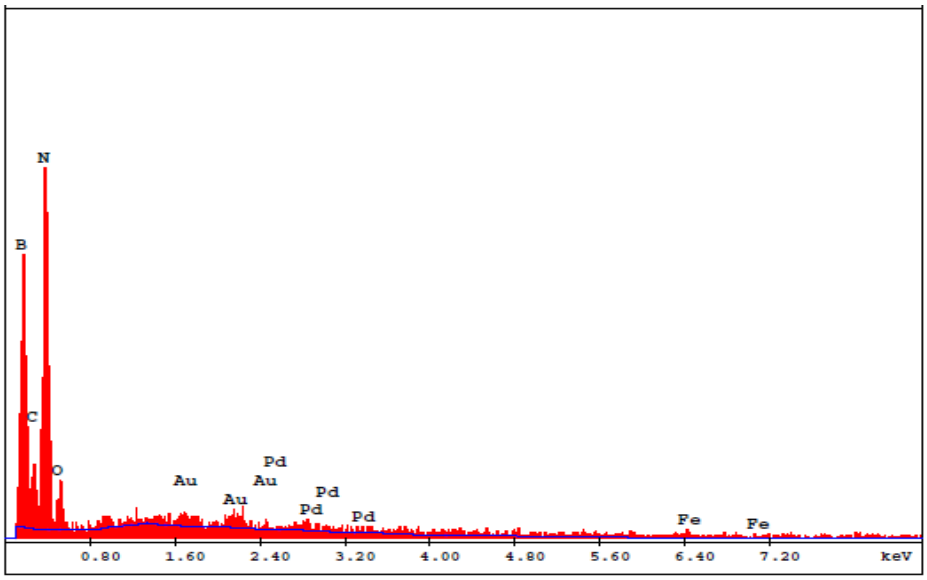

Figure 4.8 EDX spectrum of boron nitride produced from boron and iron (UP-BN-M).

4.1.4 Thermogravimetric analysis of synthesized material (TGA)

Figure 4.9 shows TGA curves of purified BN synthesized using iron oxide in air and nitrogen environment, respectively. Approximately 1% weight loss was noticed for iron oxide samples below 200^{o}C which might be due to removal of moisture in the samples. This shows the oxidation and thermal stability of BN up to 900^{o}C in both air and nitrogen environment.

Figure 4.10 shows TGA curves of purified BN synthesized using iron in air and nitrogen environment, respectively. Weight loss of approximately 2.7% and 2.2 % were observed for samples analyzed in air (Figure 4.10 a) and in nitrogen (Figure 4.10b). This might be due to removal of some impurities and moisture in the samples. Same and gradual decrease in the weight for both air and nitrogen environment was observed. This behavior showed only removal of impurities, not formation of other compounds.

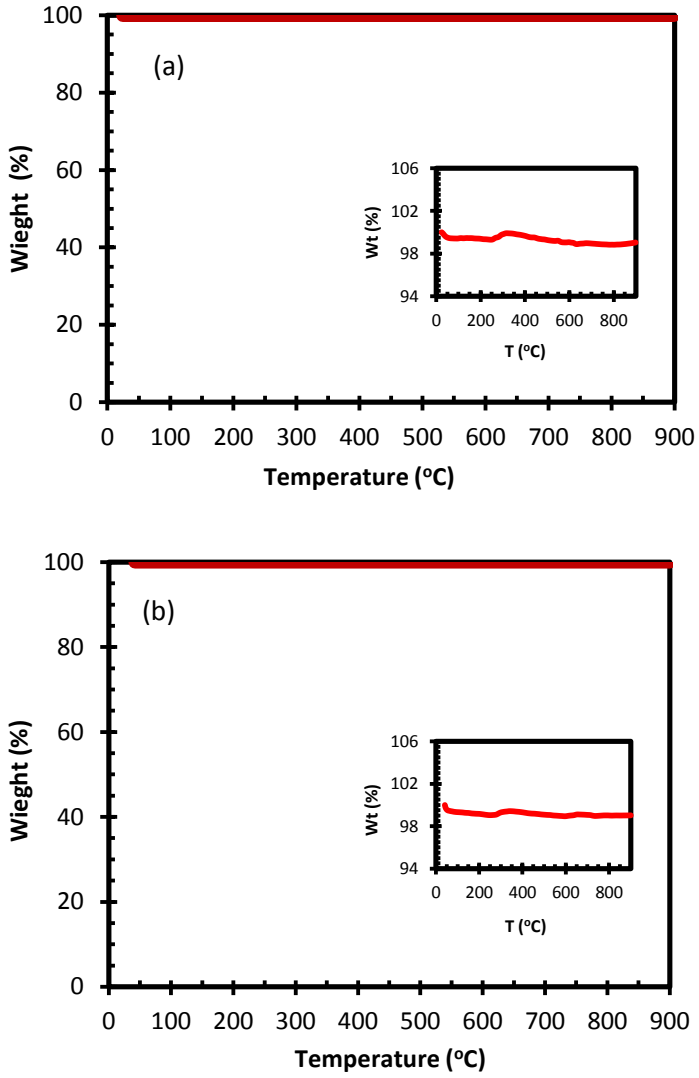

Figure 4.9 TGA curve of purified BN (P-BN-MO-6) synthesized from boron and iron oxide under (a) air and (b) nitrogen environment.

BN have excellent oxidation resistance capability compared to CNTs [50] that can be observed in thermogravimetric analysis curves shown above. Therefore BN might be used as a catalyst or catalyst support in temperature range of 200-900 ^{o}C.

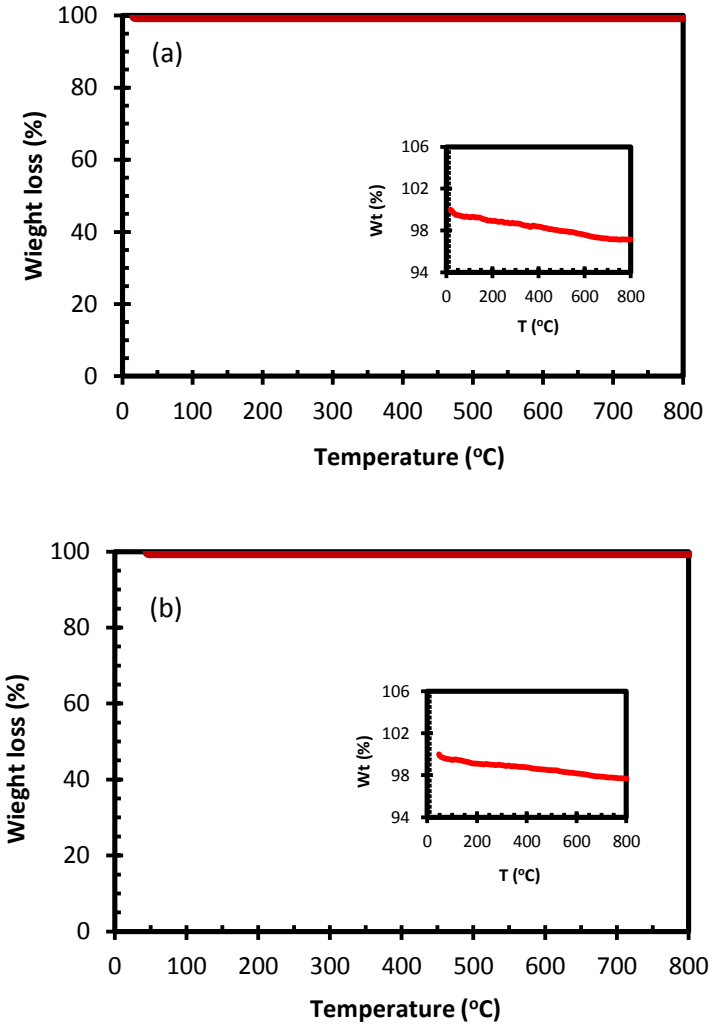

Figure 4.10 TGA curve of purified BN (P-BN-M-1) synthesized from boron and iron under (a) air and (b) nitrogen environment.

4.1.5 Scanning Electron Microscopy

Scanning Electron Microscopy (SEM) was performed in order to get information about dimensions and morphology of synthesized boron nitride materials.

In Figure 4.11, SEM images of BN synthesized using metal oxide (Fe_2O_3) are shown. SEM images showed the presence of nanotubes in the material produced by the

method used in this study. Generally nanotubes with outer diameter of 10-300 nm (Figures 4.11 and 4.12) were observed but most of the nanotubes have outer diameter in the range of 15-100 nm. The nanotubes with up to several microns long were produced. Agglomeration of BNNTs can be observed between nanotubes. Figures 4.11 a and b show agglomeration of nanotubes.

In Figure 4.11 c, d and e magnified images of BNNTs are shown that are mostly entangled. Some straight and long cylindrical nanotubes were also observed one of them shown in Figure 4.11f. The diameter and length of this particular nanotube between the red arrows were 59 nm and 2.91 microns, respectively. The diameter of the nanotube shown in Figure 4.11 d by red arrows is 49 nm. Also some longer nanotubes were observed in SEM images.

In Figure 4.12, SEM images of BNNTs produced using Fe. Large number of entangled nanotubes can be observed in Figure 4.12 a and b. Nanotubes pointed in Figure 4.12 a and b have diameters of 118 nm and 215 nm, respectively. Cylindrical nanotube can be seen in Figure 4.12 c with diameter and length of 40.9 nm and 688.2 nm, respectively. Few very large nanotubes were also observed one shown in Figure 4.12 d (diameter: 428.9 nm, length~5.02 µm). A spherical particle in Figure 4.12 e is iron and its diameter is around 5.01 µm. A very dense agglomeration of nanotubes protruded from a spherical iron particle is shown in Figure 4.12 e. This high density of nanotubes on the spherical iron is the evidence of root growth mechanism in the formation of nanotubes rather than tip growth mechanism. SEM images of some other samples are given in Appendix B.

Magnified image of iron particle surface in Figure 4.13a shows nanotube (outer diameter of 55 nm) grown perpendicular (red arrows) to the surface of the iron particle as well as nanotubes grown horizontally on the surface of iron particle. The spherical particle is iron which was confirmed from EDX analysis (Figure 4.13c) and Back Scattered Electron (BSE) image (Figure 4.13b) during SEM analysis. Some of the bright spots pointed by red arrows on BSE image (Figure 4.13 b) are iron particles and also a large iron peak in Figure 4.13 c can be observed.

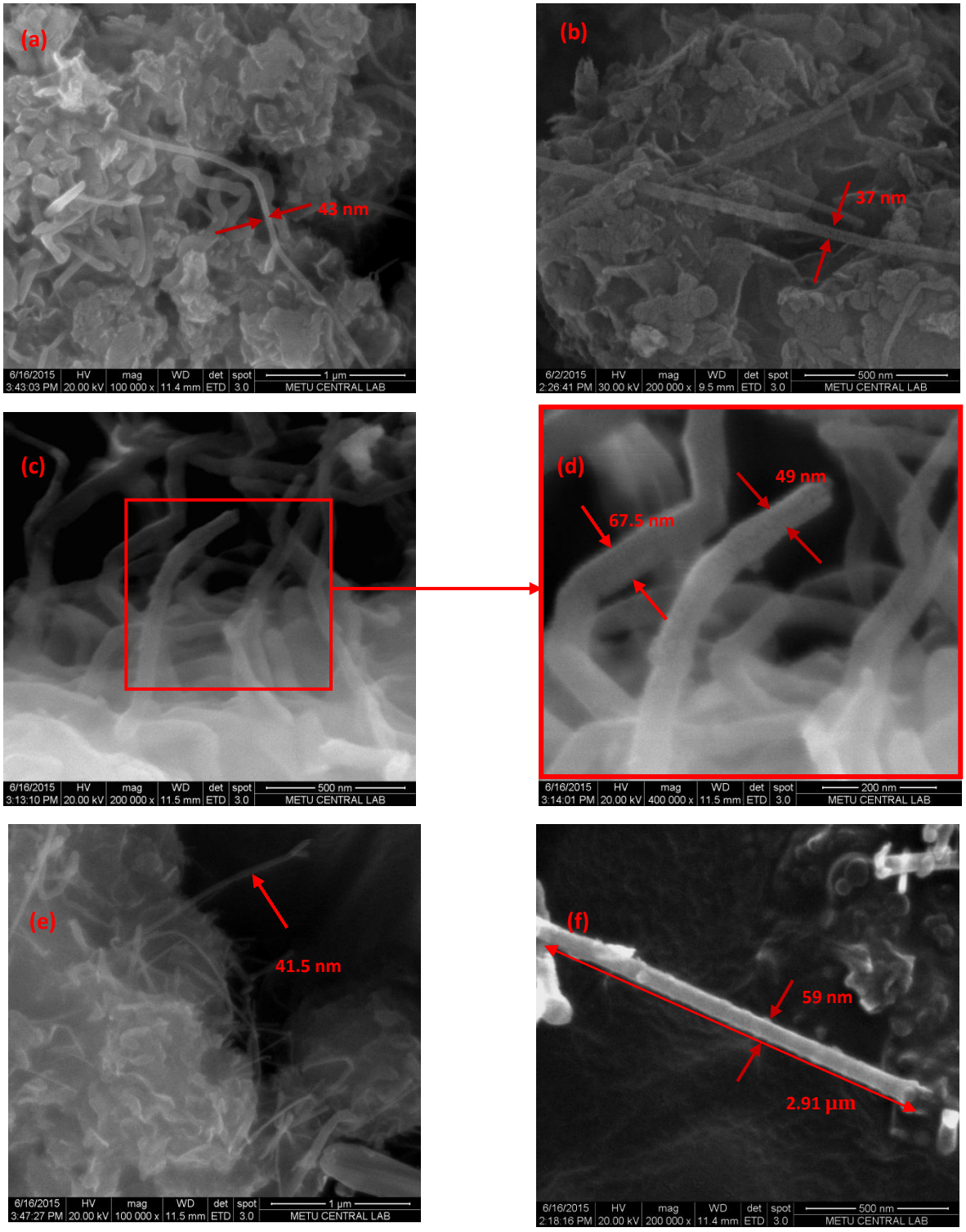

Figure 4.11 SEM images of BNNTs produced using iron oxide unpurified (a and e) purified (b, c, d and f) samples. (d) 400000x magnification (c) 200000x magnification

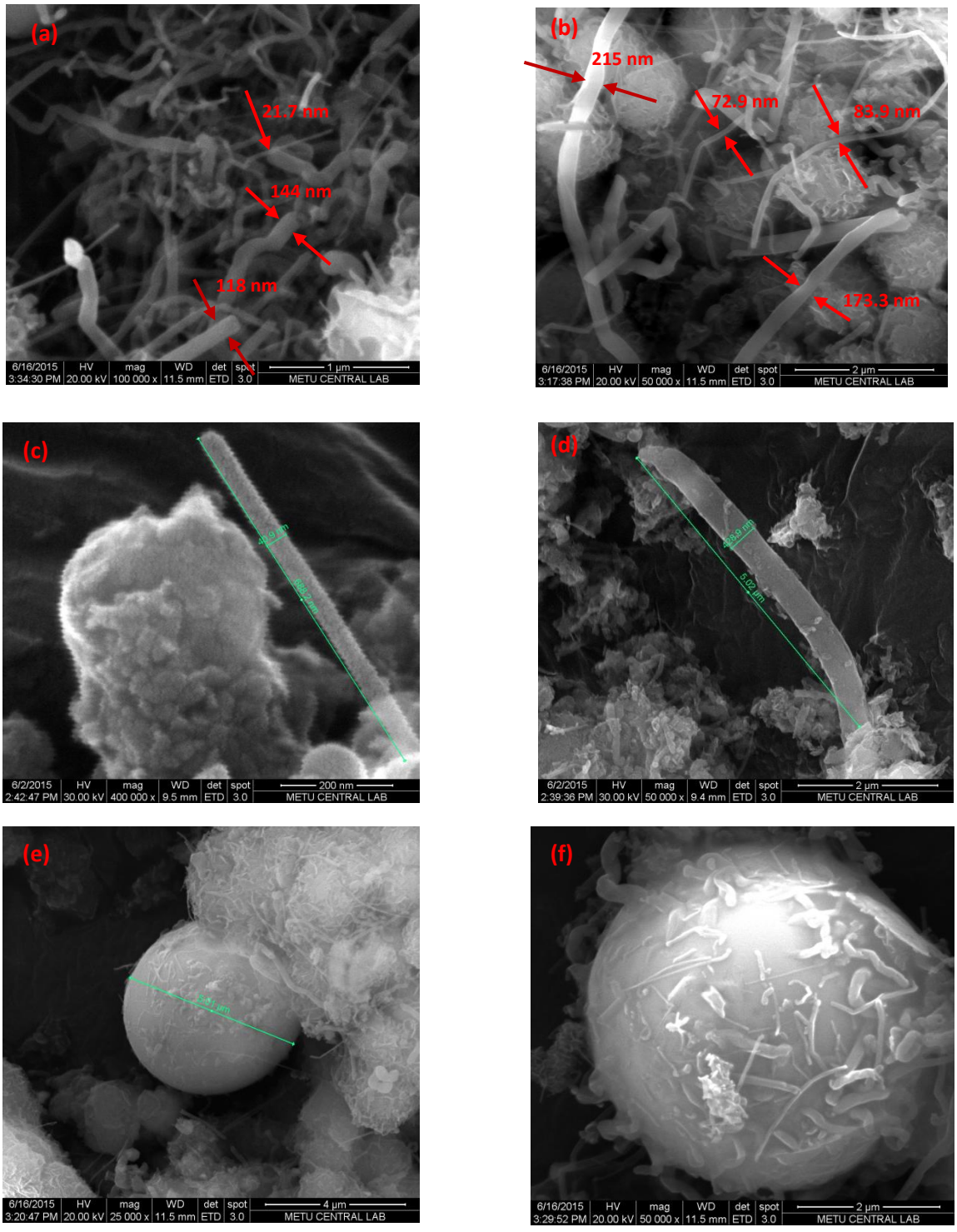

Figure 4.12 SEM images of BNNTs produced using iron unpurified (a, b, e, and f) and purified (c and d) samples.

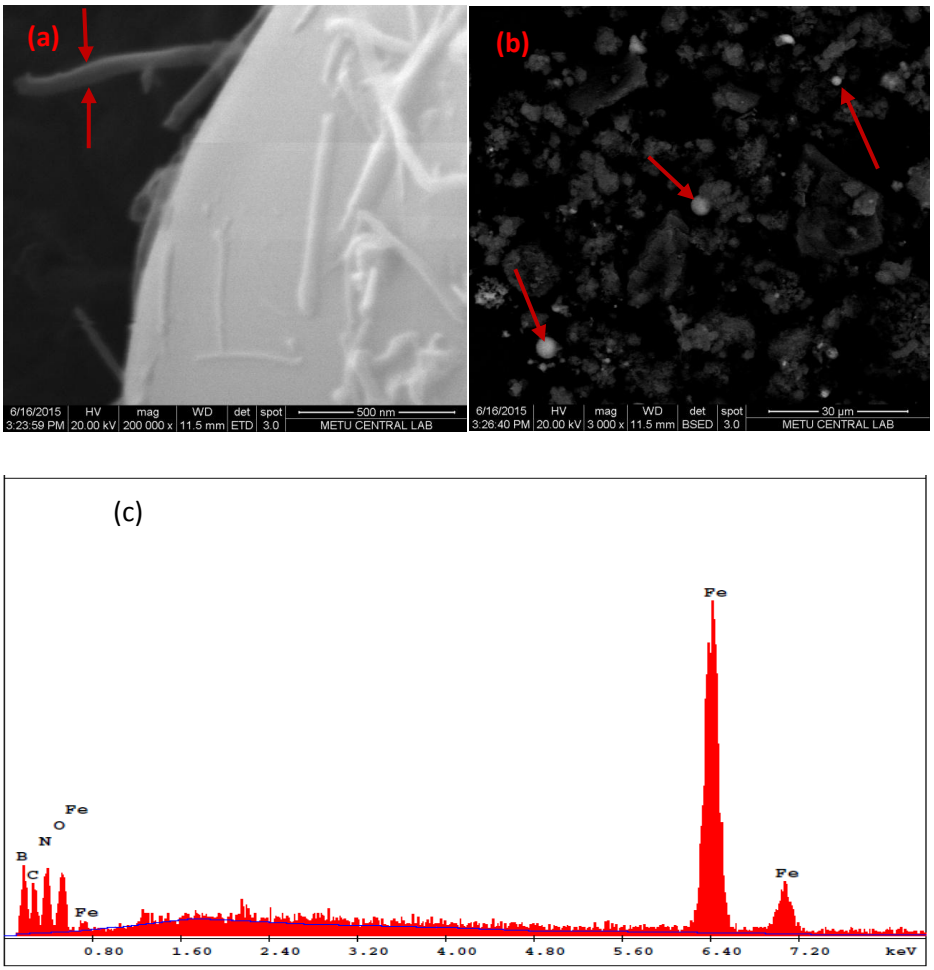

Figure 4.13 SEM images of iron particles found in material synthesized iron: (a) iron particle (b) back scattered electron image (c) EDX spectra of sample shown in (a).

It can be concluded from SEM results that considerable amount of nanotubes were obtained with different geometries from both type of precursors materials (Fe_2O_3 and Fe). Almost the same yield and type of nanotubes were produced from both types of precursor materials and samples synthesized at different times.

4.1.6 Transmission Electron Microscopy

The synthesized purified BNNTs were analyzed for detail images of individual nanotube on Transmission Electron Microscope (TEM). In Figure 4.14 TEM images of purified BNNTs synthesized using iron oxide are shown. Both bamboo like and cylindrical nanotubes with closed and open ends (Figure 4.14 c) were observed. Nanotubes were all multi-walled. In Figure 4.14 a and b bamboo-like and hallow cylindrical nanotubes can be observed with outer diameters of 45.6 nm and 45 nm and the inner diameters of 17 nm and 15 nm, respectively. In the magnified image (Figure 4.14 c) open end nanotube can be seen with an outer diameter of 35 nm. The inner diameter of the nanotube (Figure 4.14 c) at the narrow region (yellow arrows) was about 6.3 nm while in the broad region (red arrows) inner diameter was 14 nm.

Multi-walled bamboo-like nanotube in Figure 4.14 d has inner diameter varying from 7.6 nm to 11.5 nm while the outer diameter was about 40 nm. The wall thickness of the nanotube in Figure 4.14 d was 15 nm (red arrows).

In Figure 4.15 TEM images of BNNTs synthesized from boron and iron are given. Multi-walled cylindrical and bamboo-like nanotubes were observed in TEM images similar to BNNTs synthesized using iron oxide. In Figures 4.15a and b long straight cylindrical nanotubes were seen with outer diameters of about 32.6 nm and 28.9 nm, respectively. Bamboo-like nanotube was seen in Figure 4.15 c and d. The outer diameters of nanotubes pointed out by red arrows in Figure 4.15 c and d were found to be 38.9 nm and 92 nm, respectively. The small nanotube in Figure 4.15 d (yellow arrow) has a diameter of 34.5 nm. Some other bamboo-like nanotubes can also be seen in Figure 4.15 d. The black spots seen in some of the nanotubes are due to impurities attached to the nanotubes.

Both bamboo-like and hollow cylindrical nanotubes were observed in the material synthesized from boron and iron or iron oxide. The inner (Figures 4.14 c and d) and outer diameters (Figures 4.14 a and 4.15 b) of some of the nanotubes were not uniform and there were slight variations in both outer and inner diameters.

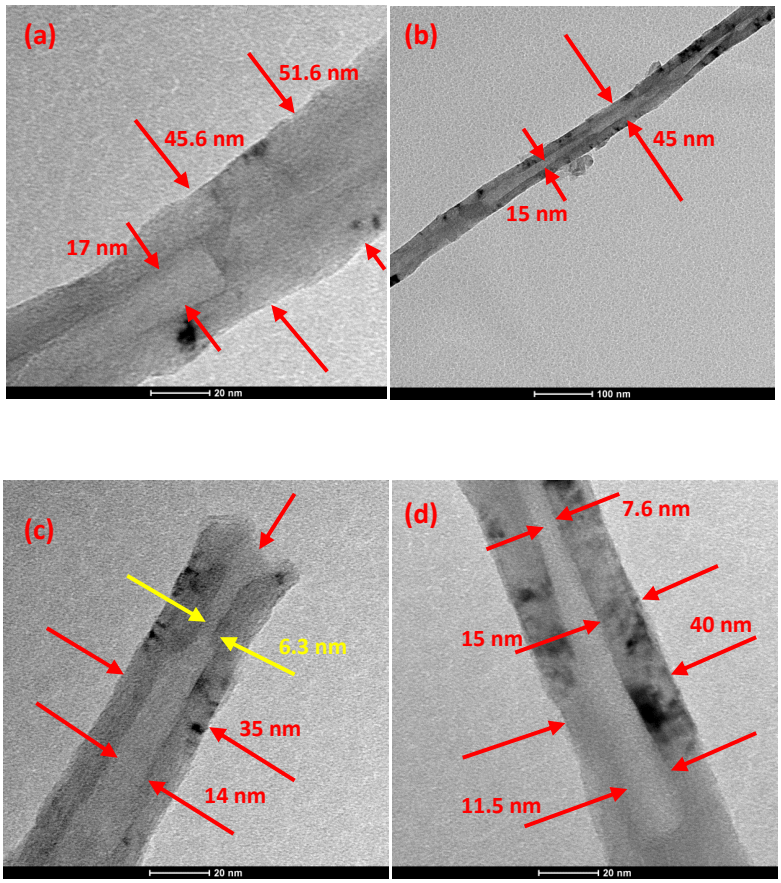

Figure 4.14 TEM images of purified BNNTs produced using Fe_2O_3

In the material synthesized using iron more cylindrical nanotubes were observed as compared to the iron oxide. More bamboo-like nanotubes were observed in the material synthesized using iron oxide. Some other TEM images of the samples are given in Appendix C.

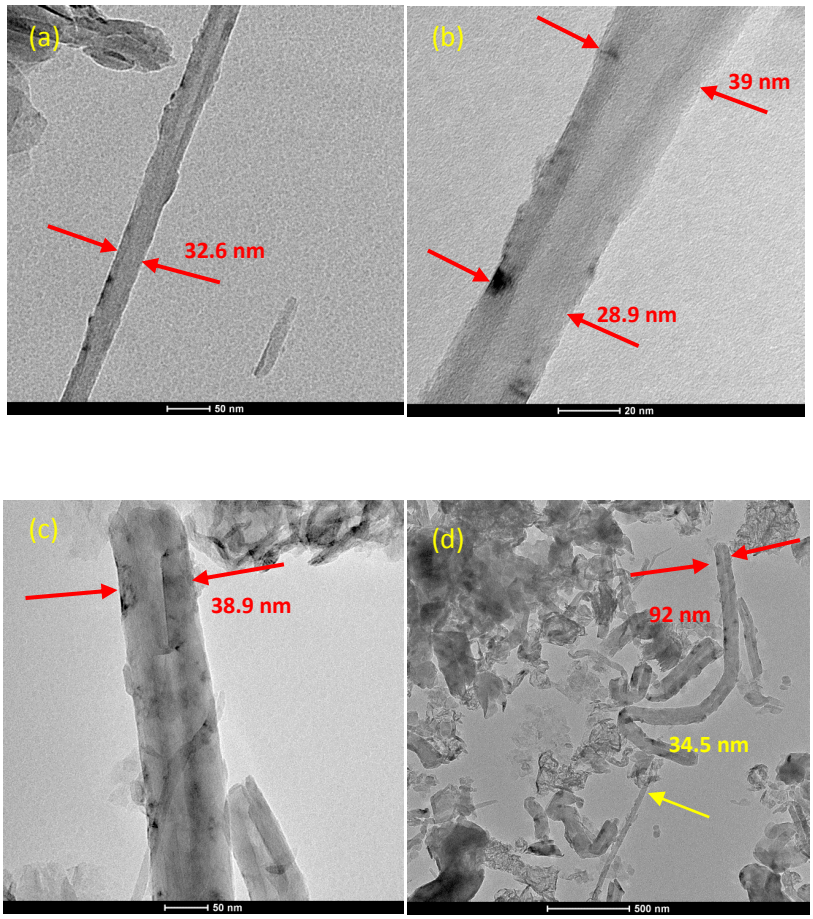

Figure 4.15 TEM images of purified BNNTs produced using Fe

4.1.7 Nitrogen adsorption and surface characterization

Textural properties of boron nitride nanotube were investigated using nitrogen adsorption. Brunauer–Emmett–Teller (BET) surface area, total pore volumes and pore size distributions were determined using nitrogen adsorption. In Figure 4.16, nitrogen adsorption and desorption isotherms of as-synthesized (unpurified) BNNTs are shown while nitrogen isotherms for purified BNNTs can be observed in Figure 4.17. Isotherms obtained for BNNTs resemble Type-II isotherm which suggests that adsorption occurs on non-porous or material with pores other than micropores. Hysteresis was obtained due to capillary condensation in mesopores. The hysteresis obtained resembles to both

Type A and Type B which indicate the presence of cylindrical and slit like pores. So hysteresis showed that adsorption occurred inside the nanotubes as well as between the walls of multi-walled nanotubes. The starting point of hysteresis was at P/P_o value of 0.46. The isotherms for the as-synthesized material (Figure 4.16) showed that mostly mesopores and considerable macropores but little amount of micropores were also present. Macropores were present due the small void spaces in the agglomeration of entangled nanotubes.

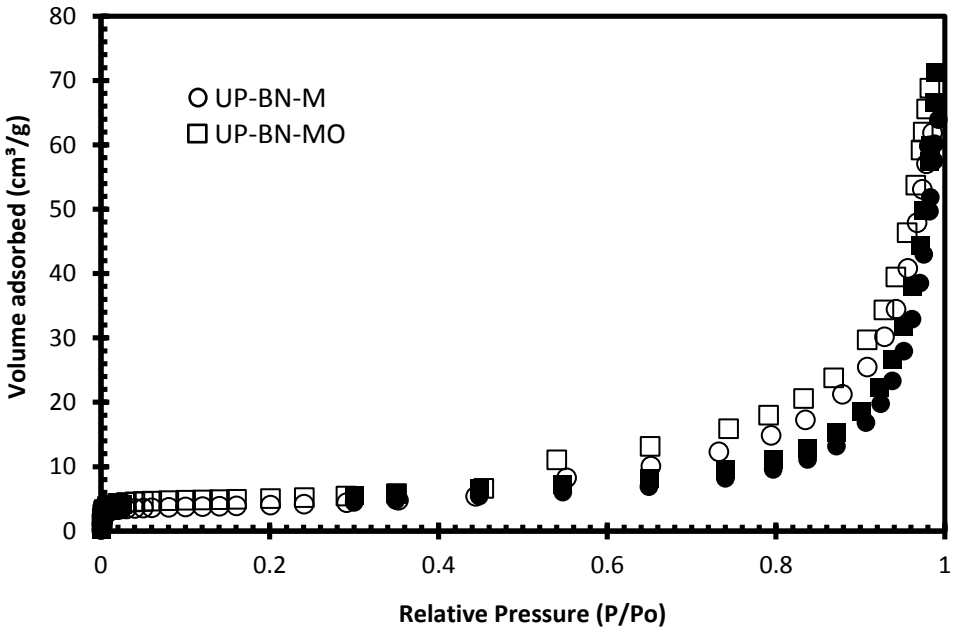

Figure 4.16 Nitrogen isotherms of unpurified BNNTs synthesized using Fe_2O_3 (filled symbols: Adsorption branch; empty symbols: Desorption branch)

From the Figure 4.16, volumes of adsorbed nitrogen gas were found to be 48 cm^3/g and 4.2 cm^3/g at P/P_o values of 0.96 and 0.02, respectively. From Figure 4.17, volumes of adsorbed nitrogen gas were found to be 259.5 cm^3/g and 27.2 cm^3/g at P/P_o values of 0.96 and 0.02, respectively. It was observed from the isotherm in Figures 4.16 and 4.17 that the amount of nitrogen adsorbed at relative pressure (P/P_o) 0.96 for purified BNNTs was more than 5 times as compared to as-synthesized material. Almost the same

increase was noticed in the value of nitrogen adsorbed in micropore region at P/P_o 0.02. The volume percent adsorbed in micropores was around 10 percent of the total volume adsorbed at P/P_o 0.96. For almost all the purified samples there were approximately 10% micropores, 70-75 % mesopores and 10-15 % macropores. Micropore and mesopores percentages were calculated from the fraction of volume adsorbed at P/P_o values of 0.02 and 0.96 to total volume adsorbed at 0.98, respectively. Macropore percentage was calculated from the difference of volume adsorbed at P/P_o values of 0.98 and 0.96. The nitrogen adsorbed amount for purified samples was much higher than the as-synthesized material because in the as-synthesized material there were a lot of impurities which were removed after purification. The total pore volumes of BNNTs produced from Fe_2O_3 and Fe were found to be 0.44 cm^3/g and 0.45 cm^3/g at P/P_o value of 0.98, respectively. Total pore volumes for as-synthesized material were 0.09 cm^3/g and 0.08 cm^3/g produced from Fe_2O_3 and Fe, respectively. Five time increase was also noticed in total pore volumes after purification. The calculations related to BET surface area are given in Appendix D.

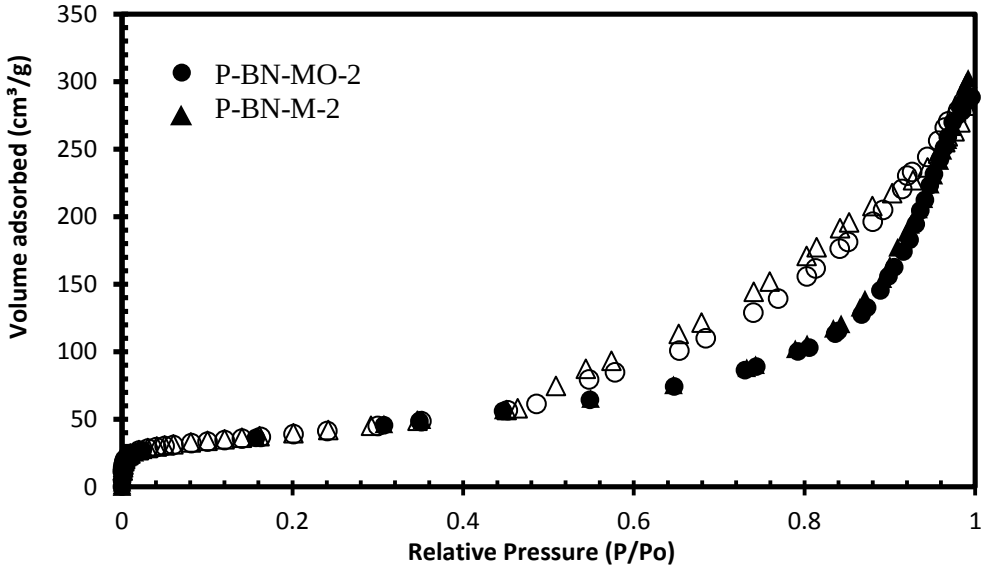

Figure 4.17 Nitrogen isotherms of purified BNNTs synthesized using Fe_2O_3 or Fe, (Filled symbols: Adsorption branch; empty symbols: Desorption branch)

In general, isotherms obtained for both samples synthesized using iron oxide and iron were almost same. These results revealed that no considerable difference in the structure of nanotubes was observed no matter which precursor was used for synthesis.

Brunauer-Emmett-Teller (BET) surface area of purified BNNTs synthesized from boron and iron oxide was found to be 145.2 m^2/g as compared to 23.80 m^2/g BET surface area of unpurified BNNTs. BET surface area of purified BNNTs synthesized from iron was observed to be 141.43 m^2/g as compared to 19.41 m^2/g of unpurified sample. On other hand the BET surface area of CNTs with walls more than 15 is about 200 m^2/g [72]. An increase in surface area of about 6 to 7 times was observed after purification of the materials. This might be due to the removal of impurities and unreacted reactants. Unpurified samples also contain lot of agglomerated nanotubes (Figures 4.11, Figure 4.12) which were debundled after purification. It was found that during purification process the amount of sample reduced to half of the initial amount in these start of purification which suggested that significant amount of impurities (site products, unreacted reactants) has been removed from the as-synthesized product. It can be observed from the isotherm that the micropores and mesopores significantly increased after purification.

Before and after purification, a difference in the shapes of hysteresis loops was observed for both samples. It can be observed in Figures 4.16 and 4.17 that the width of hysteresis loop increased after purification which shows the presence of more mesopores in purified samples compared to unpurified samples. It may be due to the removal of impurities and unreacted materials from the pores and opening the ends of the nanotubes by removal of unreacted boron and iron particles during purification. The opening of pores or the end of nanotubes allowed the gas molecules to enter inside the cylindrical nanotubes and that is why more gas was adsorbed in purified samples. The shape of hysteresis loop is almost the same for both the purified samples synthesized using Fe_2O_3 and Fe. Using iron oxide or iron as a starting material for BNNTs synthesis did not affect the amount of mesopores.

Isotherms of four (4) purified samples synthesized using Fe_2O_3 and three (3) purified samples produced using Fe are shown in Figure 4.18. The overall shape of all the purified samples isotherms was found to be almost same which shows the reproducibility of BNNT by the method used in this study. These materials were produced using iron oxide and iron at different time using same condition. Little difference in some of the isotherms was observed which may be due to some impurities in some of the samples. Almost exactly the same behavior was observed in the micropore and monolayer coverage regions of all sample. The amount of nitrogen adsorbed at a relative pressure (P/P_o) of 0.96 was very close for each samples produced at different times. BET surface areas and total pore volume of some samples produced at different times using same conditions are shown in Table 4.1. The average surface area and total pore volume for all the purified samples were found to be 133.66 m^2/g and 0.42 cm^3/g, respectively.

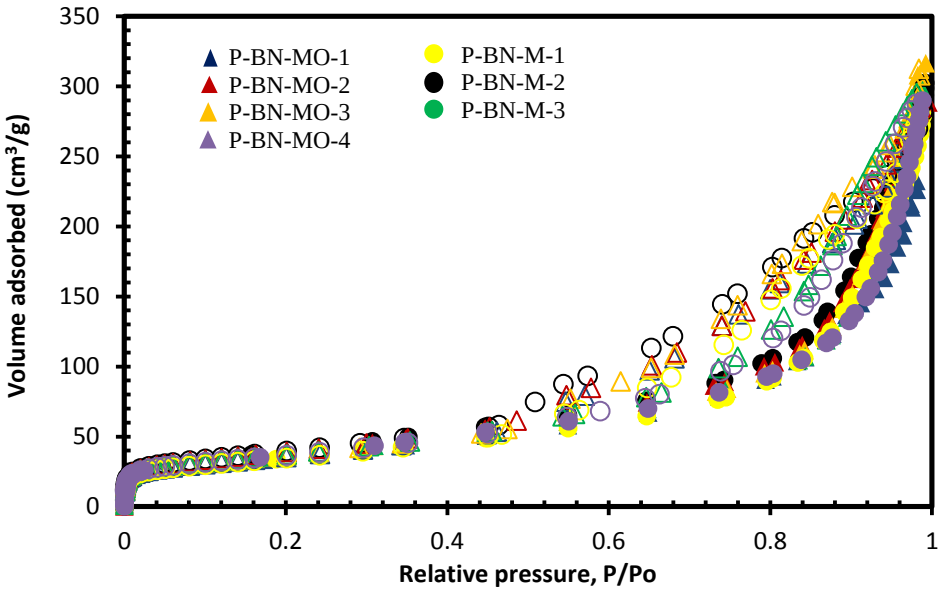

Figure 4.18 Nitrogen isotherms of purified BNNTs synthesized using Fe_2O_3 or Fe (filled symbols: Adsorption branch; empty symbols: Desorption branch)

Table 4.1 BET surface area and total pore volume of BNNTs synthesized at 1300^{o}C using iron oxide or iron (sample names were explained in Chapter 3)

Sample	BET Surface Area (P/P_o 0.05-0.3) (m^2/g)	Total Pore Volume (P/P_o 0.98) (cm^3/g)
P-BN-MO-1	126.63	0.36
P-BN-MO-2	145.20	0.44
P-BN-MO-3	131.20	0.46
P-BN-MO-4	130.42	0.41
P-BN-M-1	122.70	0.40
P-BN-M-2	141.43	0.45
P-BN-M-3	132.80	0.43
UP-BN-MO	23.80	0.09
UP-BN-M	19.41	0.08

4.1.7.1 Pore size distribution

Pore size distribution plots (Figure 4.19) were obtained using Barrett-Joyer-Hallender (BJH) method in the relative pressure range of 0.40-0.96. Main peak was observed at 41.7 Å for the sample synthesized from iron oxide (P-BN-MO-2) and presence of a small peak at 66.6 Å was also observed for this sample. For the sample synthesized from iron (P-BN-M-2) main peak was observed at 37.5 Å. Average pore

size for iron (Fe) sample was found to be smaller than that of iron oxide (Fe_2O_3). The presence of main peak in mesoporous region showed that nanotubes diameters were in mesoporous region. A small peak near 70 Å can also be observed. The diameters of nanotubes are not uniform which is consistent with SEM results. Some macropores were also observed in the purified material because of the agglomeration between the nanotubes. In Figure 4.19, pore size distributions of two other samples synthesized under same conditions at different times are compared. The BJH plots for all samples were found to be almost identical in shape with slight difference in the average peak values which is consistent with isotherm shapes.

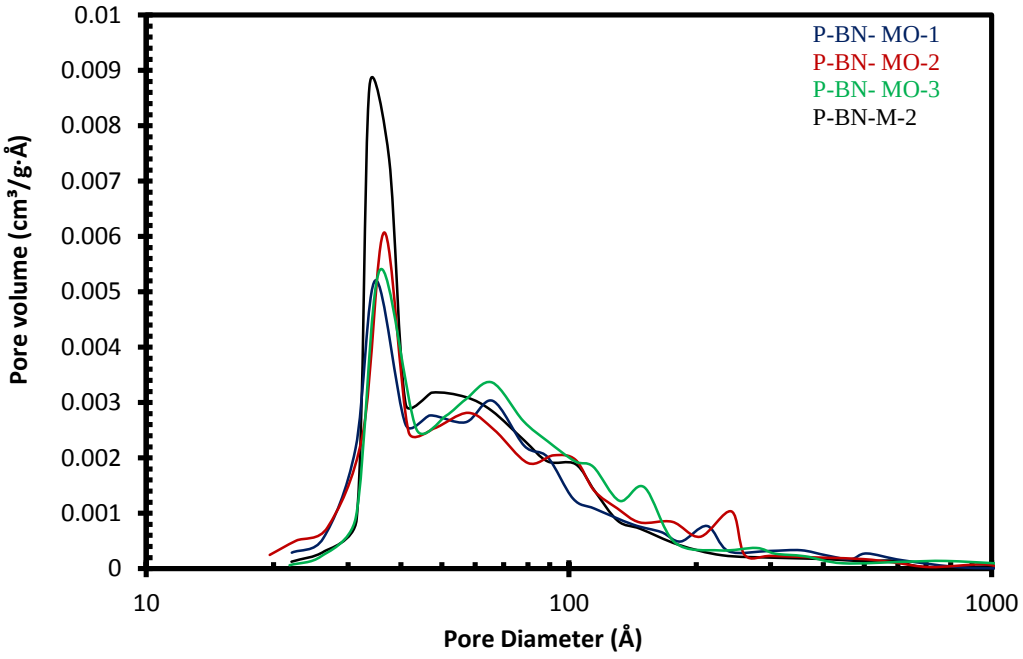

Figure 4.19 BJH pore size distribution of purified BNNTs synthesized at different times using Fe_2O_3 or Fe

Horvath-Kawazoe (H-K) micropore size distribution for slit geometry is shown in Figure 4.20. For sample synthesized using iron oxide the peak was on 9.1Å while the

main peak for iron sample was observed at 9.3Å. The pore distribution curves for both samples were observed to be almost same. Micropore peak was obtained due to adsorption of N_2 between the walls of multi-walled nanotubes and nanotubes with very small diameters.

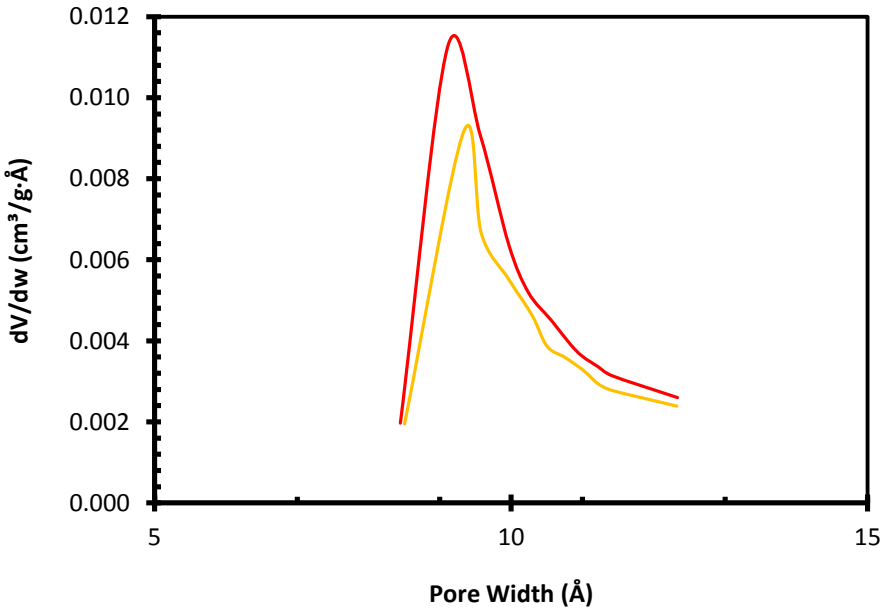

Figure 4.20: Horvath-Kawazoe (H-K) micropore size distribution (slit geometry) for purified BNNTs synthesized at different time at 1300^{o}C using Fe_2O_3 (Red: P-BN-MO-2) or Fe (orange: P-BN-M-1)

4.1.7.2 t-plots

This method was developed by Lippen and De Boer to analyze microporous materials [57]. This method allows the estimation of micropore volume and micropore area. t-plots for the sample synthesized using iron oxide is shown in Figure 4.21. There are two linear regions in the curve shown by straight lines in the figure. When the upper linear region is extrapolated to the adsorption axis the intercept corresponds to micropore volume which was found to be 0.05 cm^3/g for this sample. Similarly micropore volume for the sample synthesized using iron (Figure 4.22) was found to be

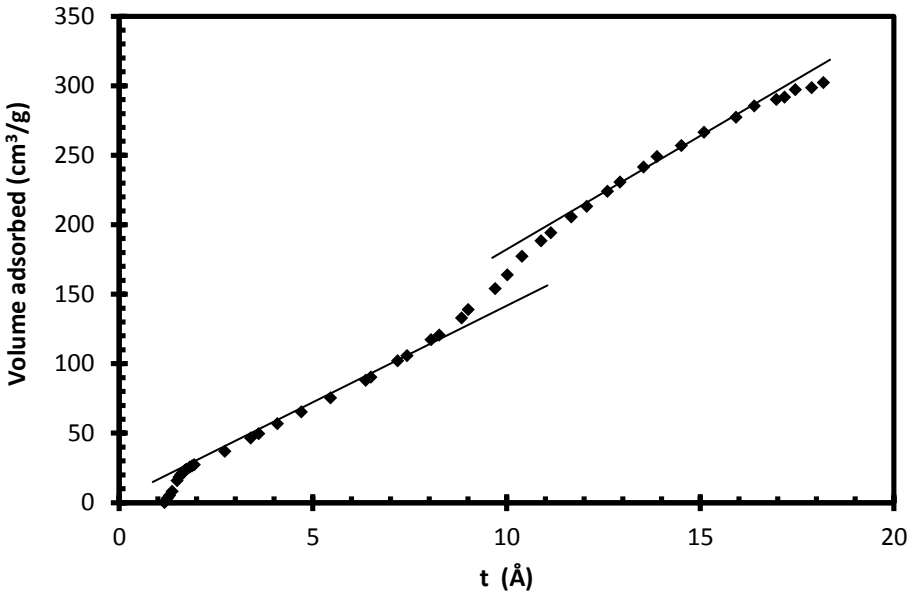

Figure 4.21 t-plot for purified BNNTs synthesized using Fe_2O_3 (P-BN-MO-1)

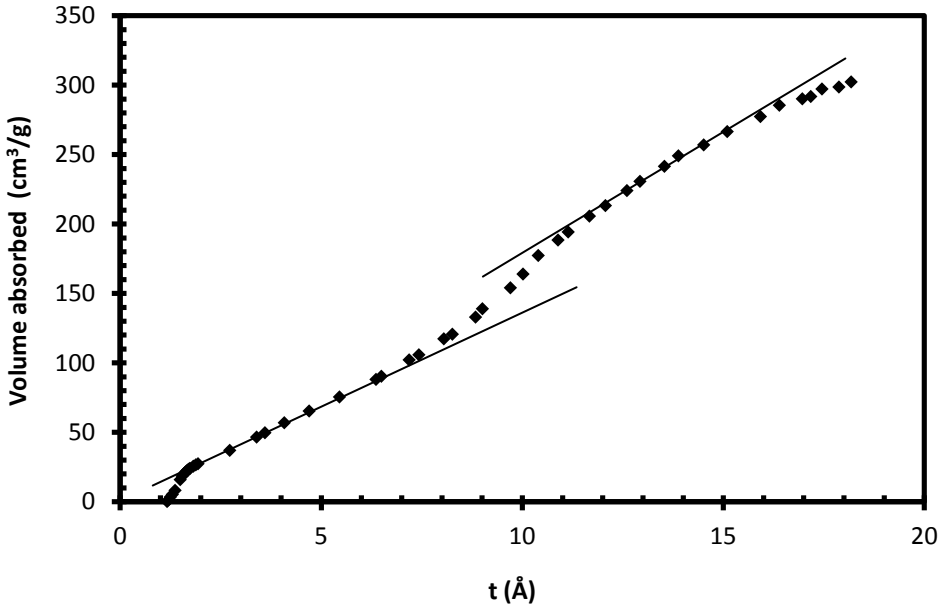

Figure 4.22 t-plot for purified BNNTs synthesized using Fe (P-BN-M-2)

be 0.05 cm^3/g. The slope of lower linear region in the t-plot gives total surface area while the slope of upper linear region gives external surface area (S_{ext}: surface area excluding micropore surface area). The difference of total surface area and S_{ext} gives micropore surface area of the material [57]. The micropore surface areas for both samples were found to be 11.14 m^2/g. From t-plot results it was concluded that both samples contain almost the same amount of micropores.

4.1.8 Carbon dioxide adsorption

For micropore analysis carbon dioxide adsorption technique was used. Due to small diameter of carbon dioxide as compared to nitrogen [71], carbon dioxide adsorption technique is preferred over nitrogen adsorption for micropore analysis. Also, CO_2 analysis was carried out at 273.15 K and at this temperature diffusion rate of molecules in tortuous and small micropores is higher [57].

In Figure 4.23, carbon dioxide adsorption isotherm for different BNNTs samples synthesized at different times are shown. It was observed that quantity of carbon dioxide adsorbed by purified BNNTs produced using metal oxide (Fe_2O_3) was higher as compared to BNNTs produced using metal (Fe) precursor. This might be suggested that metal oxide samples were considerably more microporous than iron samples or samples synthesized from metal (Fe) were not well purified that is why they adsorbed less amount of carbon dioxide. Quantity of CO_2 adsorbed by unpurified samples was almost same. Using CO_2 adsorption data and Dubinin-Radushkevich (D-R) method [57], micropore volumes of purified samples were found to be 0.053 cm^3/g and 0.040 cm^3/g for BNNTs produced from iron oxide (Fe_2O_3) and iron (Fe), respectively. The micropore volumes for unpurified samples synthesized using iron oxide or iron were observed to be 0.0046 cm^3/g and 0.003 cm^3/g. As-synthesized samples adsorbed less quantity of carbon dioxide. This might be due to presence of impurities and unreacted reactants were present in unpurified samples which suggested that reactant iron oxide and iron are nonporous.

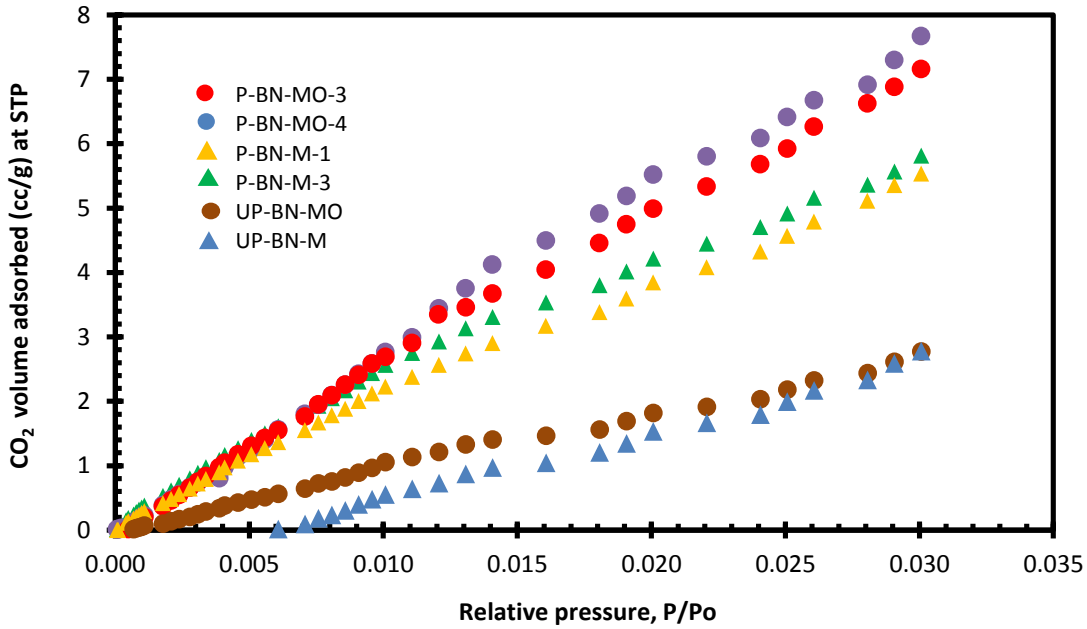

Figure 4.23 CO_2 adsorption isotherms of purified and unpurified BNNTs synthesized at different times using Fe_2O_3 or Fe

The micropore volumes for both the samples using t-plot and nitrogen adsorption data were found to be same (0.05 cm^3/g). The shapes of isotherms were almost same. The difference in the micropore volumes may also be due to not well purified sample or use of different portions of the same sample in the analyses. Carbon dioxide adsorption technique is used for microporous material and our material was not microporous so the results of micropore volume were same for both nitrogen and carbon dioxide adsorption.

4.1.9 Chemical adsorption

Chemical adsorption analysis of BNNTs was performed using ammonia as a probe molecule in order to find the surface acidity. TPD curves are shown in Figure 4.24 for purified BNNTs synthesized using iron oxide and iron. The first peak between 75-325^oC in Figure 4.24b corresponds to weak adsorption on the non active surface sites

while the second peak between 380-760^{o}C corresponds to chemisorption of ammonia on actives sites. The area under the two peaks can quantify the number of active sites available. Almost the same peaks were also observed for iron sample (Figure 4.24a) between 110-420^{o}C and 435-760^{o}C. Calibration curve for the chemisorption analysis of BNNTs is given in Appendix E. Total acidity was calculated using the calibration curve and area under the TPD curve. TPD results revealed the presence of some acid sites on

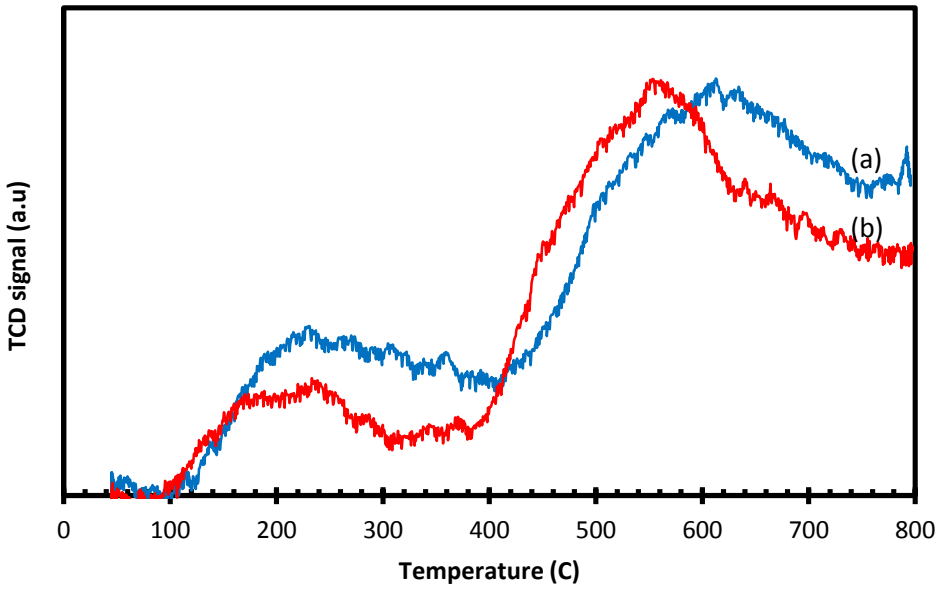

Figure 4.24 TPD spectra of purified BNNTs synthesized using iron oxide (red, P-BN-MO-5) and iron (blue, P-BN-M-1) (Probe gas: ammonia)

the material. The total acidity was found to be 0.136 and 0.155 mmol NH_3/g for BNNTs synthesized using iron oxide and iron, respectively. The total acidity is comparable to Ni/Al-SBA-15 catalyst [73] and zeolites (Mordenite) [74] which suggested the possibility of using BNNTs as a catalyst.

4.1.10 Solid density measurement

Skeletal density of powder product was measured using gas pycnometer technique. A gas pycnometer detects change in pressure from the displacement of gas by solid material. Then by using ideal gas law, first volume was calculated for a given amount and density was calculated using weight of sample. Helium gas was used in analysis. The densities of purified and unpurified boron nitride nanotubes synthesized using iron and as-synthesized sample were found to be 2.4 g/cm^3 and 1.3 g/cm^3, respectively. The density of h-BN is 2.3 g/cm^3 [75] which is almost equal to the purified BNNTs. The density of CNTs is about 1.6 g/cm^3 which is less compared to BNNTs. The calculations used for density measurement are given in Appendix F.

CHAPTER 5

CONCLUSIONS AND RECOMMENDATIONS

- Boron nitride nanotubes were successfully synthesized from the reaction of powder mixture of boron and iron oxide or iron with gaseous ammonia in a tubular reactor.

- X-ray diffraction analysis showed that hexagonal boron nitride, rhombohedral boron nitride, and boron-iron compound (FeB_{49}) were solid phases in the as-synthesized material in addition to boron and iron.

- Multi-walled hallow cylindrical and bamboo-like nanotubes with outer diameter range of 10-300 nm were obtained.

- The purified BNNTs showed Type-II isotherm with hysteresis resembling to both Type A and Type B suggesting presence of slit like and cylindrical pores.

- The highest BET surface area of purified BNNTs synthesized using iron oxide and iron were 145.2 m^2/g and 141.4 m^2/g, respectively.

- The average pore diameters and micropore volumes of purified BNNTs synthesized using iron oxide and iron were 41.7 Å and 37.5 Å, respectively.

- Micropores volume for both samples was found to be 0.05 cm^3/g using nitrogen sorption and for carbon dioxide sorption these were 0.053 cm^3/g and 0.040 cm^3/g for iron oxide and iron samples, respectively.

- Chemical adsorption analysis showed the presence of some acid active sites on the BNNT material. So there is possibility of use of BNNTs as catalyst.

- Properties of BNNTs synthesized from iron are relatively good compared to iron oxide.

- In future, adsorption of BNNTs can be observed using different gases like hydrogen.

- Achieving synthesis of BNNTs with single or few walls can greatly increase their specific surface area which could eventually enhance the adsorption and catalytic properties.

- Doping of metal particles on BNNTs can be achieved for tuning its electrical and catalytic properties like previously metal particles doped on CNTs.

- Funtionalization of BNNTs can be done to change their acidic degree.

REFERENCES

[1] Dai, L. "*Carbon nanotechnology: recent developments in chemistry, physics, materials science and device applications*", 1st edition, Amsterdam, Elsevier Science, 2006

[2] A.S. Milev, G. S. K. Kannangara, "*Nanotechnology*", in J. I. Kroschwitz., A. Seidel (Eds), *Kirk-Othmer Encyclopedia of Chemical Technolology*, Fifth Edition, vol. 17, Wiley, NJ, pp 1-29, 2005.

[3] John Mongillo, "*Nanotechnology 101*". Westport, Connecticut US: Greenwood Press, 304, 2007.

[4] Iijima, S., "*Helical microtubules of graphitic carbon*", Nature, 354, p 56, 1991.

[5] Chopra, N.G., Luyken, R.J., Cherrey, K., Crespi, V.H., Cohen, M.L., Louie, S.G., Zettl, A., "*Boron nitride nanotubes*", Science, vol. 269, no. 5226, p. 966-67, 1995.

[6] Gogotsi, Y. *Nanomaterials Handbook*, Taylor and Francis group,779, 2006

[7] F. Lamari Darkrima, P. Malbrunota, G.P. Tartagliab, *Review of hydrogen storage by adsorption in carbon nanotube*, International Association for Hydrogen Energy, 27, 193–202, 2002.

[8] Ma, R., Bando, Y., Zhu H., Sato,T., Xu,C., Wu,D., *Hydrogen Uptake in Boron Nitride Nanotubes at Room Temperature*, Journal of American Chemical Society (JACS), 124, 7672-767, 2002.

[9] Tang,C., Bando,Y., Ding,X., Qi,S., Golberg,D., *Catalyzed Collapse and Enhanced Hydrogen Storage of BN Nanotubes*, Journal of American Chemical Society (JACS), 124, 14550-14551, 2002.

[10] Lee,C.H., Zhang,D.,Yap, Y.K., *Functionalization, Dispersion, and Cutting of Boron Nitride Nanotubes in Water*, Journal of Physical Chemistry, C, 116, 1798–1804, 2012.

[11] Ferreira, T. H., Marino, A., Rocca, A., Liakos, I., Nitti,S., Athanassiou, A., Mattoli,V., Mazzolai, B., , Edesia M.B. de Sousa, Ciofani, G., *Folate-grafted boron nitride nanotubes: Possible exploitation in cancer Therapy*, International Journal of Pharmaceutics 481, 56–63, 2015.

[12] Gao, C., Guo, Z., Liu, J. H., Huang, X. J., "*The new age of carbon nanotubes: An updated review of functionalized carbon nanotubes in electrochemical sensors",* The royal society of chemistry, Nanoscale, 4, 1948–1963, 2012.

[13] Dau, H., *Carbon Nanotubes: Synthesis, Integration, and Properties*, Accounts of Chemical Research, 35, 1035-1044, 2002.

[14] Dresselhaus, M.S., Gene, D., Phaedon, A., *Carbon Nanotubes: Synthesis, Structure, Properties, and Application* , Springer, 2001.

[15] Milev, A.S., Kannangara, G.S.K., Wilson, M.A., "*Kirk-Othmer encyclopedia of chemical technology*", 5th ed., John Wiley & Sons, Inc, 2000.

[16] Mongillo, J., "*Nanotechnology 101*", Westport Conn.: Greenwood Press, 2007

[17] Kim, P., Shi, L., Majumdar, A., and McEuen, P. L., *Thermal transport measurements of individual multiwalled nanotubes*, *Physical Review Letters* 87, 2155021-4 , 2001.

[18] Rubio, A., Corkill, J, L., Cohen, M, L., *Theory of graphitic boron nitride nanotubes*, Phys. Rev. B: Condens. Matter Mater. Phys., 49, 5081–5084, 1994.

[19] Ishigami, M., Sau, J, D., Aloni, S., Cohen, M, L., Zettl, A., *Observation of the giant stark effect in boron-nitride nanotubes*, Phys. Rev. Lett., 94, 056804, 2005.

[20] Golberg, D., Bando, Y., Huang, Y., Terao, T., Mitome, M., Tang, C., Zhi, C., *"Boron Nitride Nanotubes and Nanosheets",* American chemical society, VOL. 4 ,NO. 6, 2979–2993, 2010

[21] Chopra, N.G., Zettl, A., "*Measurement of the elastic modulus of a multi-wall boron nitride nanotube*", Solid State Communications, vol. 105, no. 5, p. 297-300, 1998.

[22] Kuntz, D, M., *"Design and synthesis of Boron Nitride Nanomaterials*", MS thesis Department of Chemistry and Biochemistry, Northern Illinois University De Kalb, Illinois, December 2013.

[23] Wang J., Lee, C, H., Bando, Y., Golberg, D.,Yap, Y, K., "*Multiwalled Boron Nitride Nanotubes: Growth, Properties, and Applications",* B-C-N Nanotubes and Related Nanostructures, Springer Science , Business Media, LLC, 2009.

[24] Duclaux, L., Nysten, B., Issi, J-P., Moore, A. W., *Physical Review* B 46, 3362-7, 1992.

[25] Qiang, H, W., Mickelson, W., John, C., Zettl, A., *Boron Nitride Nanotube Peapods,* Applied Physics Letters 81, 1110-2, 2002.

[26] Wang J., Lee, C, H., Bando, Y., Yap, Y, K.,, *Recent advancements in boron nitride nanotubes*, Nanoscale, The Royal Society of Chemistry, 2, 2028-2034, 2010.

[27] Ishigami, M., Aloni, S., Zettl, A., "*Properties of Boron Nitride Nanotubes*", Scanning Tunneling Microscopy/spectroscopy and related Techniques: 12 international Conference, 2003 American Institute of Physics, 0-7354-0168-3, 2003

[28] Zhou, Z., Zhao, J., Chen, Z.,. Schleyer, P. V. R., "*Atomic and electronic structures of fluorinated BN nanotubes: computational study"*, J. Phys. Chem. B, 110, 25678-25685, 2006.

[29] Meyer, N., Renders, C., Lanckman, R., Devillers, M., Hermans, S.,"*Gold as active phase of BN-supported catalysts for lactose oxidation"*, Applied Catalysis A: General 504, 549–558, 2015.

[30] Meyer, N., Devillers, M., Hermans, S., "*Boron nitride supported Pd catalysts for the hydrogenation of lactose"*, Catalysis Today 241, 200–207, 2015.

[31] Zhi , C. Y., Bando, Y., Tang, C., Golberg, D., "*Engineering of electronic structure of boron-nitride nanotubes by covalent functionalization",,* Phys. Rev. B 74, 153413, 2006.

[32] Demir, C., *"Production of Boron Nitride Nanotubes and their uses in Polymer Composites",* MS thesis Chemical Engineering Middle East Technical University Ankara, Turkey, November, 2010.

[33] Ahmad, P., Khandaker, M. U., Khan, Z. R., Amin, Y. M.," *Synthesis of boron nitride nanotubes via chemical vapor deposition: a comprehensive review"*, Royal Society of Chemistry (RSC) Adv., 5, 35116, 2015.

[34] Loiseau,A., Willaime, F., Demoncy, N., Hug, G., Pascard, H., "*Boron Nitride Nanotubes with Reduced Numbers of Layers Synthesized by Arc Discharge"*, The American Physical Society, volume 76,0031-9007/96/76(25)/4737(4),1996.

[35] Lu, X., Feng, L., Akasaka. T., Nagase, S., "*Current status and future developments of endohedral metallofullerenes"*, Chem. Soc. Rev., 41, 7723–7760, 2012.

[36] Golberg, D., Bando, Y., Eremets, M., Takemura, K., Kurashima, K., Yusa, H.," *Nanotubes in boron nitride laser heated at high pressure"*, Applied Physics Letters, 69, 2045–2047, 1996.

[37] Ando, Y., Zhao, X., Sugai, T., Kumar, M., "*Growing carbon nanotubes*." Materials today, 22-29, 1369-7021, 2004

[38] Chen, Y., Chadderton, L. T., Gerald, J. F., Williams, J. S.," *A solid-state process for formation of boron nitride nanotubes"*, Appl. Phys. Lett., 74, 2960–2962, 1999.

[39] Chen, I. Y., "*Nanotubes and Nanosheets: Functionalization and Applications of Boron Nitride and Other Nanomaterial"s*, CRC Press, Feb 13, 2015

[40] Han, W., Bando, Y., Kurashima, Y., Sato, T.," *Synthesis of boron nitride nanotubes from carbon nanotubes by a substitution reaction"*, Applied Physics Letters volume 73, number 21 3085, 1998.

[41] Lourie, O. R., Jones, C. R., Bartlett, B. M., Gibbons, P. C., Ruoff, R. S., Buhro, W. E., "*CVD growth of boron nitride nanotubes"*, Chem. Mater., 12, 1808–1810, 2000.

[42] Tang, C., Bando, Y., Huang, Y., Yue, S., Gu, C., Xu, F., Golberg, D.," *Fluorination and electrical conductivity of BN nanotubes"*, J. Am. Chem. Soc., 127, 6552–6553, 2005.

[43] Lee, C. H., Wang, J., Kayatsha, V. K., Huang, J. Y., Yap, Y. K.," *Effective growth of boron nitride nanotubes by thermal chemical vapor deposition"*, Nanotechnology, 19, 455605 (5pp), 2008.

[44] Kayastha, V. K., Wu, S., Moscatello, J., Yap, Y. K.," *Synthesis of Vertically Aligned Single- and Double-Walled Carbon Nanotubes without Etching Agents"*, J. Phys. Chem. C, 111, 10158–10161, 2007.

[45] Tang, C., Bando, Y., Sato, T., "*Catalytic growth of boron nitride nanotubes"*, Chem. Phys. Lett., 362, 185–189, 2002.

[46] Tang, C., Lamy de la Chapelle, M., Li, P., Liu, Y., Dang, Y., Fan, S.," *Catalytic growth of nanotube and nanobamboo structures of boron nitride"*, Chem. Phys. Lett., 342, 492–496, 2001.

[47] Tang, C., Bando, Y., Sato, T., Kurashima, K.," *A novel precursor for synthesis of pure boron nitride nanotubes"*, Chem. Commun., 1290–1291, 2002.

[48] Ahmad, P., Khandaker, M. U., Amin, Y. M.," *Synthesis of boron nitride nanotubes by argon supported thermal chemical vapor deposition"*, Phys. E, 67, 33–37, 2015.

[49] Kim, M. J., Chatterjee, S., Kim, S. M., Stach, E. A., Bradley, M. G., Pender, M. J., Sneddon, L. G., Maruyama, B.," *Double-walled boron nitride nanotubes grown by floating catalyst chemical vapor deposition"*, Nano Lett., 8, 3298–3302, 2008.

[50] Golberg, D., Bando, Y., Tang, C., Zhi, C., "*Boron nitride nanotubes"*, Adv. Mater., 19, 2413–2432, 2007.

[51] Guo, L., Singh R.,"*Catalytic growth of boron nitride nanotubes using gas precursor"s"*, Phys. E, 41, 448–453, 2009.

[52] Su, C. Y., Chu, W. Y., Juang, Z. Y., Chen, K. F., Cheng, B. M., Chen, F. R., Leou, K. C., Tsai, C. H.," *Large-scale synthesis of boron nitride nanotubes with iron-supported catalysts"*, J. Phys. Chem. C, 113, 14732–14738, 2009.

[53] Ma, R., Bando, Y., Sato, T.,"*CVD synthesis of boron nitride nanotubes without metal catalysts"*, Chem. Phys. Lett., 337, 61–64, 2001.

[54] http://cnx.org/contents/9bbbe39c-a840-4461-882c-e31f8a0125e6@2/Chemical-Vapor-Deposition, last accessed date: December 31, 2015.

[55] Mercan, O., "*Production of boron nitride using chemical vapor deposition"*, MS Thesis, Chemical Engineering department, Middle East Technical University Ankara, February, 2014.

[56] Campbell, S. A., *Fabrication Engineering at the Micro- and Nanoscale*, 4th Edition. Oxford University Press, 2013.

[57] Lowell, S., Shields, J. E., Thomas, M. A., Thommes, M., "*Characterization of porous solids and powders: surface area, pore size and density*", 4th edition, Netherlands, Springer, Netherlands: Springer, 347, 2006.

[58] Narita, I., Oku, T., "*Synthesis of boron nitride nanotubes by using YB6 powder"*, Solid State Communications 122, 465–468, 2002.

[59] Zhoua, G. W., Zhanga, Z., Baib, Z. G., Yub, D. P., "*Catalyst effects on formation of boron nitride nano-tubules synthesized by laser ablation"*, Solid State Communications 109, 555–559, 1999.

[60] Yu, D. P., Sun, X. S., Lee, C. S., Bello, I., Lee, S.T., Gu, H. D., Leung, K. M., Zhou, G. W., Dong, Z. F., Zhang, Z., "*Synthesis of boron nitride nanotubes by means of excimer laser ablation at high temperature"*, Applied Physics Letters, volume 72, number 16, 1998.

[61] Dai, J., Xu, L., Fang, Z., Sheng, D., Guo, Q., Ren, Z.,Wang, K., Qian, Y.," *A convenient catalytic approach to synthesize straight boron nitride nanotubes using synergic nitrogen source"*, Chemical Physics Letters 440, 253–258, 2007.

[62] Cai, P., Chen, L., Shi, L., Yang, Z., Zhao, A., Gu, A., Huang, A., Qian, Y., "*One convenient synthesis route to boron nitride nanotube"*, Solid State Communications 133, 621–623, 2005.

[63] Yu, J., Chen, Y., Wuhrer, R., Liu, Z., Simon, Ringer, P., "*In Situ Formation of BN Nanotubes during Nitriding Reactions"*, Chem. Mater., 17, 5172-5176, 2005.

[64] Chen, Y., Conway, M., Williams, J. S., Zou, J., "*Large-quantity production of high-yield boron nitride nanotubes"*, J. Mater. Res., Vol. 17, No. 8, Aug 2002.

[65] Özmen D., Sezgi, N. A., Balcı, S., "*Synthesis of Boron Nitride Nanotubes from Ammonia & a Powder Mixture of Boron & Iron Oxide"*, Chem. Eng. J., 219, 28–36, 2012.

[66] Noyan, S., "*Production of boron nitride nanotubes from reaction of NH_3 with boron and iron powder mixture*" MS thesis Chemical Engineering department, Middle East Technical University Ankara Turkey, September, 2012

[67] Ferreira, T. H., Omelas da Silva, P. R., Dos Santos, R. G.,De Sousa, E. M . B., " *A Novel Synthesis Route to Produce Boron Nitride Nanotubes for Bioapplications"*, Journal of Biomaterials and Nanobiotechnology, 2, 426-434, 2011.

[68] Seo, D., Kim, J., Park, S. H., Jeong, Y. U., Seo, Y. D., Lee, S. H., Kim, J., "*Synthesis of boron nitride nanotubes using thermal chemical vapor deposition of ball milled boron powder"*, Journal of Industrial and Engineering Chemistry,19, 1117–1122, 2013.

[69] Lim, S. H., Luo, J., Ji, W., Lin, J., "*Synthesis of boron nitride nanotubes and its hydrogen uptake"*, Catalysis Today 120, 346–350, 2007.

[70] Webb, P. A., "*Volume and Density Determinations for Particle Technologists"*, Micromeritics Instrument Corporation, 2/16/2001 report.

[71] Mehio, N., Dai, S., Jiang, D., "*Quantum Mechanical Basis for Kinetic Diameters of Small Gaseous Molecules"*, J. Phys. Chem. A, 118, 1150−1154, 2014.

[72] Ok, S. *"Adsorption properties of carbon nanotubes"* MS thesis Chemical Engineering department, Middle East Technical University Ankara Turkey, August 2005.

[73] Lindo, M., Vizcaı´no, A.J., Calles, J.A., Carrero, A.,"*Ethanol steam reforming on Ni/Al-SBA-15 catalysts: Effect of the aluminium content",* International journal of hydrogen energy, 35, 5895 – 5901, 2010.

[74] Niwa., M, Katada., N., *"Measurements of acidic property of zeolites by temperature programmed desorption of ammonia",* Catalysis Surveys from Japan, Baltzer Science Publishers 1, 215 – 226, 1997.

[75] Low, I. M., "*Ceramic Matrix Composites - Microstructure, Properties and Applications"*, Woodhead Publishing, p 346 (613), 2006.

APPENDIX A

X-RAY DIFFRACTION DATA

A.1 XRD data of synthesized material and reference compounds

XRD data of BN nanotubes synthesized using Fe_2O_3 and Fe and other reference materials are given in Tables A.1- A.6.

Table A.1 XRD data of BN synthesized at 1300°C and boron to iron oxide ratio of 15 and ammonia flow rate of 125cm^3/min

2θ(°)	**Intensity (I/I_o)**	**d (Å)**
26.4	100	3.3733
44.5	41.78	2.0343
41.9	26.42	2.1544
65.2	17.43	1.4297
75.9	15.00	1.2526
77.3	14.38	1.2333
38.5	13.93	2.3364
54.3	10.78	1.6880
82.2	10.51	1.1718

Table A.2 XRD data of BN synthesized at 1300°C and boron to iron ratio of 15 and ammonia flow rate of 125 cm^3/min

2θ(°)	**Intensity (I/I_o)**	**d (Å)**
26.40	100	3.3733
41.90	24.53	2.1543
42.19	23.58	1.1470
44.75	22.64	2.0235
75.99	15.09	1.2513
54.97	11.79	1.6691
82.06	10.85	1.1734
82.44	10.38	1.1690
65.12	9.90	1.4313
78.27	9.43	1.2204
38.46	6.60	2.3388

Table A.3 XRD Data of Hexagonal BN

Catalog No: 34-0421 **Hexagonal BN** **Radiation:CuKa1(λ:1.5406Å)**			
d(Å)	**2θ (°)**	**Intensity(I/I_o)**	**h k l**
3.328	26.76	100	0 0 2
2.169	41.59	23	1 0 0
2.062	43.87	10	1 0 1
1.817	50.14	16	1 0 2
1.663	55.16	12	0 0 4

Table A.3 (cont'd)

d(Å)	2θ (º)	Intensity(I/I_o)	h k l
1.550	59.55	<2	1 0 3
1.319	71.41	5	1 0 4
1.252	75.93	13	1 1 0
1.172	82.17	14	1 1 2
1.134	85.51	<3	1 0 5
1.109	87.94	<3	0 0 6
1.084	90.53	<3	2 0 0
1.031	96.66	3	2 0 2
1.000	100.68	10	1 1 4
0.908	115.93	<4	2 0 4
0.831	135.63	<4	0 0 8
0.830	136.14	4	1 1 6

Table A.4 XRD data of rhombohedral BN

Catalog No: 45-1171 **Rhombohedral BN** **Radiation:CuKa1(λ:1.5406Å)**			
d(Å)	**2θ (º)**	**Intensity(I/I_o)**	**h k l**
3.334	26.71	100	0 0 3
2.119	42.61	20	1 0 1
1.989	45.56	12	0 1 2
1.666	55.06	8	0 0 6
1.638	56.07	4	1 0 4

Table A.4 (cont'd)

d(Å)	2θ (º)	Intensity(I/I_o)	h k l
1.470	63.18	2	0 1 5
1.251	75.95	8	1 1 0
1.193	80.41	<3	1 0 7
1.172	82.11	11	1 1 3
1.112	87.66	<3	0 0 9
1.077	91.23	<3	0 2 1
1.059	93.22	<3	2 0 2
1.001	100.62	7	1 1 6
0.831	135.85	4	1 1 9
0.816	141.13	4	2 1 1
0.808	144.53	4	1 2 2

Table A.5 XRD data of cubic iron

Catalog No: 06-0696 **Cubic iron** **Radiation:CuKa1(λ:1.5406Å)**			
d(Å)	**2θ (º)**	**Intensity(I/I_o)**	**h k l**
2.026	44.67	100	1 1 0
1.433	65.20	20	2 0 0
1.170	82.33	30	2 1 1
1.013	98.94	10	2 2 0
0.906	116.38	12	3 1 0
0.827	137.13	6	2 2 2

Table A.6 XRD data of iron oxide

Catalog No:33-0664 **Fe_2O_3** **Rad:CuKa1 (λ:1.5406)**					
d(Å)	**2θ (º)**	**Intensity(I/I_o)**	**h**	**k**	**l**
3.684	24.14	22	0	1	2
2.700	33.15	100	1	0	4
2.519	35.61	75	1	1	0
2.292	39.28	4	0	0	6
2.207	40.85	24	1	1	3
2.077	43.52	4	2	0	2
1.840	49.48	59	0	2	4
1.694	54.09	72	1	1	6
1.636	56.15	2	2	1	1
1.603	57.43	8	1	2	2
1.485	62.45	17	0	1	8
1.453	63.99	55	2	1	4
1.413	66.03	<2	1	2	5
1.349	69.60	6	2	0	8
1.311	71.94	21	1	0	10
1.306	72.26	12	1	1	9
1.259	75.43	17	2	2	0
1.227	77.73	9	3	0	6
1.214	78.76	4	2	2	3
1.189	80.71	11	1	2	8
1.163	82.94	12	0	2	10
1.141	84.91	17	1	3	4
1.103	88.54	17	2	2	6
1.076	91.34	5	0	4	2
1.055	93.71	18	2	1	10
1.042	95.24	<3	1	1	12
1.039	95.66	8	4	0	4
0.989	102.28	11	3	2	8
0.971	104.91	<3	2	2	9
0.960	106.61	14	3	2	4
0.958	107.02	11	0	1	14
0.951	108.08	14	4	1	0

APPENDIX B

SEM IMAGES OF PURIFIED BNNTs

B.1. SEM Images of BNNTs Synthesized Using Iron Oxide

SEM images of purified BNNTs synthesized using iron oxide are given in Figures B.1-B.4

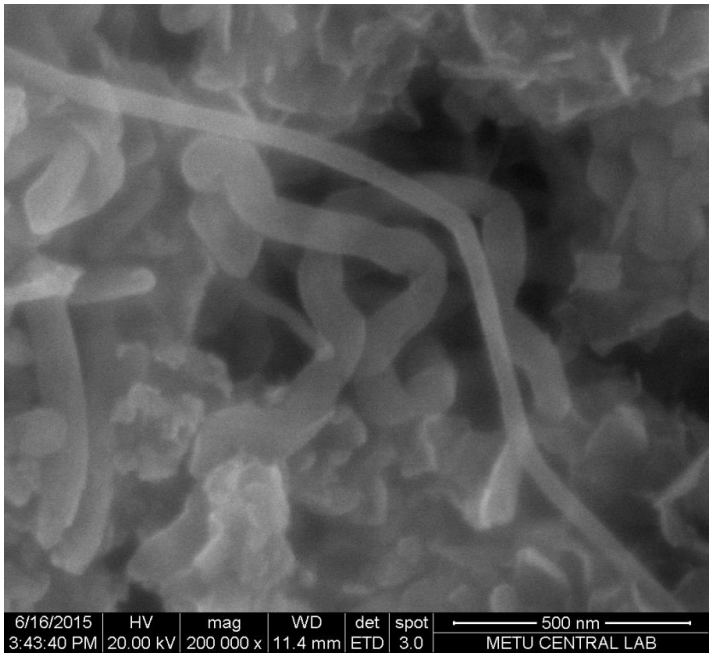

Figure B.1 SEM image of BNNTs (UP-BN-MO) synthesized using iron oxide at 1300^{o}C

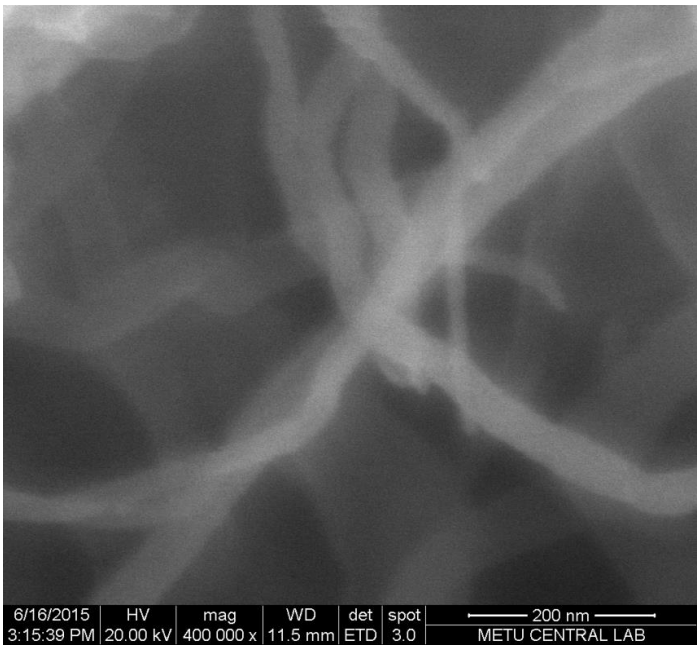

Figure B.2 SEM image of BNNTs (P-BN-MO-4) synthesized using iron oxide at 1300ºC

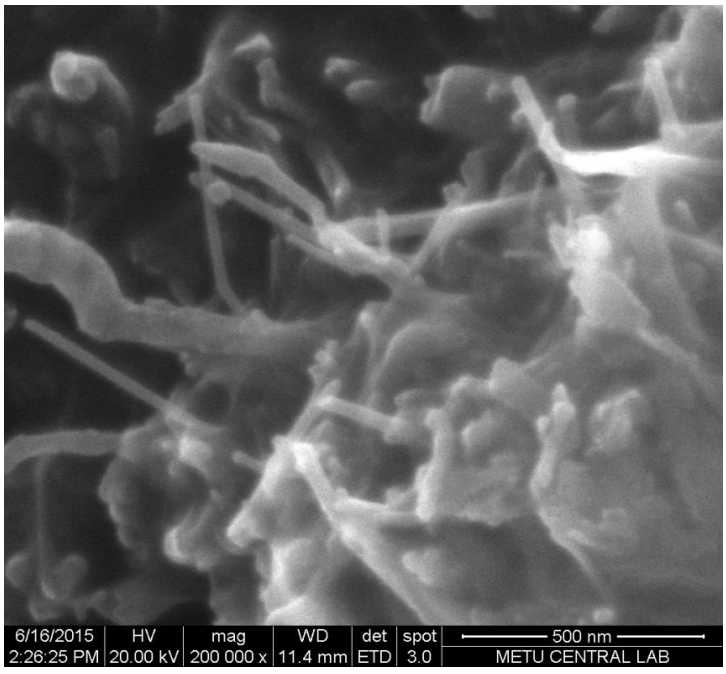

Figure B.3 SEM image of BNNTs (P-BN-MO-6) synthesized using iron oxide at 1300ºC

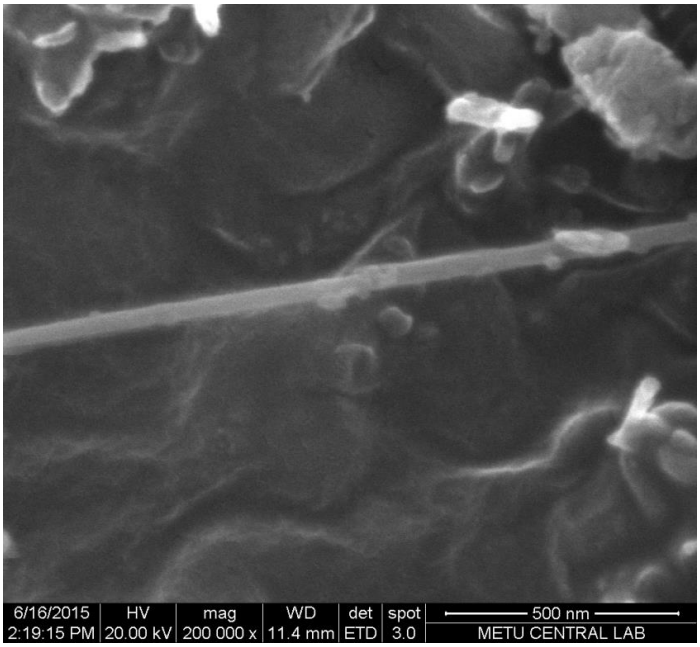

Figure B.4 SEM image of BNNTs (P-BN-MO-6) synthesized using iron oxide at 1300^{o}C

B.2. SEM Images of BNNTs Synthesized Using Iron

SEM images of BNNTs synthesized using iron are shown in Figures B.5-B.6

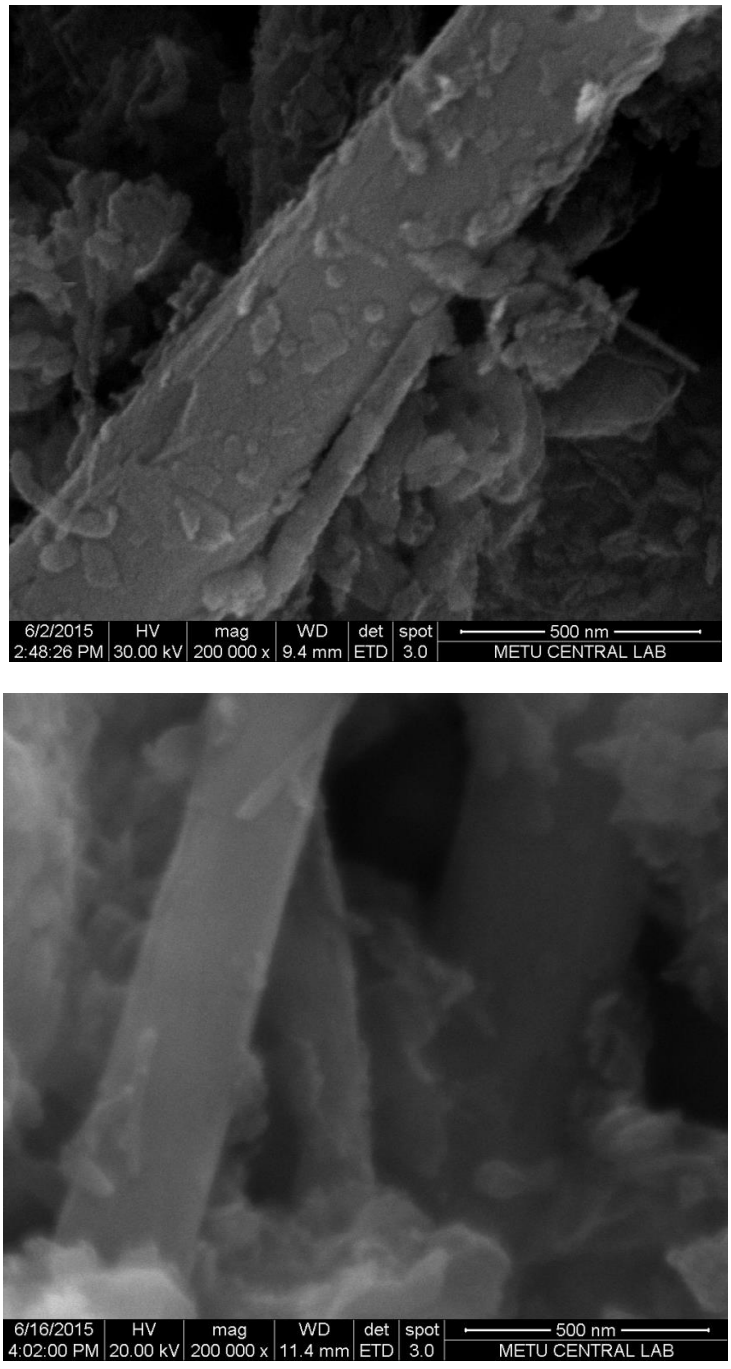

Figure B.5 SEM images of BNNTs (P-BN-M-1) synthesized using iron at 1300^{o}C

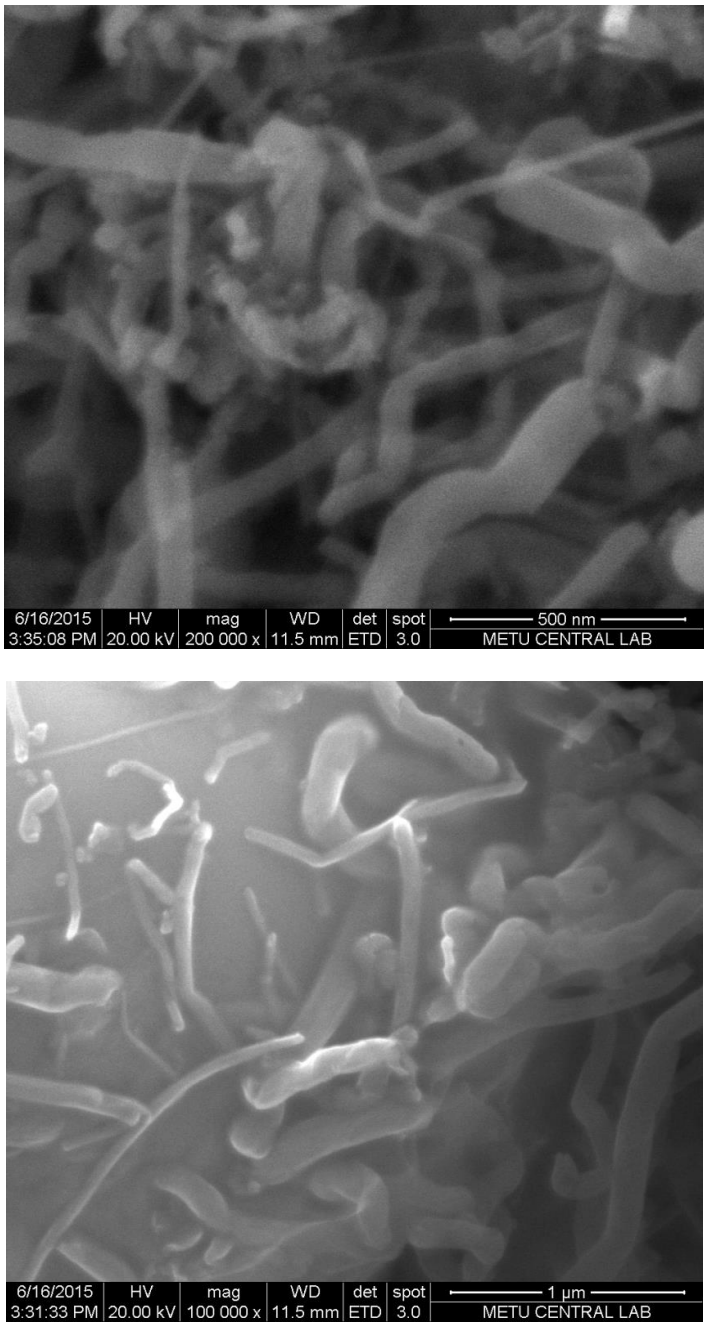

Figure B.6 SEM images of BNNTs (UP-BN-M) synthesized using iron at 1300^{o}C

APPENDIX C

TEM IMAGES OF PURIFIED BNNTs

TEM images of purified BNNTs synthesized using iron oxide and iron are shown in Figures C.1-C.6, respectively

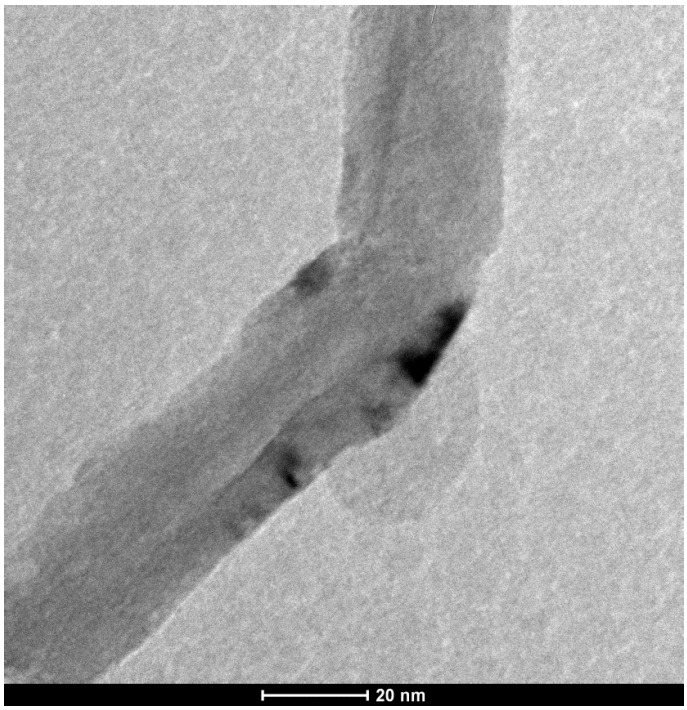

Figure C.1 TEM image of purified BNNT (P-BN-MO-2) synthesized using iron oxide at 1300^{o}C

Figure C.2 TEM image of purified BNNT (P-BN-MO-2) synthesized using iron oxide at 1300^{o}C

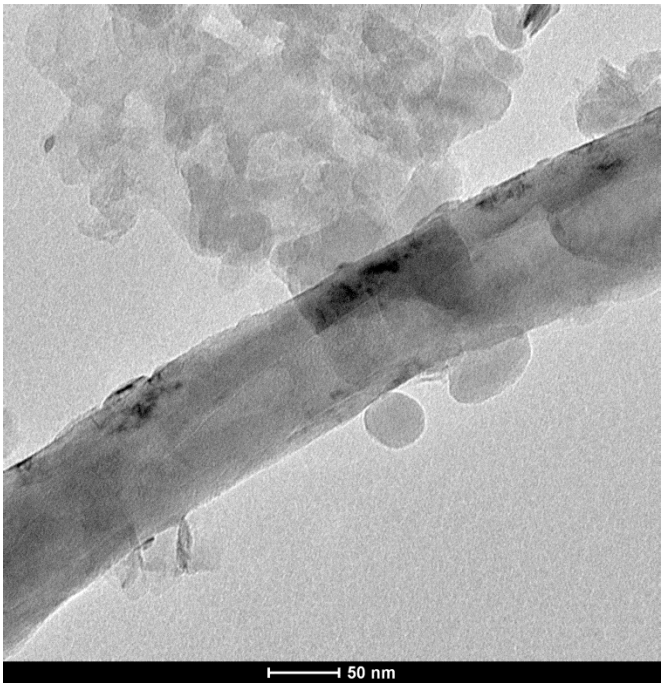

Figure C.3 TEM image of purified BNNT (P-BN-MO-2) synthesized using iron oxide at 1300^{o}C

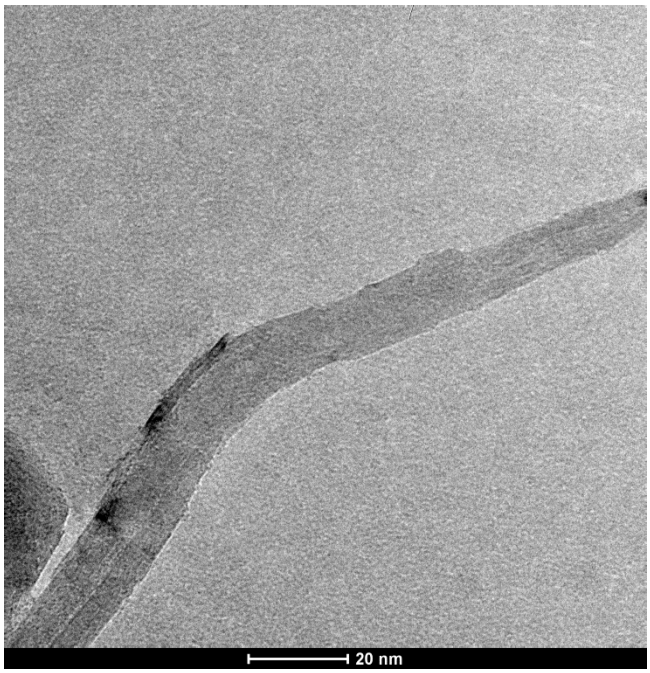

Figure C.4 TEM image of purified BNNT (P-BN-MO-2) synthesized using iron oxide at 1300ºC

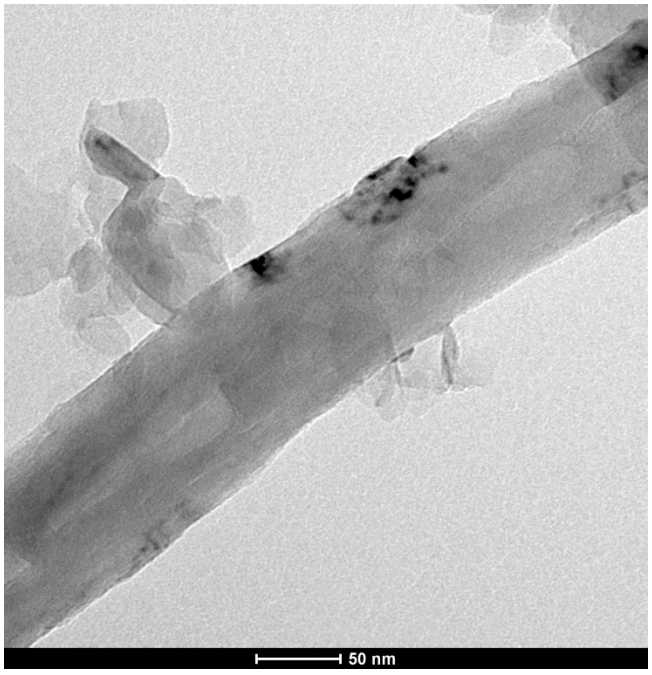

Figure C.5 TEM image of purified BNNT (P-BN-M-1) synthesized using iron at 1300ºC

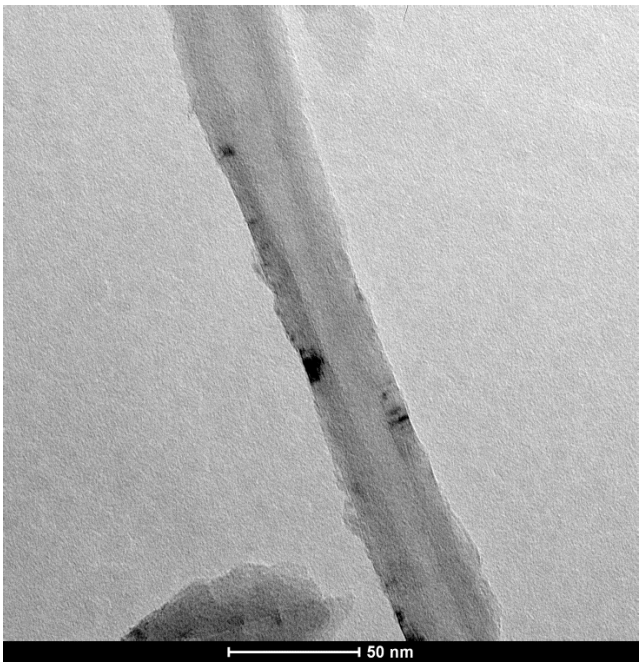

Figure C.6 TEM image of purified BNNT (P-BN-M-1) synthesized using iron at 1300ºC

APPENDIX D

BET SURFACE AREA CALCULATIONS

The Brunauer-Emmett-Teller (BET) method is the most widely used procedure for the determination of the surface area of solid materials and involves the use of BET equation (1). Where V is the amount of gas adsorbed at a relative pressure, P/P_o, V_m is amount of gas adsorbed in the monolayer on solid surface and C is BET constant; indication of the magnitude of the adsorbate/adsorbent interaction.

$$\frac{1}{V_m\left(\left(P_0/P\right)-1\right)} = \frac{1}{V_m C} + \frac{C-1}{V_m C}\left(\frac{P}{P_0}\right) \qquad (1)$$

$$s = \frac{C-1}{W_m C} \qquad (2)$$

$$i = \frac{1}{W_m C} \qquad (3)$$

The BET equation requires a linear plot of $1/[V(P_o/P - 1)]$ versus relative pressure (P/P_o). For most solids nitrogen is used as adsorbate . The BET equation is applied to the data in the P/P_o range of 0.05-0.30. The standard multipoint BET procedure requires a minimum of 3 points in this range. Equation (2) and (3) is the slope and intercept of the BET plot, respectively. V_m can be obtained using equation (4).

$$V_m = \frac{1}{s+i} \qquad (4)$$

The total surface area of the sample can be calculated from the following equation

$S= (V_m* A* N_A)/22400$

Example:

BET surface area of a sample (P-BN-MO-2) is calculated as an example. All the surface area values used in this work are calculated and not taken from the equipment results sheets.

Table D.1 Relative pressure (P/P_o) and volume adsorbed (V) data used for calculation of surface area

Relative Pressure (P/Po)	**V (cm^3/g)**	**$1/[V(P_o/P - 1)]$**
0.299790332	45.04137854	0.009506
0.240724966	41.29399399	0.007678
0.201127702	39.00658702	0.006454
0.162763456	36.90334172	0.005268
0.140647984	35.69348956	0.004585
0.120382452	34.58091073	0.003958
0.100367059	33.45243456	0.003335
0.081390802	32.33461236	0.00274
0.060314342	30.93374964	0.002075
0.050008437	30.16631726	0.001745

A graph (Figure D.1) is plotted between P/P_o and $1/ [V (P_o/P)-1]$ and from the slope and intercept the surface area is calculated

Using slope and intercept BET surface area can be calculated as

Slope= 0.0296

Intercept= 0.0004

$V_m=1/ (0.0296+0.0004)$

$V_m= 33.33\ cm^3/g$

BET surface area= $(33.33*16.2*10^{-20}*6.023*10^{23})/22400$

BET surface area= 145.2 m^2/g

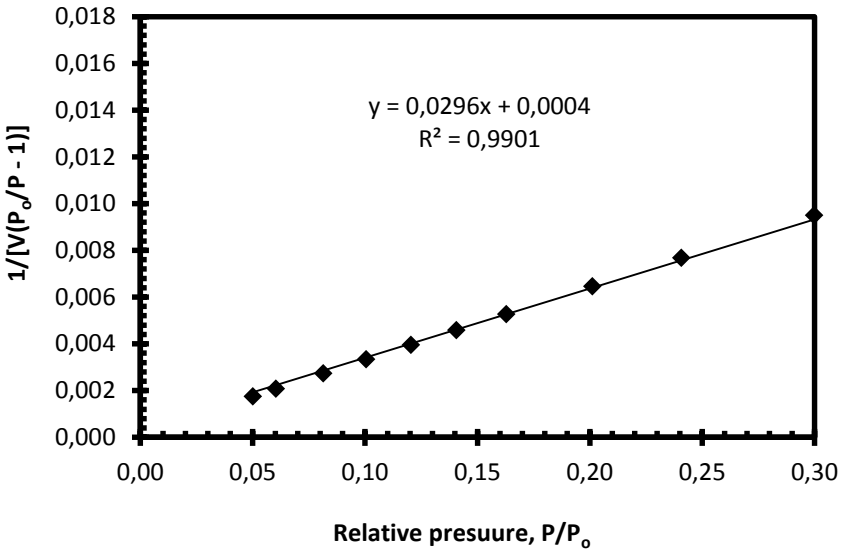

Figure D.1 Plot between 1/ [V(P_o/P - 1)] and relative pressure for surface area calculations

APPENDIX E

CHEMICAL ADSORPTION AND TOTAL ACIDITY

Figure E.1 shows the calibration curve obtained for the chemisorption analysis of BNNTs using ammonia as a probe gas. Table E.1 shows the area under the curve calculated from using the chemisorption curves for BNNTs. Also the temperature ranges in which peaks are obtained are shown in Table E.1.

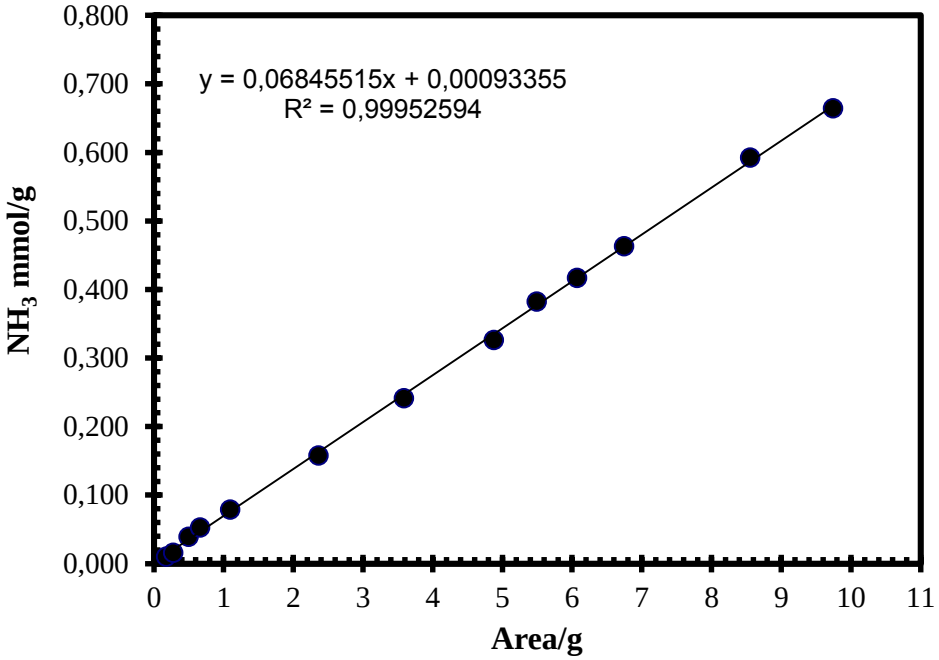

Figure E.1 Calibration curve for NH_3 chemisorption

Table E.1 Area under the curve and total acidity calculation

P-BN-M-1	**Area 1st peak (110 - 420 ºC)**	**Area 2nd peak (435- 760 ºC)**	**Total Area/g**	**Total acidity (mmol NH_3/g)**
	0.58926	1.66674	2.25600	0.15537
P-BN-MO-5	**Area 1st peak (73 - 325 ºC)**	**Area 2nd peak (380- 760 ºC)**	1.98030	0.13650
	0.27011	1.71019		

APPENDIX F

DENSITY MEASUREMENT CALCULATIONS

Skeletal density of powder product was measured using gas pycnometer technique. A gas pycnometer detects change in pressure from the displacement of gas by solid material. Volume was calculated using gas law. Density was calculated using volume and mass of sample used in experiment. Helium gas was used as displacement fluid in the equipment as it is inert and due to small atomic size it can penetrate to very small pores and it is assumed that He gas behaves ideally. Figure 3.4 shows the general schematic of the gas pycnometer. Equipment consists of sample chamber (V_{cell}), reference chamber of precisely known volume (V_{exp}), gas flow control valve, and pressure transducer. The sample was charged into the sample cell and gas was allowed to pressurize the chamber up to 20 psig. The pressure was recorded (P_1) then the valve between sample and reference chambers was slowly opened in order to allow the gas to expand. The pressure was reduced after expansion and when equilibrium was achieved pressure value (P_2) was recorded. Volume and density of the sample were calculated using these pressure, volume and weight of the sample. Analysis was performed at ambient temperature.

$$V_{sample} = Vcell + \frac{Vexp}{1-(P1/P2)} \quad [64]$$

where V_{sample} is the calculated volume of sample and P_1, P_2 are recorded directly from the digital display on the equipment and V_{cell} is the volume of sample chamber/cell.

The pressure data obtained from the equipment for purified BNNTs sample (P-BN-M-3) is given in Table F.1. Gas law was used to calculate the volume of sample and from the volume and known mass of sample density was calculated.

Table F.1 Pressure readings from apparatus for calculation of density

P_1 (psi)	**P_2 (psi)**
19.876	11.289
19.891	11.295
19.955	11.361
19.916	11.312
19.953	11.332

P_1 is the pressure before opening the valve between the sample and reference chambers and P_2 is the pressure after opening that valve. For density measurements the average values of pressures given in Table F.1 were used. Volume of sample chamber/cell (V_{cell}) was measured by taking pressure values using a metal sphere of known volume in the sample chamber as follow.

$$V_{cell} = \frac{Vc(P1-P2)}{P1-P2-(P/P2(P1e-P2e)} = 6.27\ cm^3$$

V_c is volume used for calibration which was taken from equipment manual (2.42 cm^3)

Here P_1 and P_2 are the pressures when sphere was present in the sample chamber. P_{1e} and P_{2e} are the pressures measured before and after opening the valve between the chambers when the sample cell was empty.

Volume of reference or expansion (V_{exp}) chamber was calculated from V_{cell}

$V_{exp} = V_{cell}(P_{1e}-P_{2e})/P_{2e}$

$V_{exp} = 4.76 cm^3$

Then, volume of sample was calculated from the V_{cell} and V_{exp}

$V_{sample} = V_{cell} - \frac{Vexp}{\left(\frac{P1}{P2}\right)-1} = 0.006\ cm^3$

Here P_1 and P_2 are the pressures when sample was present inside the sample chamber 0.0145 g of sample was used in the experiment so the density of sample was obtained as

Density of sample = 0.0145 g/0.006 cm^3 = 2.4 g/cm^3